Title	Study of 180mTa Decay and Development of Ultra-low Background Gamma-ray Spectrometry
Author(s)	Chan, Wei Min
Citation	大阪大学, 2017, 博士論文
Version Type	VoR
URL	https://doi.org/10.18910/61506
rights	
Note	

OSAKA UNIVERSITY
GRADUATE SCHOOL OF SCIENCE

Study of ^{180m}Ta Decay and Development of Ultra-low Background Gamma-ray Spectrometry

Wei Min CHAN

SUBMITTED IN SUPPORT FOR THE DEGREE OF
DOCTOR OF PHILOSOPHY IN PHYSICS

March 2017

Abstract

Among all nuclear isomers that exist in nature, tantalum-180m (^{180m}Ta) has the longest half-life of more than 10^{16} years. Due to the highly forbidden transition with large spin parity difference from ground state, its half-life is yet to be finalized up until now. To achieve the most sensitive detection of ^{180m}Ta decay, ultra-low background condition is essential. In this research, a new ultra-low background HPGe detector system of CANDLES Collaboration was developed at Kamioka Underground Observatory and utilized to observe the rare decay of ^{180m}Ta. Two phases of tantalum physics run were completed, which Phase II has further background reduction on the detector system. The detector performance and background condition during the tantalum measurement were analyzed. Monte Carlo simulation was constructed for the new detector system to obtain the detection efficiency and study the interaction of γ-rays with detector. To further reduce the background level, a new type of pulse shape discrimination (PSD) method for coaxial Ge detector was developed. Using the new PSD method, Compton background event at energy region less than 200 keV can be rejected effectively. By combined the experiment data in Tantalum Phase I and Phase II, physics runs with total livetime of 358.2 days was obtained. With various background reduction techniques and long-term tantalum measurement, the world most stringent half-life limit of ^{180m}Ta has been successfully achieved.

Preface

The dissertation is organized as the following:

First, the interesting facts about isomer ^{180m}Ta and motivation of this research will be described. The ^{180m}Ta decay experiments performed by various research groups for the passed year and improvement that can be done are presented in the first chapter.

In the following chaper 2, focus will be put on the detector system and experiment set up that have developed in this research. The ^{180m}Ta decay is very rare event, hence it is essential to minimized the background level during measurement. Development of a new γ-ray spectrometry at ultra-low background underground laboratory is another main pursue in this study. For ^{180m}Ta study, there were two sets of data, Phase I and Phase II, which corresponds to different experiment setting. The experiment site, detector system, data acquisition system and tantalum sample will be described in detail.

As all the physical preparations were done, chapter 3 will concentrate on the way how raw data were processed for long-term measurement. The DAQ of detector system, DSP has the speciality to digitized and recorded pulse shape of each event, the interpretation of data file will be further mentioned in this section. Furthermore, methods and analysis used to process 3 different runs: tantalum physics run, energy calibration run and background run are included in this chapter.

For chapter 4, analysis of experiment result will be discussed. From Tantalum Phase I (300.6 days) and Phase II (57.6 days) measurements, a long-term low background level γ-ray spectrum was obtained, where numerous weak natural radionuclide became observable with enough statistic.

Pulse shape of each event is important for background reduction using discrimination method, which will be further talked in chapter 5. The Monte Carlo simulation for HPGe detector is summarised in Chapter 6. In this chapter, construction of detector geometry by GEANT4, verification of simulation model and detection efficiency is shown.

Finally, in chapter 7, all the analysis will be combined to conclude the $T_{1/2}$ of ^{180m}Ta. The final result of the efficiency and sensitivity of ^{180m}Ta will be fully explained in this chapter. Compare with the latest published experiment, the best lower limit of $T_{1/2}$ was obtained.

Table of Contents

List of Abbreviations

^{180m}Ta	Isomer of Tantalum-180
γ	Gamma radiation
CANDLES	Neutrinoless double beta decay experiment: CAlcium fluoride for the study of Neutrinos and Dark matters by Low Energy Spectrometer
DAQ	Data AcQuisition system
DSP	Digital Signal Processor
FEP	Full Energy Peak
FWHM	Full Width Half Maximum of energy peak
FWTM	Full Width Tenth Maximum of energy peak
HPGe	High Purity Germanium detector
HV	High Voltage
LN_2	Liquid Nitrogen
NIM	Nuclear Instrumentation Module standard
PSA	Pulse Shape Analysis
PSD	Pulse Shape Discrimination
ROI	Region Of Interest
UPS	Uninterruptible Power Supply

Chapter 1

Introduction of Tantalum-180m Decay

1.1 Physics Motivation

Discovery of Tantalum-180

In 1955, a group of scientists in Knolls Atomic Power Laboratory has discovered a new naturally occurring isotope of tantalum, Tantalum-180 (^{180}Ta) which was obscured by stable ^{181}Ta isotope [1]. They made a tantalum ribbon filament as thermal ionization sample, then used a multiplier to count individual positive ions and obtained the ratio of ^{180}Ta to ^{181}Ta isotopes. The natural abundances of ^{181}Ta and ^{180}Ta were found to be 99.988 % and 0.012 %, respectively. In fact, the group had not realized at that time, that all the observed ^{180}Ta isotopes were actually nuclear isomer, Tantalum-180m (^{180m}Ta).

Interesting facts about ^{180m}Ta

When nucleons of an atomic nucleus were excited and temporary stayed at a metastable state, it is called a nuclear isomer. Generally, nucleus in excited state will decay immediately in the order of pico-second, however typical isomer's $T_{1/2}$ is in the order of nano-second. ^{180m}Ta has the longest isomer $T_{1/2}$ lower limit with more than 4.5 $\times 10^{16}$ years, as reported by HADES group in 2016 [2]. The next nearly stable isomer with long $T_{1/2}$ is ^{166m}Ho with $T_{1/2}$ of 1.2 $\times 10^3$ years [3], which is 13 orders of magnitude shorter than ^{180m}Ta.

Among all isotopes, ^{180m}Ta is the only isomer existing in nature and the rarest stable nuclide in the solar system. The odd-odd nuclide ^{180}Ta has the interesting property of having a short-lived ($T_{1/2}$ = 8.1 hours) $J\pi$ = 1+ ground state and a very long-lived $J\pi$ = 9 isomeric state at 77 keV. In ground state, ^{180}Ta is very unstable and will soon decay after production. Hence, all the tantalum sample that present in the nature are only composed of ^{181}Ta (stable) and ^{180m}Ta.

Since the discovery of ^{180m}Ta in 1954, there were numerous experimental groups attempted to observe the decay. At this point, the $T_{1/2}$ of ^{180m}Ta is yet to be determined.

The purpose of this research is to determine and set a more stringent lower limit for the half-life of ^{180m}Ta, by utilized ultra-low background gamma-ray spectrometry.

1.2 The Nucleosynthesis Puzzle of ^{180m}Ta

The nucleosynthesis of this natures rarest isotope ^{180m}Ta has remained an unsolved puzzle, because it bypassed the major s- and r-process mechanisms. Various nucleosynthesis processes (s- , r-, p-, -) [4, 5, 6] and astrophysical production sites (supernovae, AGB stars, cosmic radiation) have been proposed to explain its very low abundance. Few possible production paths were described by Nemeth [4], as shown in Figure 1.1.

The ratio of the population of the metastable isomer to the total production of this isotope is a crucial hint in all the possible production path. When ^{180m}Ta was produced, it is in a high-temperature photon bath where the transition rate and branching ratio between the ground state and the isomer is affected by the changing temperature [7]. The studies on nucleosynthetic history and production site of ^{180m}Ta are important topics for astrophysics.
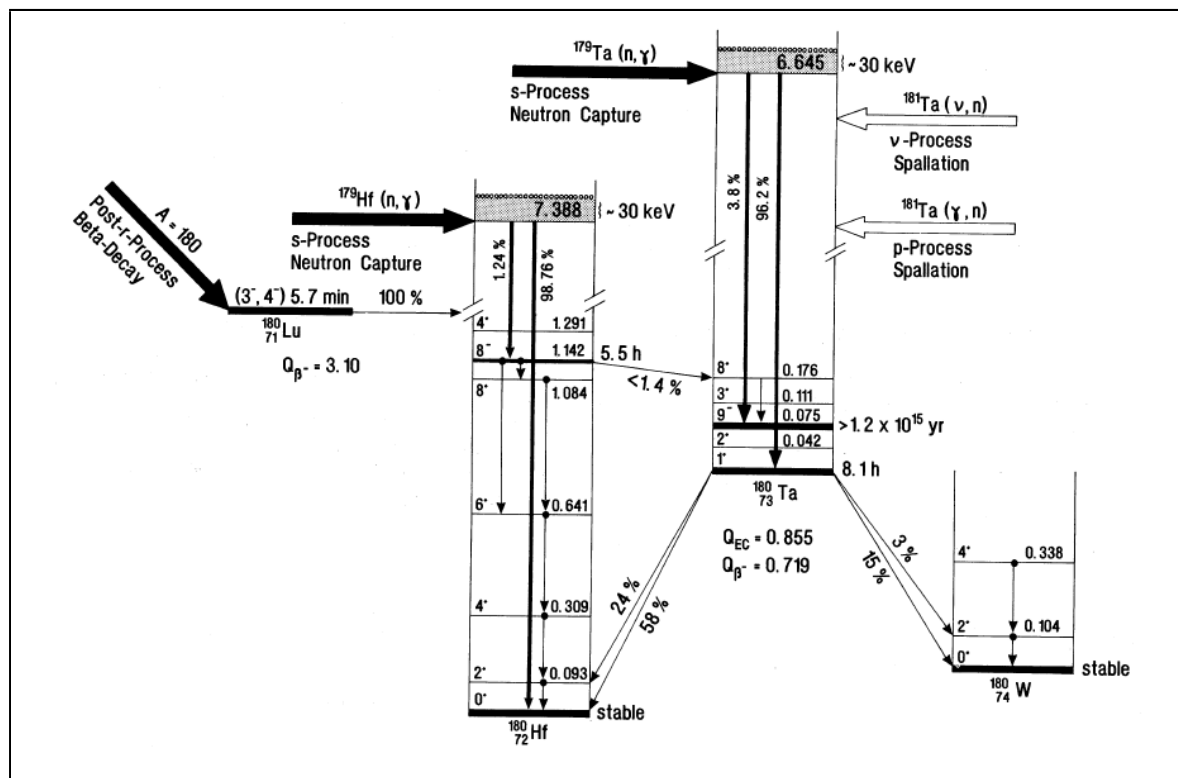
Figure 1.1: Proposed production paths of ^{180m}Ta [4]

1.3 Decay Scheme of ^{180m}Ta

As shown in Figure 1.2, the three decay paths of ^{180m}Ta are,

1. Isomeric transition to ground state

2. Beta minus decay to ^{180}W

3. Electron capture to ^{180}Hf

The isomeric transition from $J\pi = 9\text{-} \to 1+$ was found to be very unlikely with lifetime greater than 10^{27} yr [8]. Hence, it is feasible to detect the six cascading γ-rays from β- and EC decays that indicate the decay of ^{180m}Ta from third-forbidden non-unique transition.
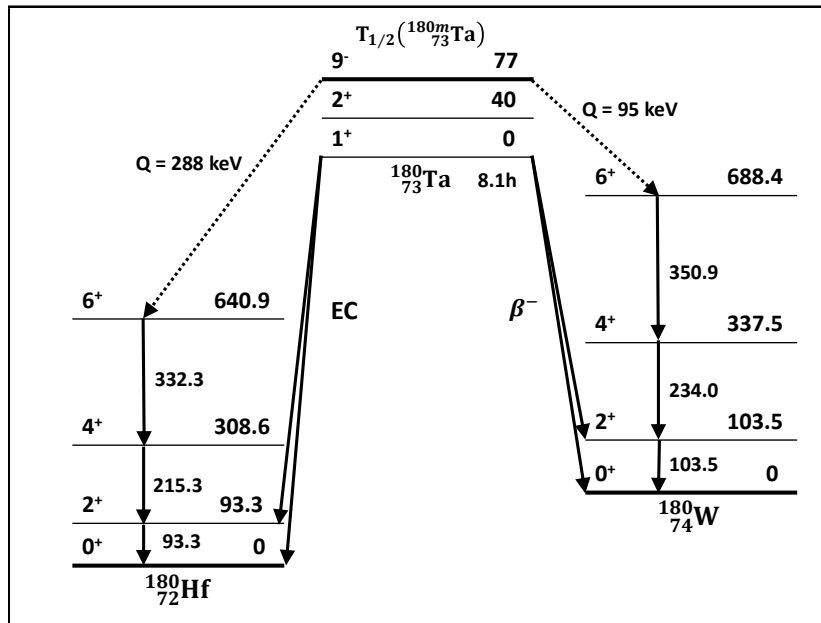
Figure 1.2: Decay Scheme of ^{180m}Ta

Since ^{180m}Ta can undergoes β- and EC decays to ^{180}W or ^{180}Hf, by detecting the cascading γ-rays of the decay, detection of ^{180m}Ta is confirmed. The decay scheme based on values published in Nuclear Data Sheets [9, 10].

1.4 Log ft Value of Beta Decay

For Log ft value of all beta decay nuclides, only one nuclide with third forbidden non-unique transition was obtained [11]. The nuclide is ^{87}Rb with Log ft value of 17.5. Third forbidden non-unique beta decay is far above the normal distribution of first and second transitions. The ^{180m}Ta decay is also a third forbidden non-unique transition of $J\pi = 9\text{-} \to 6+$ as shown in previous decay scheme, and the lower limit of Log ft value (β-) is 22.9. Hence, it has almost reached the highest beta decay limit and indicate the chance to observe the ^{180m}Ta decay.
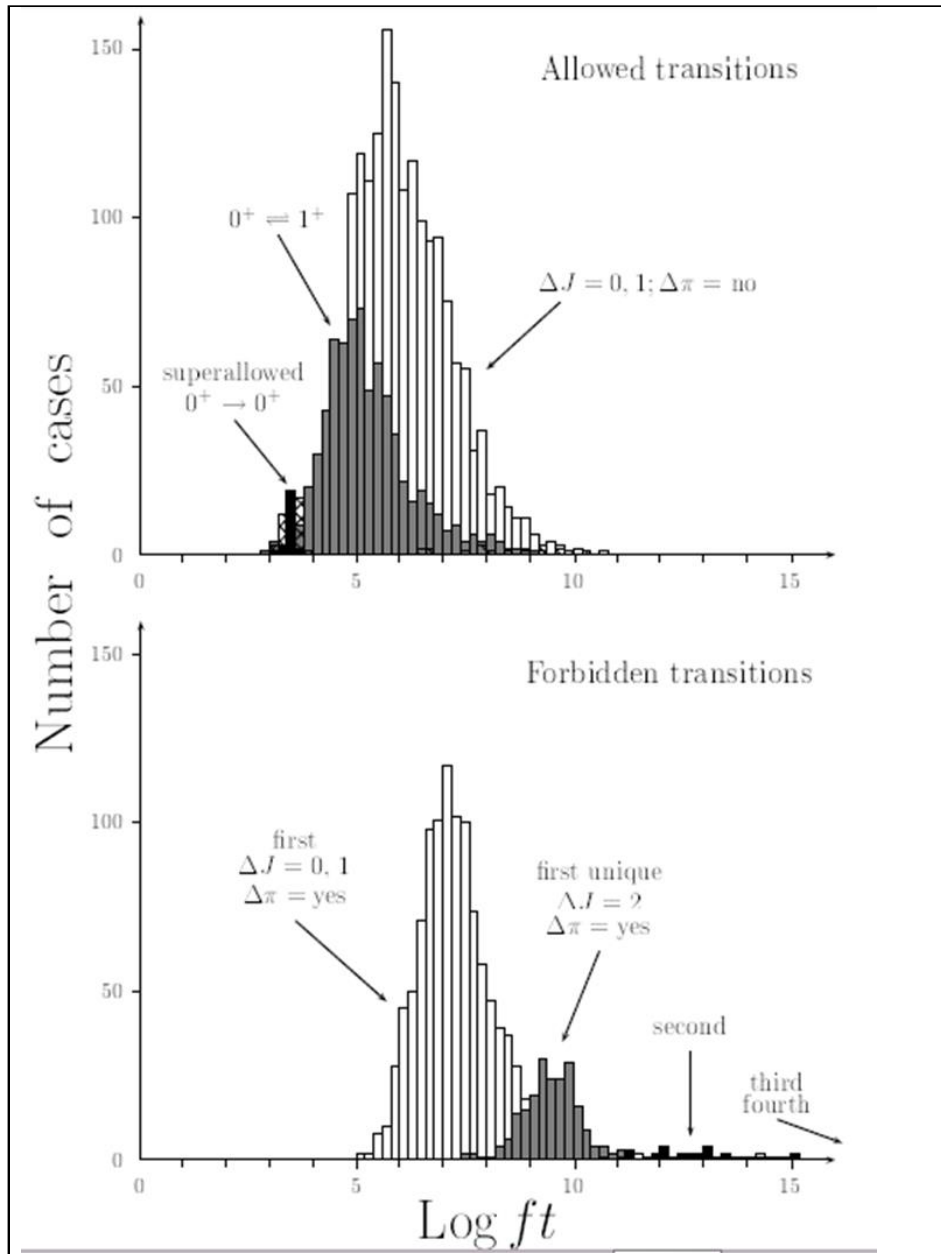
Figure 1.3: Statistical study of Log ft distribution for beta decay transition [11].

1.5 Present Status of ^{180m}Ta Decay Search

Since 1955 [12], scientists has been interested to obtain the half-life of ^{180m}Ta, the most widely accepted $T_{1/2}$ is done by Cumming in 1985 [13]. In recent years, after the available of underground laboratory with ultra-low background gamma-ray spectrometry, scientist has regain the interest to further determine the lower limit of this isotope or even set set an exact value to its half-life.

Kishimoto group has done a measurement to search for the $T_{1/2}$ of ^{180m}Ta at Oto Underground Cosmo Laboratory in year 1999 and obtained a lower limit of 2.6 $\times 10^{15}$ yrs. The tantalum spectrum obtained is shown in Figure 1.4. The consequent experiment was done by a research group of HADES and published results in year 2006, 2009 and 2016 [14, 10, 2]. The journal published spectrum obtained from HADES in year 2009 is shown in Figure 1.5. The latest lower limit of $T_{1/2}$ for ^{180m}Ta is 4.5 $\times 10^{16}$ yrs [2]. The main published results of ^{180m}Ta decay search is listed in Table 1.1.

Table 1.1: Comparison of published ^{180m}Ta decay search

Research Group	Cumming 1985 [13]	Oto 1998 [15, 16]	Hult 2006 [14]	Hult 2009 [10]	Lehnert 2016 [2]
Environment	Ground	Underground	Underground	Underground	Underground
Depth (m.w.e.)	-	1200	500	500	500
Rn (Bq/m^3)	-	10	7	7	7
Tantalum (g)	0.15	479.83	606.04	1500.33	1500.33
Abundance	Ta_2O_5	Natural	Natural	Natural	Natural
Detector	Well Ge	HPGe	HPGe	2× HPGe	2× HPGe
Diameter (mm)	-	-	40	78 & 80	78 & 80
Pb Shield (cm)	-	15.0	-	18.5	18.5
Cu Shield (cm)	-	5.0	-	3.5	3.5
Measurement Duration (days)	89	51	170	68	176 + 238 (Hult 2006 & 2009)
$T_{1/2}$ **limit (yrs)**					
EC branch	3.0×10^{15}	5.2×10^{15}	1.74×10^{16}	4.45×10^{16}	2.0×10^{17}
Log ft	22.9	23.1	23.7	24.1	-
β**- branch**	1.9×10^{15}	1.9×10^{16}	1.2×10^{16}	3.65×10^{16}	5.8×10^{16}
Log ft	21.3	22.3	22.2	22.9	-
Total	1.2×10^{15}	2.6×10^{15}	7.1×10^{15}	2.0×10^{16}	4.5×10^{16}
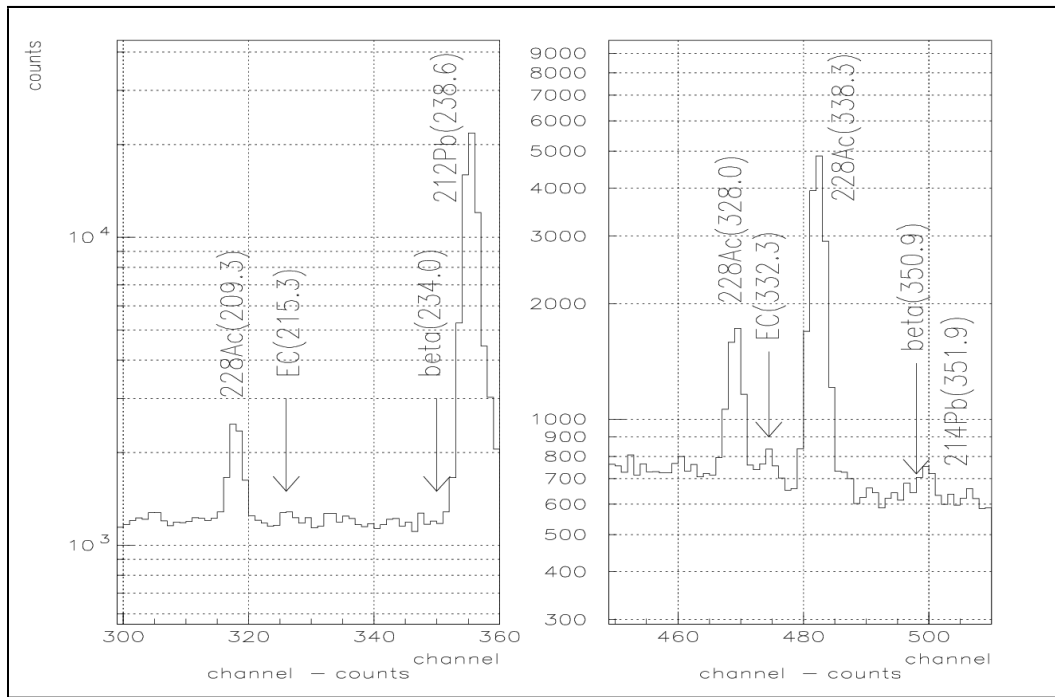
Figure 1.4: Result of Oto Underground Observatory, Shiomi 1999 [15, 16]
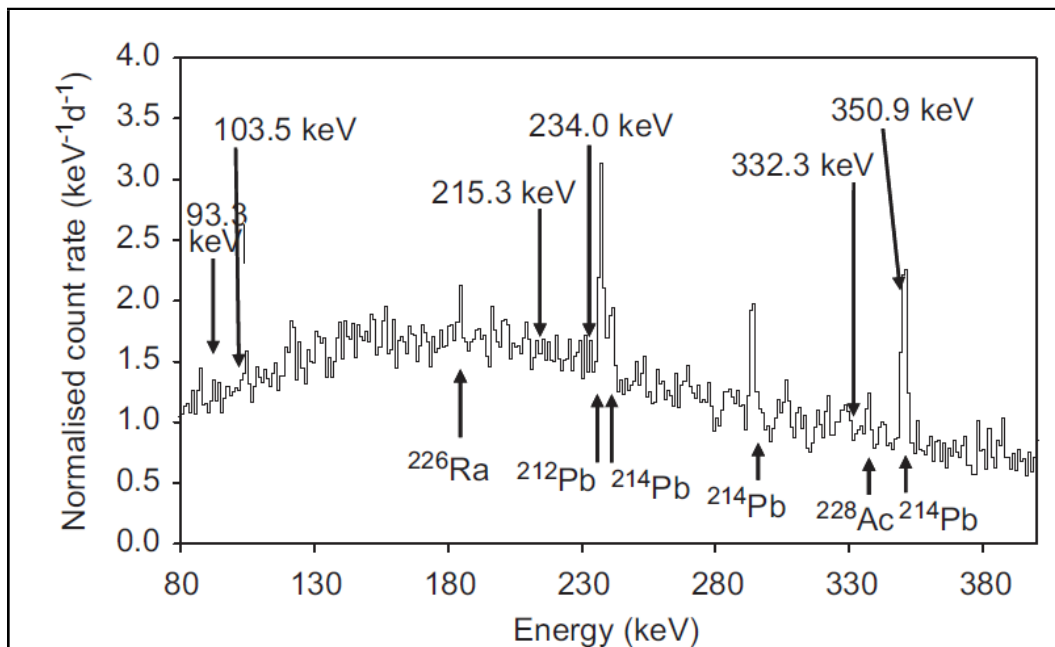
Figure 1.5: Result of HADES, Hult 2009 [10]

6

1.6 Strategy of Detection

In order to reach the most sensitive detection of ^{180m}Ta decay, a ultra-low background γ-ray spectrometer is the optimum choice. Moreover, the following strategies were proposed:

1. Low background condition: Deep underground environment with low cosmic ray flux and hermetic shielding design

2. Optimize tantalum sample configuration

3. Increase statistic of experiment data

4. Improve capability of detector system

5. Develop pulse shape discrimination method for background reduction

Chapter 2

Development of Ultra-low Background HPGe Detector System

2.1 Overview

An ultra-low background γ-ray spectrometry of CANDLES Collaboration was employed for the purpose to study the ^{180m}Ta decay. Figure 2.1 shown a schematic diagram of the major hardware components in the spectrometry system. The main component of the spectrometer was a High Purity Germanium detector (HPGe detector), which used to detect the γ radiation and then convert to recordable electric signal. Power supply for preamplifier, high voltage supply and liquid nitrogen supply for detector were necessary components to make sure the HPGe detector functions in normal condition. A sample, in particular tantalum sample in this research was placed near to the detector and protected from external radiation by passive shields. The electronic signal obtained from detector was then amplified by preamplifier and transferred to digital signal processor (DSP) for pulse processing. Next, the output data of the pro-

Figure 2.1: Schematic diagram of HPGe detector system. The major hardware components were labelled in boxes and connectio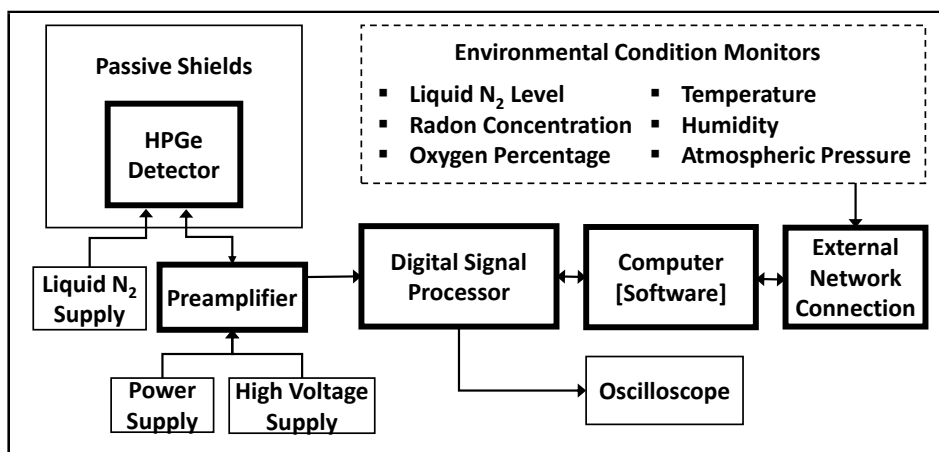ns between each component were linked with arrow lines. Thick boxes indicated the main components that involved in signal processing and data transmission.

cessed signal was recorded by software in computer and can be viewed by oscilloscope for on-site analysis. The recorded data in on-site computer were then transmitted by network connection to external server for storage and off-line analysis. In addition, the parameter setting and data taking of the DSP can be modified and controlled by the software of the on-site computer via external network connection. Environmental conditions within the experimental room such as radon concentration, oxygen percentage, liquid nitrogen level, temperature, humidity and atmospheric pressure were constantly monitored. This information was also transmitted through the external network connection or network camera. The detail of all major components will be described in the coming sections.

For the purpose of this research, a tantalum sample was measured for long-term by the γ-ray spectrometry to detect the rare decay of ^{180m}Ta isomer. Based on the improvements on shielding design, sample surface purification and DSP parameter setting, the tantalum measurement was divided into two phases, Phase I and Phase II. The Phase I measurement was conducted from July 2013 to September 2014, whereas Phase II measurement from April 2016 to June 2016. Majority of the experiment set up in both phases were the same. However, Phase II measurement was conducted with further emphasis on background reduction after realized some deficiencies in Phase I measurement. The improvements of detector system in Phase II will also be discussed in this chapter.

2.2 Experiment Location

The γ-ray spectrometer was newly developed by CANDLES Collaboration since year 2012. Timeline of the detail construction works was listed in Table A.1 of Appendix A. CANDLES is a neutrinoless double beta decay research collaboration which stands for CAlcium fluoride for the study of Neutrinos and Dark matters by Low Energy Spectrometer [18]. For double beta decay experiment, ultra-low background condition is very essential, therefore careful selection of low radioactivity material was required [19]. The γ-ray spectrometer or HPGe detector system is aimed to measure, screen and evaluate the background level of the materi-

Figure 2.2: Illustration of CANDLES Experimental Hall at Kamioka Underground Observatory. The experimental hall was located 1000 m under the Ikenoyama Mountain, which can be accessed by horizontal tunnel. The drawing is not to scale.[17]

als (e.g. case, bolt, string) that will be assembled inside the CANDLES system. In addition, the HPGe detector system was also used for the purpose of this research.
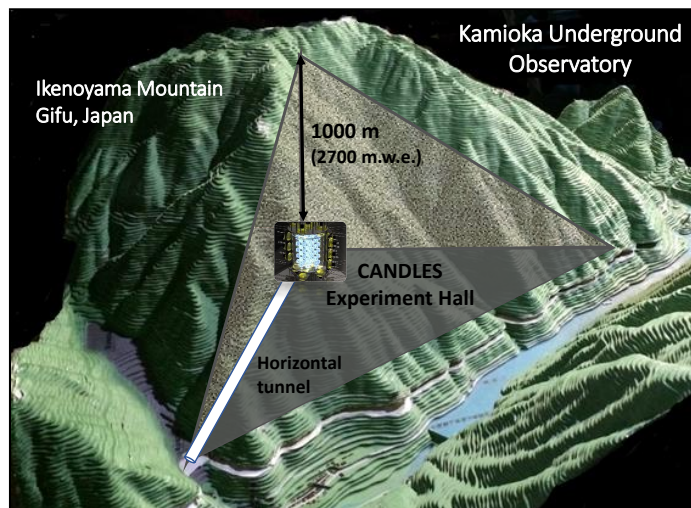
Outer space cosmic ray that mostly consists of energetic proton hit the upper atmosphere and create showers of subatomic debris, such as muon and neutrino. In order to achieve ultra-low background condition for rare event detection, underground laboratory is the ultimate choice. The overburden at deep underground acts as an effective passive shield to attenuate the cosmic rays and neutron activation, the background level is greatly reduced as compared to an on-ground laboratory [20]. The γ-ray spectrometer is located at CANDLES Experimental Hall of Kamioka Underground Observatory [21] as shown in Figure 2.2. The Experimental Hall is divided into three main areas; Front Preparation Room, Center Experimental Hall for CANDLES system and Back Experimental Room. The HPGe detector system was placed inside the Back Experimental Room, where it is convenient to perform material screening for CANDLES. In Summer 2013, the construction of HPGe detector system was completed and data taking of Phase I Tantalum Measurement was started.

2.2.1   Environment at Kamioka Underground Observatory

Muons from cosmic ray can pass through a detector and generate unwanted background by themselves or produce secondary backgrounds of fast neutrons and cosmogenic radioactivity [23]. Due to the need of ultra-low background environment, there are several underground facilities around the world that host the frontier researches of dark matter, neutrino and neutrinoless double beta decay. For instant, Gran Sasso at Italy, Homestake at USA, and so on. As shown in Figure 2.3, muon flux reduces exponentially as the experimental site goes deeper. However, the reduction of muon flux is not simply depends on the physical depth of the experimental site, but mostly affected by the geological composition of the overburden rocks. To standardise this inconsistency, unit meter water equivalent (m.w.e.) was commonly used instead of physical depth (m). This unit shown the competence of a particular underground site to suppress muon penetration as much as the depth of water.
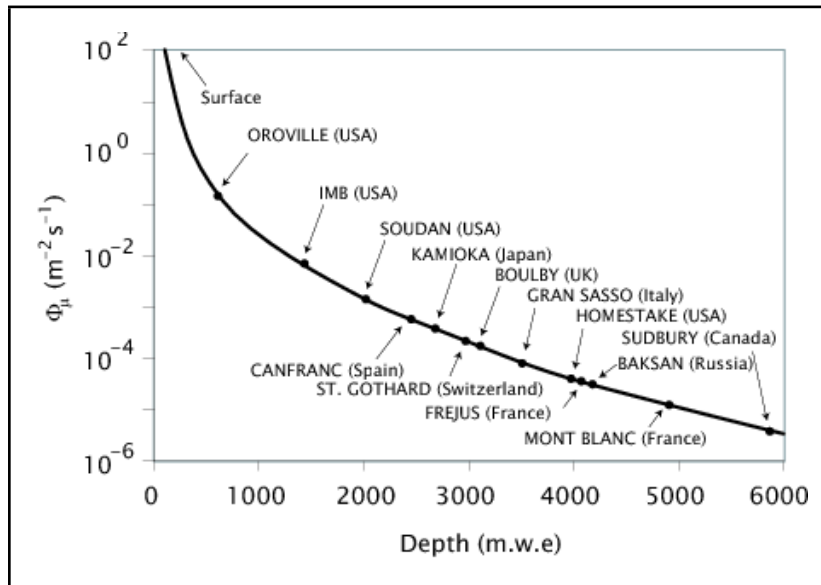

Figure 2.3: The reduction of muon flux corresponds to the depth of worldwide underground facilities [22]. Depth of Kamioka Underground Observatory is 2700 m.w.e.

Kamioka Underground Observatory is the deepest underground scientific facility at Japan, with physical depth of 1000 m which corresponds to 2700 m.w.e.. The muon flux at Kamioka is $3 \times 10^{-3}\ m^{-2}s^{-1}$, that is 5 order magnitude lower than surface of the Earth. The thermal neutron flux and non-thermal neutron flux are $8.25 \pm 0.58 \times 10^{-2}\ m^{-2}s^{-1}$ and $11.5 \pm 1.2 \times 10^{-2}\ m^{-2}s^{-1}$ respectively, as reported by A. Bettini in the review of underground laboratories [24].

The observatory is located under the Ikenoyama Mountain, with horizontal tunnel reach to the center part of experimental halls. This horizontal access provides the advantages of easy drive-in and transportation of large experiment apparatus. Available space can be build on demand and the support facilities on ground were well established. Besides CANDLES, Kamioka is also the experimental site for many other international frontier research groups in nuclear and particle astrophysics. For examples, Super-Kamiokande for neutrino physics, KamLAND for double beta decay and neutrino studies, XMASS and NEWAGE for dark matter search, and CLIO (KARGA) for gravitational wave observation [25].

2.3   Detector System

Decay of unstable nuclei will emit radiation in the form of α particle, β particle or γ-ray. In case of ^{180m}Ta, γ-ray detection is the method to identify the emission of cascading γ-rays from excited state to ground state after electron capture or β^- decay. Detector is a device to convert the radiation into electric signal which contains information of that particular radiation. To maintain a normal function of the detector, in particular HPGe detector, a comprehensive system has to be built to support the detector's requirement, harvest signal information, and monitor surrounding environ-
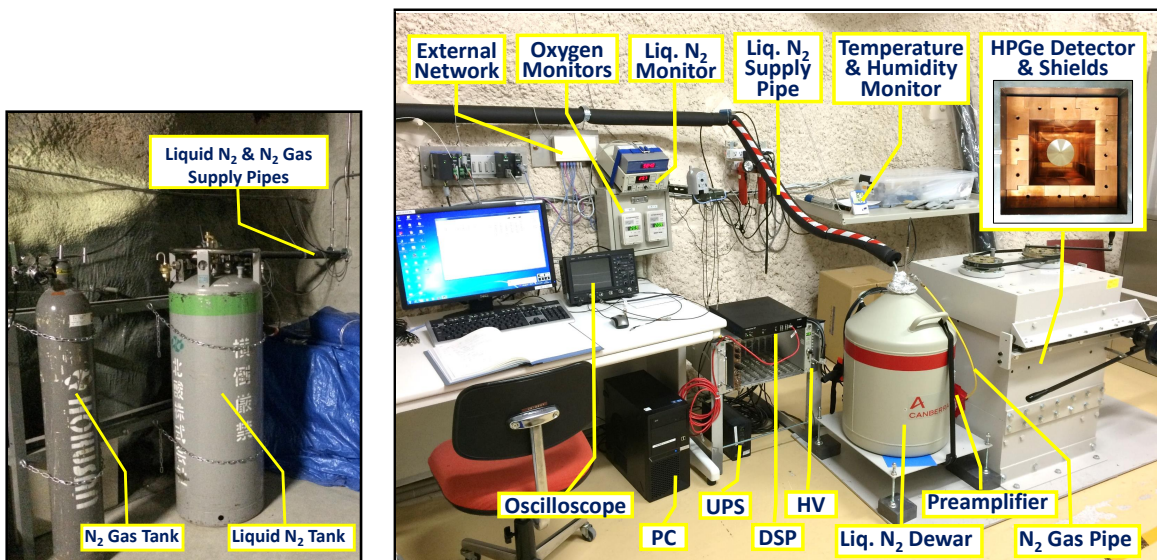

Figure 2.4: Photographic images of the whole HPGe detector system of CANDLES Collaboration. (right) Hardware including HPGe detector, data acquisition system and monitors at Back Experimental Room. (left) Reservoirs of liquid nitrogen and nitrogen gas which placed outside of the experimental room.

ment condition. A photo of the fully developed γ-ray spectrometer is shown in Figure 2.4, which main hardware components have also been labelled in Figure 2.1.

2.3.1   HPGe detector

The main component of the γ-ray spectrometry, HPGe detector is a standard electrode closed coaxial Ge detector (SEGe, Model GC5019) manufactured by CANBERRA Industries Inc. as shown in Figure 2.5 [26].

Germanium crystal   HPGe detector's crystal is a cylindrical high purity p-type germanium crystal with net impurity level about 10^{10} atoms/cm^3. The crystal size is 65 mm in diameter and 64 mm in length. When the germanium crystal was produced, the top edge was slightly rounded by bulletization procedure to improve charge collection, then a cylindrical hole was drilled at the bottom for core contact location [27]. For p-type Ge detector, the outer surface of the germanium crystal was diffused with lithium atoms and inner surface was implanted with boron atoms. Lithium is electron donor, which makes a n+[1] contact electrode with typical thickness of 0.5 mm at outer surface. On the other hand, boron which is electron acceptor, creates an p+ contact electrode with typical thickness of 0.3 μm at the inner surface. In prin-

Figure 2.5: Inner configuration of standard electrode coaxial Ge detector produced by CANBERRA Industries Inc. [26]

ciple, HPGe detector is a P-I-N structure semiconductor diode[2]. When reverse bias voltage applied, the whole germanium crystal between the contact electrodes will be depleted and creates a depletion region for active radiation detection. However, the lithium-diffused crystal surface is inactive to radiation detection, called as dead layer. As time passed, the lithium atoms can diffused deeper into the crystal volume and dead layer thickness increased [28].

Inner structure   The germanium crystal is supported by an aluminium holder and two rings at side. There are also core signal contact, Teflon insulator, high voltage contact, copper cryostat that connected to the crystal, not drawn in Figure 2.5. The entire crystal and its supporting components are sealed inside an high purity aluminium endcap of 83 mm diameter, 0.8 mm thick at top and 1.5 mm thick at side. The space inside endcap is keep in ultra-high vacuum condition to ensure effective cooling of the crystal. All materials used inside the HPGe detector were carefully selected for ultra-low radioactivity.

---

[1]Symbol '+' indicates high dopant concentration

[2]P-I-N diode is intrinsic semiconductor (I) sandwiched by positively doped (P) and negatively doped (N) contacts

Detector feature   CANBERRA HPGe detector is capable to detect X-ray and γ-ray in energy range from 40 keV to around 10 MeV. The relative efficiency corresponds to 3 inch NaI detector is $\geq$ 50 %. Furthermore, the detector has excellent energy resolution and peak shape. The energy resolution, FWHM is 1.0 keV at 122 keV and 1.9 keV at 1332 keV. Peak shape, FWTM/FWHM is 1.90, whereas Peak to Compton ratio is 64 [26].

2.3.2   Liquid Nitrogen Refill System

For semiconductor material, band gap around 0.5 eV to 4 eV is exists between valence band and conduction band. The band gap of germanium is 0.67 eV [29], which is very low. At room temperature, the charge carriers in germanium crystal can be generated by thermal excitation and produce reverse leakage current. Therefore, the crystal must be kept at low temperature during radiation measurement, which commonly cooled down by liquid nitrogen (LN_2) to 77 K.

Standard HPGe detector is accompanied with cryostat and preamplifier. For this detector system, the liquid nitrogen cryostat is U-type Integral with 30 litre dewar (Model 7915-30ULB, CANBERRA [30]), which the detector chamber and dewar share the same vacuum. During transportation, caution procedure must be taken to ensure the detector is properly attached to the dewar, to avoid vacuum failure. The HPGe detector and cyrostat are assembled with low-background shields as shown in Figure 2.6. U-type cryostat model was specially chosen to keep the preamplifier and dewar outside of the shields, only the HPGe detector was placed inside the shields. This set-up minimizes the external radioactivity originated from electronics inside the preamplifier and simplified the liquid nitrogen filling process.

LN_2 filling procedures LN_2 is a consumable resource in the detector system, the usage rate is around 1.37 litre/day. Therefore, filling of LN_2 to the dewar is a routine work to maintain the HPGe detector's well performance. If the LN_2 supply was depleted and bias voltage is continuously applied, the temperature of the Ge crystal will rinse up enormously, causing excessive thermally generated current and damage to the preamplifier.

The LN_2 filling system in Back Experimental Room is shown in Figure 2.4. On top of the dewar, there are three tubes connected to the LN_2 supply pipe, LN_2 level monitor and boil-off N_2 gas pipe. Instead of measuring the volume of LN_2 in the dewar, a capacitance-based level sensor is reached to the bottom of the dewar and measures the remaining LN_2 height in centimeter scale. The LN_2 level monitor (Model 186, AMI) is capable to monitor accurate LN_2 height inside the dewar with resolution of 0.1 cm. When LN_2 level dropped below a certain pre-set lower limit, the monitor will give out warning alarm and provide automatic refill function. The LN_2 supply pipe is connected to a LN_2 reservoir tank outside of the experimental room, which is regularly provided by Kamioka Mine Company upon request.

During HPGe detector measurement period, shift worker of the CANDLES will perform a daily check on the LN_2 level and refill the LN_2 manually in weekly basis. HPGe

Side View

Top View

Figure 2.6: Schematic drawing of HPGe detector, cryostat and shields. (Top) View from side and (Bottom) from top when top Pb shield is opened. Components that drawn in bold lines indicate the integral cryostat system, vacuum is shared between the detector chamber and liquid nitrogen dewar. The external passive shields are customized for the detector, where preamplifier is placed outside of the shield to minimize external radioactivity. Dimension of length is in millimeter, drawing not to scale.

detector is extremely sensitive to mechanical vibration. For example, scratching the dewar surface or small vibration during LN_2 filling process will produce high frequency microphonics noise to the detector [31]. Therefore, the time and duration of weekly LN_2 filling were recorded to check the effect of microphonics noise on the radiation measurement. The analysis and rejection of this kind of noise will be further discussed in Chapter 3.

Boil-off N_2 gas   The LN_2 that evaporated to gas phase in dewar is channelled to the shield chamber by a small gas pipe. The boil-off N_2 gas is flowed from the bottom of the HPGe detector, filled up the entire space within the shields, then out of a small hole at top side. The good use of boil-off N_2 gas is one of the effective method to achieve ultra-low background condition for the detector. Since N_2 gas is constantly flowing within the closed shield chamber, the background radioactivity caused by radon gas can be greatly suppressed. High concentration of N_2 gas can lead to dangerously low oxygen level in a closed room, especially for underground site. Hence, two oxygen monitors are permanently allocated at the opposite sides in the experimental room for safety purpose.
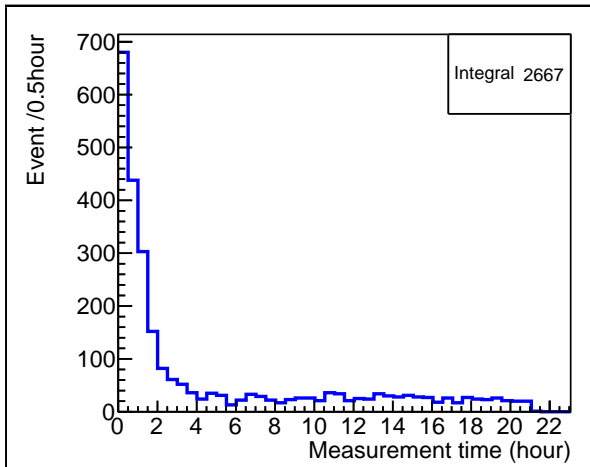

Figure 2.7: Reduction of event rate after flowed with boil-off N_2 gas

In a typical measurement, Figure 2.7 shown a dramatical reduction of event rate after started to flow with boil-off N_2 gas. Before starting this measurement, the shield chamber was opened to change a new sample. During this occasion, normal air which contains radon gas was filled inside the space of the chamber. After closed the chamber, boil-off N_2 gas was started to flow. At the beginning of this measurement, event rate was extremely high (1360 event/hour), mainly caused by background radiation from radon gas. After flowing boil-off N_2 gas for more than 4 hours, the event rate was reduced greatly to 6 %, with less than 80 event/hour. The reduction was less affected by the decay of radon ($T_{1/2}$ of ^{222}Rn is 3.82 days [3]), but mainly caused by the rejection of normal gas out of the system. The event rate also became stable with the constant flow of N_2 gas. This result proved the effectiveness of boil-off N_2 gas to suppress radon gas inside the shield chamber. Setting a good air ventilation in the system can help the nitrogen gas to flow from the bottom of the detector, fill in any possible small gap between the shields, thus force out the normal air that contained high concentration of radon gas via the top side's hole.

N_2 gas supply   As mentioned above, the event rate was extremely high at the beginning after shield chamber had been opened. Boil-off N_2 gas can reduce the radon effect, but stability of event rate takes several hours and waste a lot of measurement time. This situation becomes more serious if a sample has short half-life or many samples

need to be measured one-by-one in a short-term. The solution is to add an additional N_2 gas supply that flow rate and duration can be controlled. A N_2 gas tank is placed beside the LN_2 tank and linked to the experimental room by gas supply pipe as shown in Figure 2.4. The boil-off N_2 gas pipe on top of the dewar can be disconnected and then connects to the N_2 gas supply pipe. To achieve ultra-low background condition, if the shield chamber had been opened, N_2 gas will be circulated inside the chamber for 20 minutes, with flow rate of 7 litre/minute. Then, the pipe will be reconnected to the boil-off N_2 outlet of the dewar for long-term measurement.

2.3.3 High Voltage and Preamplifier

In order to create depletion region that is active to radiation detection, bias voltage has to be supplied to the HPGe detector. Moreover, in order to minimize the electrical noise, a detector signal should be amplified as soon as possible after produced. These two functions was performed by the preamplifier that attached to the cryostat system. The preamplifier used in this system is Model 2002C Spectroscopy Preamplifier, produced by CANBERRA Industries Inc [32].

The HPGe detector's depletion voltage is +1100 volt and recommended bias voltage is +4500 volt. The High Voltage Supply (HV) model is 3106D produced by CANBERRA Industries Inc. NIM bin was set up to provide power supply for HV, preamplifier and ground connection. For ^{180m}Ta measurement, detector was continue running for years. Within the long-term measurement, power failure can occur in the experimental hall, causing the HV of detector increase and decrease within a short period. This is very unfavoured situation that could cause permanent damage on the depletion region of Ge detector and preamplifier.

As a solution to avoid this possible situation, Uninterruptible Power Supply (UPS, OMRON Model BY50S) was installed to the detector system. The UPS has two main function, first is to prevent the automatic recovery of power supply which increase the HV supply rapidly. The second function is provide temporary power supply to the detector in case of power failure and immediate action could be taken to turn down the HV of detector properly. High voltage was reduced or increased gradually when needed.

2.3.4 Shielding

With the advantage of 2700 m.w.e. overload of rocks to shield out the cosmic ray from the Earth surface, there are still background candidates remained in underground laboratory. Background level of the experiment set up should be considered carefully to achieve ultra-low condition. The first step is to construct passive layered shielding around the HPGe detector as presented in Figure 2.8.

Lead shield The outermost layer of the shielding is made of 9 mm of iron shield, which also functions as a container for the 2nd layer of lead shield. The 2nd layer is made of 150 mm of hermetic lead shield, which has only three segmentations. The

Figure 2.8: Photographic image of shielding layers

lead material was originated from lead blocks that used in Oto Underground Observatory and melted by Yoshizawa-LD Corporation to make the required shape. It was specially customized to minimize gap between blocks, in order to avoid radiation coming from outside of the shielding. Crane is needed during construction of the lead shield at experiment site.

Copper shield The copper shield used as the 3rd & inner most layers are oxygen-free high-conductive copper (OFHC Cu). OFHC Cu is electrolytically refined to reduce oxygen level to less than 0.001 %, at the same time, reduce the impurity level which caused background to the radiation detection. The Cu blocks were made into zig-zag shape for the same reason to minimize external radiation. Before assembly, each Cu block has surface refinement process and wiped with ethanol to avoid dust. The 3rd layer Cu shield is 50 mm thick. In Tantalum Phase II measurement, additional inner Cu were added to fill up the remained empty space in the chamber, as shown in Figure 2.9.

With the full shield, the event rate was around 750 events/day in the energy region of 40 keV to 1540 keV. The background studies of shielding, detector and sample will be discussed in Chapter 4.
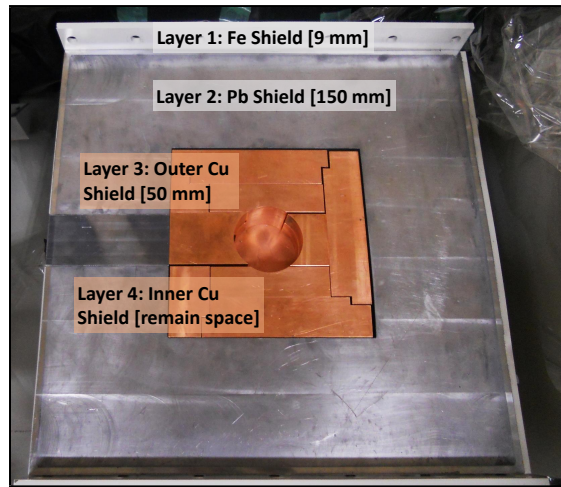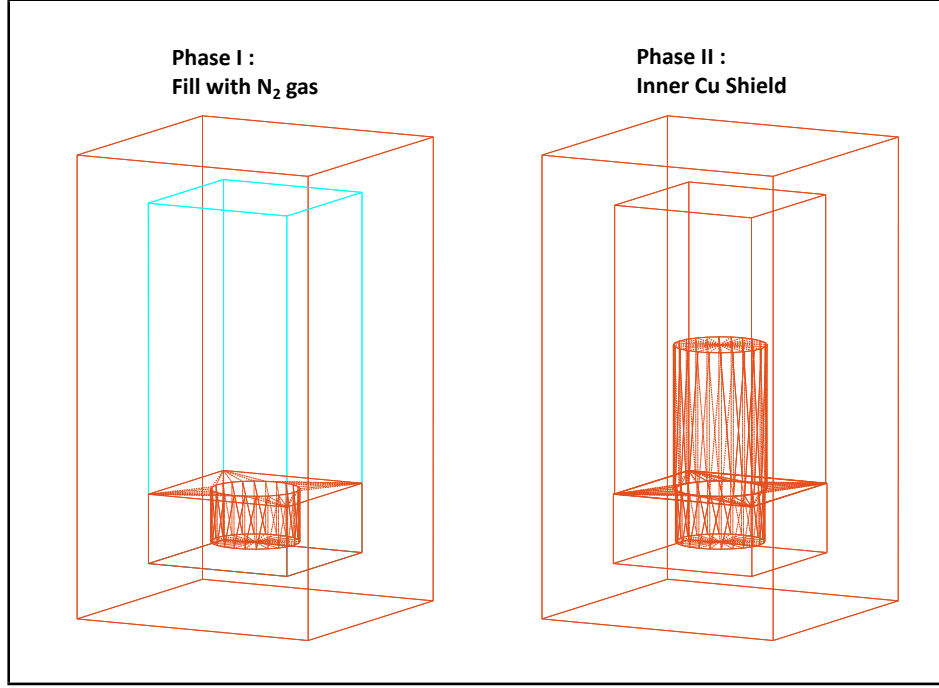
Figure 2.9: The Cu shield configuration designed for Phase I and Phase II measurements. (left) For Phase I, the inner space between outer Cu shield was filled with N_2 gas, lower part of the HPGe detector was covered with Cu shield. (right) For Phase II, the inner space was fully covered with inner Cu shield, the cylindrical space in the middle was exactly fit for detector and tantalum sample.

2.3.5 Environment Monitoring System

The environment inside the Back Experimental Room of CANDLES is monitored all days by sensors or network camera. This including room temperature, humidity, atmospheric pressure, radon concentration and oxygen concentration. Environment information is transmitted by external network connection as mentioned in Section 2.1. The temperature was maintained at 17^oc and humidity was around 40 %.

Radon concentration Radon gas is one of the major background source at underground facilities. Its concentration is a few orders magnitude higher at closed underground as compared to open ground surface because the space is surrounded with rocks that contain a lot of natural radioactivity. The radon concentration is varies with local geological condition, ventilation speed of air, and seasonal changes. The average radon concentration at Back Experimental Room of CANDLES was around 80 Bqm^{-3} (Figure 2.10). It was monitored by radon detector of SK Radon Group [33] in May 2016, during the data taking period of Tantalum Phase II. The data was taken with 10 minutes interval. Result shown a time variation of radon concentration from 10 Bqm^{-3} to 180 Bqm^{-3}, with average of 80 Bqm^{-3}.
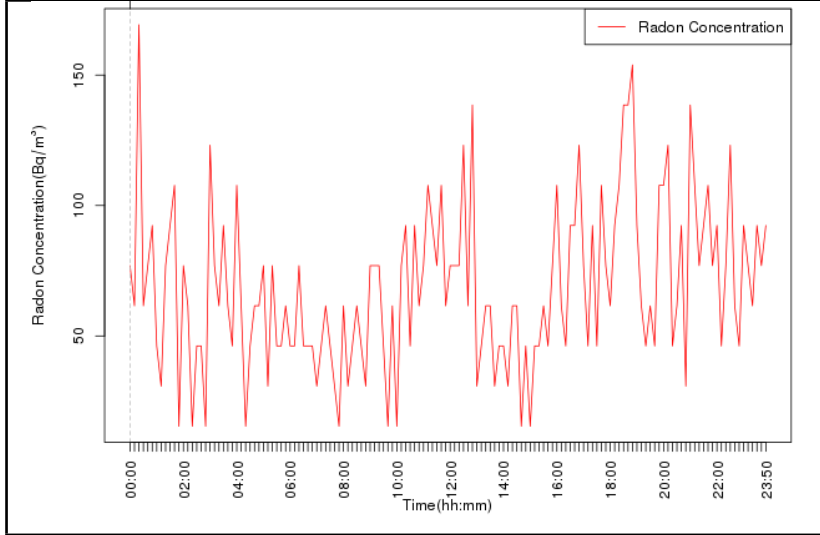
19

Figure 2.10: One day monitoring of radon concentration at Back Experimental Room of CANDLES with respect to time. The radon detection system is run by SK Radon Group [33].

2.4 Data Acquisition System (DAQ)

The DAQ of the detector is made up of preamplifier (mentioned in previous section), Digital Signal Processor (DSP), and computer that installed with the software of DSP. The schematic diagram of the DAQ system is indicated with thick boxes in Figure 2.1. Data were copied and stored in three different servers; on-site computer, research center server near the underground observatory and far distance research center server. All data can be retrieved remotely by external network.

2.4.1 Digital Signal Processor (DSP)

The main electronic system that required in γ-ray spectrometry is contained in the DSP (Model APU8002), produced by Techno AP [34]. The DSP is a non-NIM system which whole module is within a single "black box". Signal amplification, pulse shaping, ADC, pole-zero cancellation, FPGA and digital pulse processing functions were provided. The DSP is responsible to collect the detector signal from preamplifier, amplify the signal, convert to digital signal, pulse shaping, counting, convert output to analog signal for oscilloscope view, and finally transfer output in binary form to external hard disk for memory storage.

Figure 2.11: Photographic image of DSP (Model APU8002, Techno AP [34])

Hardware The circuit diagram of DSP is shown in Figure 2.12. Specifications of the hardware is listed in Table 2.1.

20

Table 2.1: DSP APU8002 Specification [35]

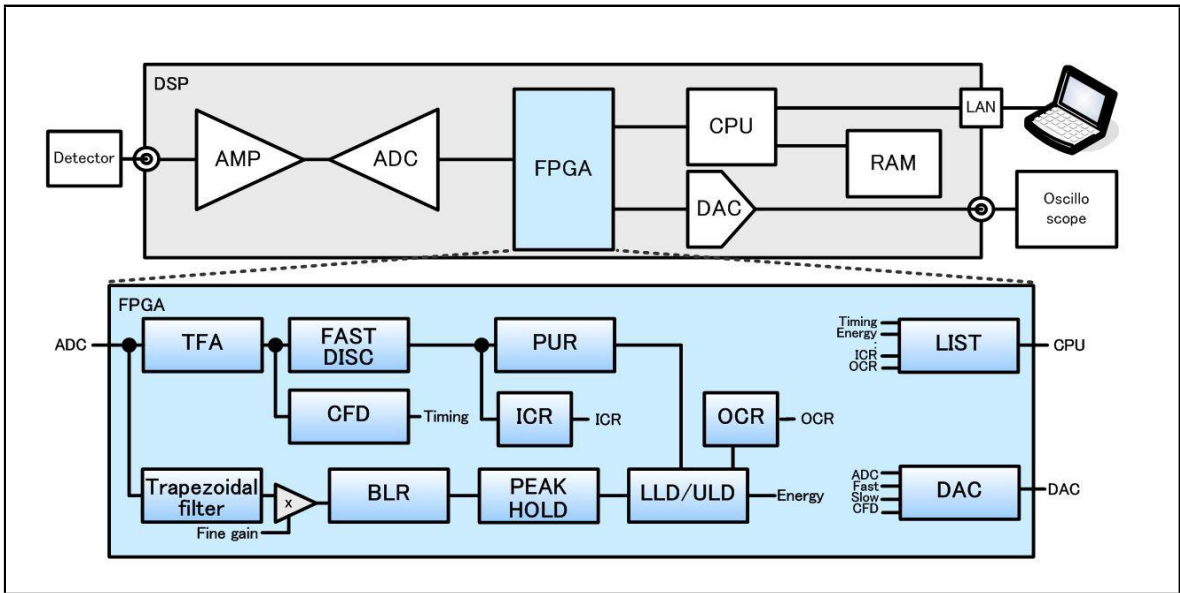| Specification	Capability
Input channel	2 CH
Energy resolution	1.7 keV at 1332 keV
Time resolution	0.625 ns (minimum unit)
Throughput rate	100 kcps
ADC sampling rate	100 MHz
Resolution	14 bit
Operation mode	Histogram, list or waveform
Function	Amplifier, Timing Filter Amplifier, CFD, DAC

Figure 2.12: DSP APU8002 circuit diagram [35]

Software   DSP setting is controlled by software installed in computer. The version of DSP software is DSP MCA 2.11.0, provided by Techno AP [36]. It has been customized for low count rate detection, which capable to recode single event with pulse shape and maximum 780 hours of measurement time. Trapezoidal filter is used for the pulse shaping. The parameters that can be adjusted including ADC gain, pole zero, trigger threshold, pulse rise time, flat top time, etc. The DSP setting is essential for shaping the signal from HPGe detector, which affects the energy resolution of the γ spectrum. The waveform output from DSP is recorded in binary format. Each event size is 300 byte, which contained information of timing, energy and rise wave form (64 points, resolution of 2 ns). To convert the binary file to ROOT file [37], a DSP analyzer was developed to abstract information from the raw data to branches of ROOT file. The data processing will be described further in chapter 3.

2.5   Tantalum Sample

The tantalum sample used in this experiment was produced by Nilaco Corporation with natural abundance. As mentioned in chapter 1, tantalum consist of 99.98% of ^{181}Ta and 0.012% of ^{180m}Ta. The tantalum sample was assembled by 6 tantalum plates, two round plate of 1 mm thick and four curved plate of 0.5 mm. After assembly, the tantalum cylinder sample was 100 mm in height and 88 mm in diameter as shown in Figure 2.13. For Phase II, the diameter was reduced to 87.3 mm to reduce space between sample and detector. The thickness of top round plate and side cylinder was 2.0 mm and 1.5 mm, respectively.

Tantalum is also a common material to detect neutron source due to it properties of neutron activation. The sample used was produced on ground, which certain percentage of radioactive ^{182}Ta was present as internal background of the sample. The decay of ^{182}Ta was observed in long term measurement and the result will be discussed in chapter 4. Since Tantalum Phase I, the sample has been stored at underground for 3.5 years. As a preparation for Phase II, it was moved on ground for cleaning procedure for a short term and transfer back to underground afterwards.
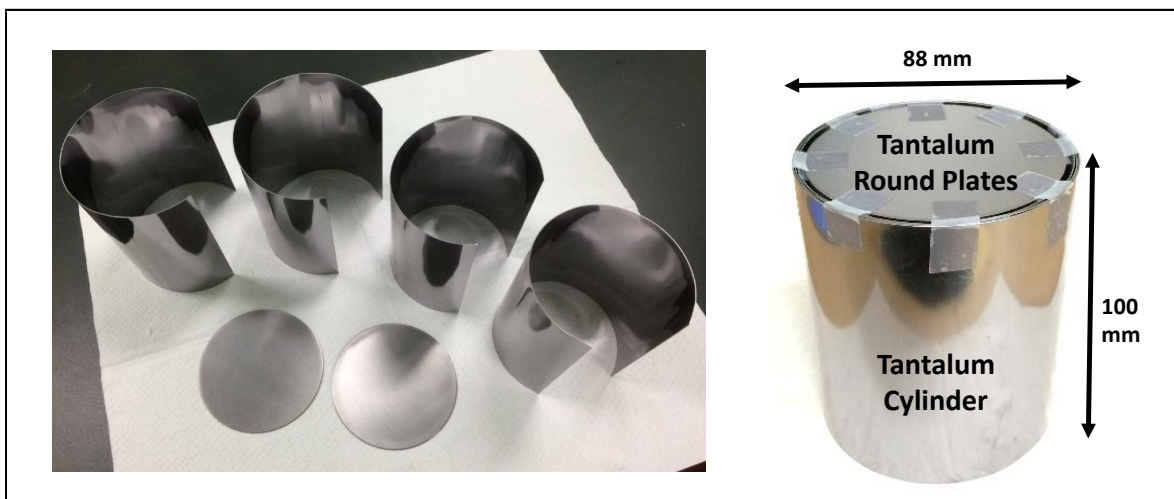
Figure 2.13: Photographic images of tantalum. (left) Segmentation of tantalum sample. (Right) Tantalum cylinder sample after assembly, with two round plates on top and three layers of cylindrical surface.

2.5.1   Acid Cleaning Procedure

In Phase 1, background peak of ^{137}Cs was found and deduced as the contribution from surface contamination of the sample. The tantalum cylinder was disassembled and sent to Minamide-Rikasyokai Corporation for proper metal cleaning procedure. The common surface cleaning process for tantalum metal is acid cleaning. The sample was returned to Kamioka Underground Observatory after the cleaning. As mentioned before, the ^{182}Ta will be created by cosmos ray on ground, hence the sample was kept at underground for 9 months before starting the Tantalum Phase II measurement.

The Acid cleaning procedure for tantalum sample:

1. Immersed in nitric acid for 5 minutes

2. Rinsed with pure water

3. Dried in clean room class 10000 for 15 minutes

4. Confirmed cleanliness by checking the sample surface

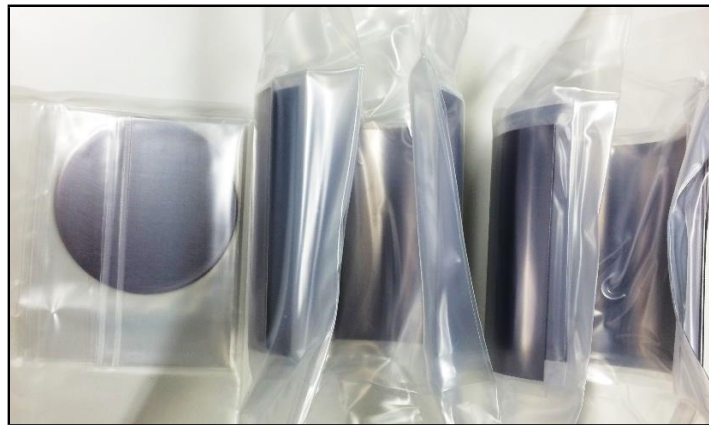5. Packed with double-layer vacuum bag inside the clean room

Figure 2.14: Vacuum packing of tantalum sample after acid cleaning procedure

Total mass   After cleaning process, the total mass of tantalum sample has reduced 1.6 % due to the acid cleaning on tantalum plate surface. The total mass of tantalum sample used in Phase I and Phase II is listed in Table 2.2.

Table 2.2: Total mass of tantalum sample

Tantalum	Phase I	Phase II
Total mass (g)	863.0 ± 0.1	848.8 ± 0.1

2.5.2   Configuration in Phase I and Phase II

The tantalum material used in Phase I and Phase II was the same sample. However, there were several modification in term of configuration. Note that in Phase II, there are no space between the tantalum cylinder and the HPGe detector cylinder surface. The space within shields which was filled with N_2 gas was now covered with inner Cu shield. The schematic drawings and photographic images of experiment set up for Tantalum Phase I and Phase II measurements are presented in Figure 2.15.
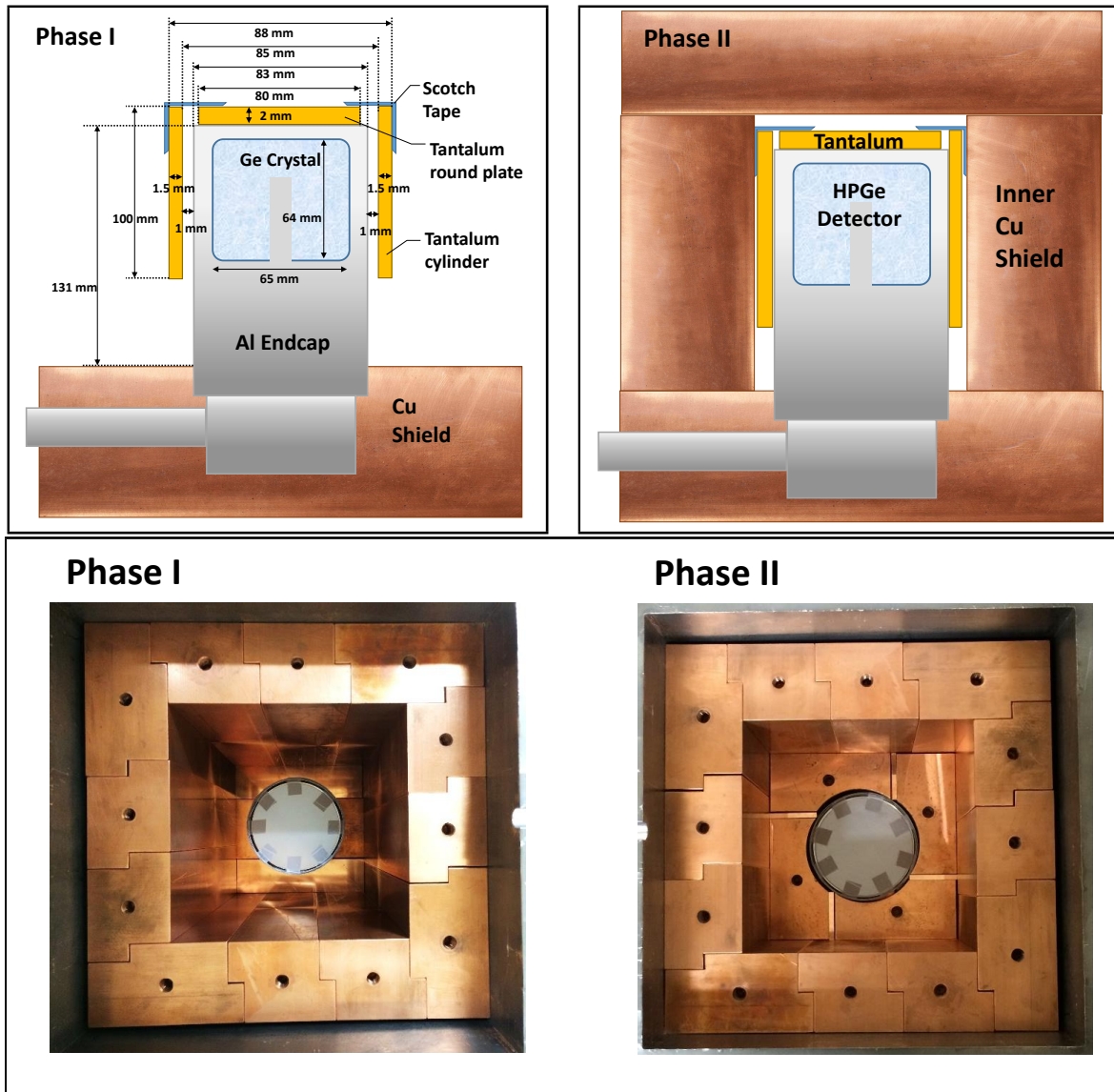
Figure 2.15: Schematic drawing of tantalum sample configurations in Phase I (top left) and Phase II (top right). Photographic images of the tantalum sample placed inside the HPGe detector is shown in the lower figure. Note that top Cu shield was not inserted when taking the photos.

Data Processing

3.1 Long-term Data Acquisition

First, the raw data from γ-ray spectrometer were transfer to storage server. Then, the binary file was converted to ROOT file by DSP analyzer. For 3rd step, the data were underwent pre-analysis to reject noise events. In 4th step, each event will be energy calibrated by using the natural radioactivity peaks presented in the spectrum. The final γ-ray spectrum was then used for data analysis. Data analysis framework used for data analysis and file format was ROOT [37], developed by CERN.

Since the interested target is extremely long half-life isomer, long-term measurement is required in this case. Three types of runs were taken; tantalum physics run, calibration run and background run. Here "run" means a set of data taken by detector for a certain period. Tantalum physics run was taken with tantalum sample, which is the main component to study the ^{180m}Ta decay and consist of long-term measurement (months) without any any chance on the detector system.

Calibration run was refer to measurement taken with γ sources that energy peaks was known. The measurement time of this run was comparatively short and taken in between of the long-term tantalum physics run. Moreover, the calibration run was used for efficiency calibration and verification for simulation model. Background run was taken without any sample inside the detector chamber and maintain the same condition (shielding, DAQ parameter setting, detector performance) as tantalum physics run. The detail of these three types of run will be discussed in the following sections.

3.2 Data Format of Time-stamp Rise Wave Event

Using the DSP, the rise wave (rising part) of each event can be recorded. The pulse shape is defined as 0 ns to 640 ns of pulse when start to rise from pedestal. The format of the DSP data is binary, which contain the information of timing (time of the event happen), pulse shape (0-640 ns of the rising part), energy (obtained by integration of 12 μs of the event from start channel). Data were copied and transfered to distance servers at research center outside of Kamioka Observatory and RCNP server of Osaka University.

3.3   Tantalum Physics Runs

From year 2013 to 2014, 237 physics runs were collected from tantalum measurement, which is classified as Phase I data. After improved the detector system and tantalum sample, 32 physics run was collected as the Phase II data. The livetime of both phases is summarized in Table 3.1. The event rate of the all physics run in Phase I & Phase II were presented in Figure 3.1. With background reduction by adding inner Cu shield, event rate in Phase II has reduced 46 % from average 50 events/hour (Phase I) to average 27 events/hour.

Table 3.1: Tantalum physics runs

Tantalum	Phase I	Phase II	Total
Physics Runs	237	32	269
Livetime (days)	300.6	57.6	358.2
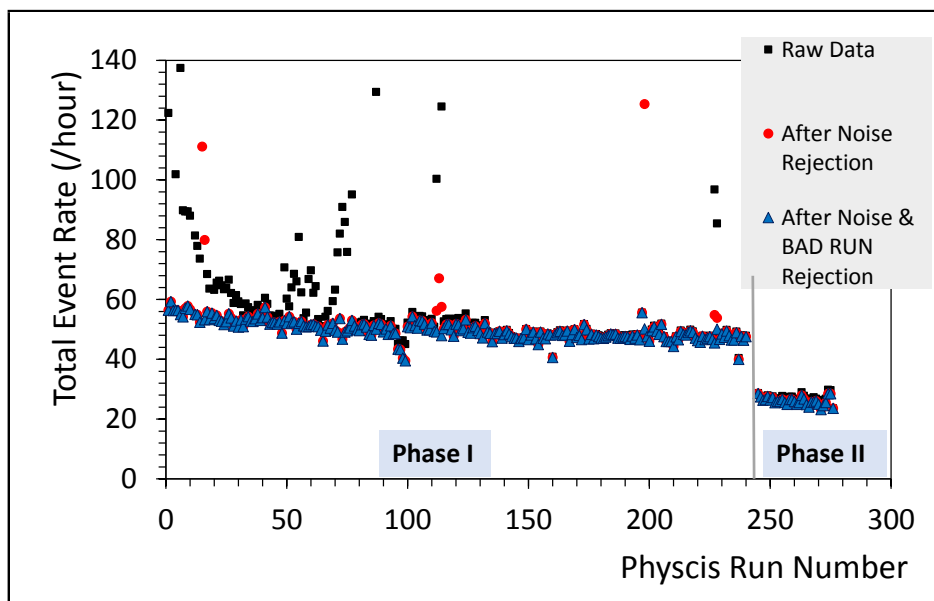
Figure 3.1: Event Rate of All Tantalum Physics Runs in Phase I and Phase II

Even though the measurement was long-term, a new run was taken after 1 2 days and the previous run was stopped and transfer for storage. The purpose of this procedure was to keep monitoring the data taking, check the event rate and identify any possible fault during measurement. Since the ROI of ^{180m}Ta is 90 keV to 360 keV, the energy range of the measurement was set between 40 keV to 1540 keV. Lower energy threshold was set at 40 keV because this value is the accepted energy range of typical standard electrode coaxial Ge detector. High energy threshold was set at 1540 keV to include the 1460.8 keV (^{40}K) peak which used for gain monitoring of every runs.

3.3.1 Monitoring of Tantalum Physics Run

To make sure the data taking is work under normal condition, pre-analysis for each run was established after taken the raw data, before going to the second stage of the analysis. Figure 3.2 shown a typical pre-analysis for tantalum physics run. Pre-analysis checked the gamma-ray spectrum, event rate, maximum pulse height correspond to energy (channel at this stage) and pulse shape of event correspond to measurement time. Gamma-ray spectrum was presented with total event correspond to each channel (energy of the event).

Background peaks of 185.7 keV (^{235}U) and 1460.8 keV (^{40}K) were identified and fitted to check the gain change. These two peaks were chosen because its highest intensity and located at lower and higher ends of the energy range. Analysis of gain stability using these two peaks will be discussed in later Section 3.4.2.3.The peak position, FWHM, total event of the background peaks were analysed in this stage. Event rate check (15 minutes interval) is more straight forward to locate if any trouble occured.
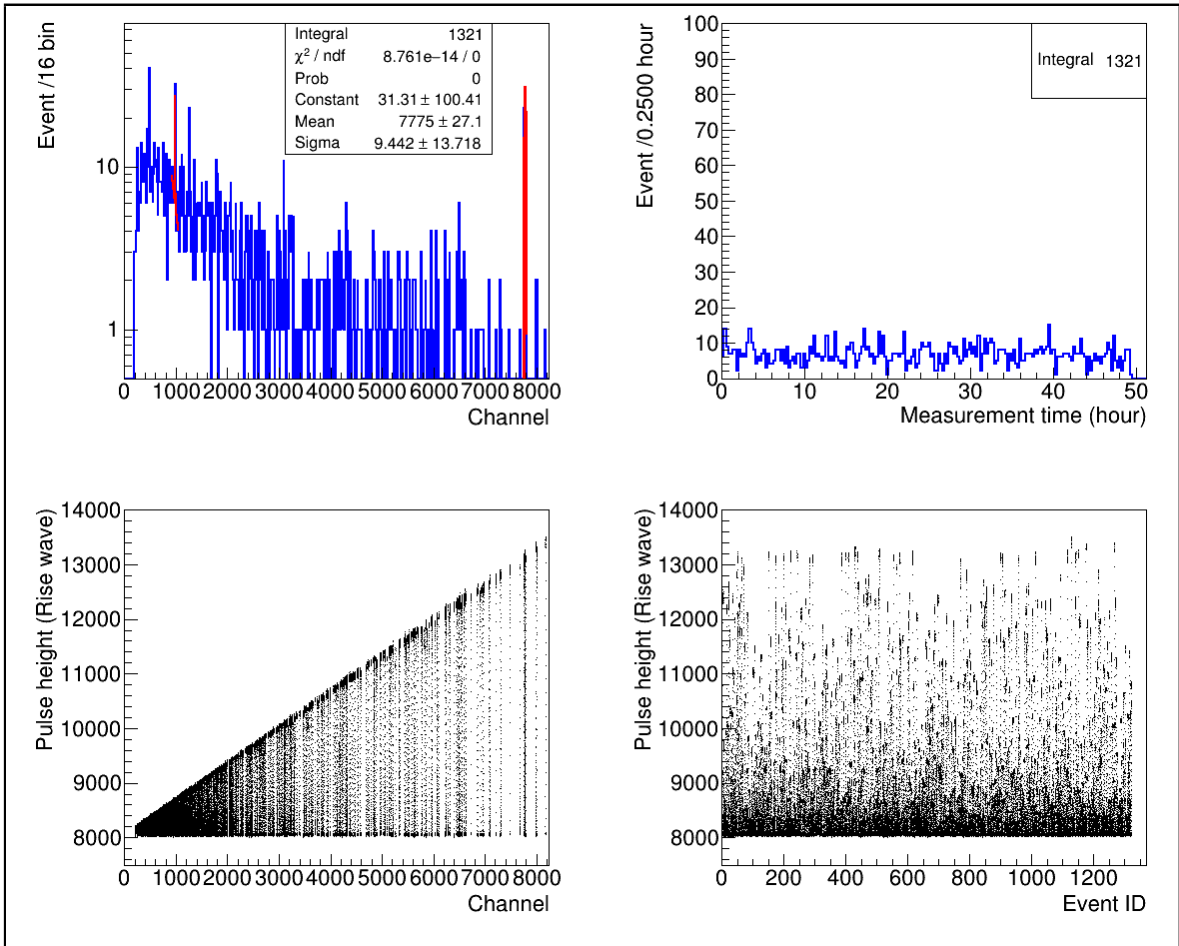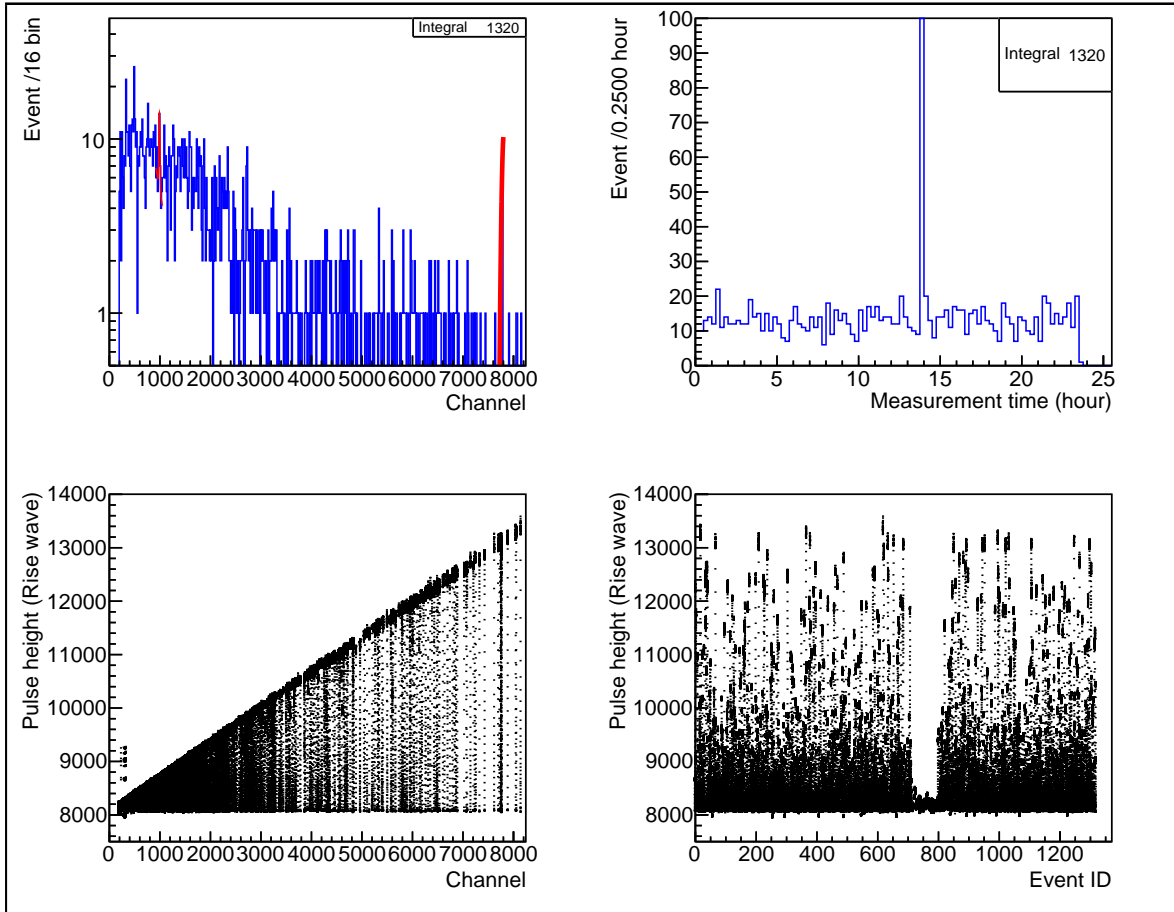

Figure 3.2: Pre-analysis and checking of a typical normal tantalum physics run. Energy spectrum (top left), event rate (top right), pulse height corresponds to channel/energy (bottom left) and pulse height corresponds to Event ID/time (bottom right) were plotted and checked during pre-analysis process.

Noise rejection As an example of abnormal tantalum physics run, with the same pre-analysis method, a physics run (Figure 3.3) plot of event rate indicated an extremely high event rate at 14th hours of measurement. The pulse height corresponds to channel plot shown some events with pulse height much higher than average, at channel 200 to 400. Moreover, the pulse height corresponds to Event ID plot also shown abnormal pulse height at Event No. 700 to 800. Further investigation revealed that these abnormal events happen at the same time during LN_2 filling, when vibration of the dewar produced a lot of microphonics noise events. This type of noise event can be rejected by pulse shape analysis type-A, which will be discussed in Section 5.1.1, or increase the timing trigger threshold of the DSP.

Monitoring all tantalum physics runs is very important for long-term measurement, as any possible change may happen around the detector system. Pre-analysis is useful to notice unexpected problem, change of gain, condition of detector system. When something abnormal happen, necessary action can be taken immediately. This is also one of the main reasons to renew physics run every one or two days. If any specific run was abnormal, it can be omitted without losing great portion of the data.

Figure 3.3: Pre-analysis and checking of an abnormal tantalum physics run. Energy spectrum (top left), event rate (top right), pulse height corresponds to channel/energy (bottom left) and pulse height corresponds to Event ID/time (bottom right) were indicated a short period of noise events with extremely high count rate.

3.3.2 Exclusion of Bad Run

From the monitoring of each physics run, abnormal runs has been identified. These runs was either rejected or split for certain time period. The following lists shown the reasons of physics run which need additional filtering.

1. Neutron source induced background

2. Radon gas effect after opened the detector chamber

3. DSP trouble during data taking

4. Low statistic run

For example, run that taken with DAQ trouble (no data taken, unstable of DAQ), high count rate due to radon gas effect (after opened the detector chamber) and due to neutron source passed by the detector system. Figure 3.4 shown a run that was split and rejected certain period of the whole run due to radon effect at the beginning of data taking. In this case, the total live time will be subtracted for the period when the event was rejected.
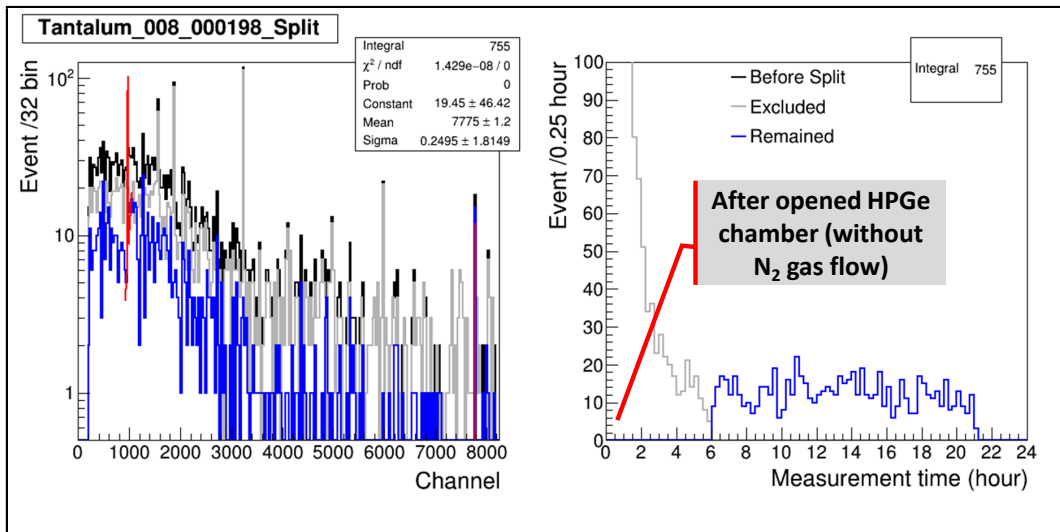
Figure 3.4: Energy spectrum (left) and event rate (right) of a physics run that has high radon effect after HPGe detector chamber has been opened. Raw data (black line), excluded bad event (grey line) and remained good event (blue line) were plotted.

Neutron effect Regarding the neutron source effect, the detector system is located at one of the experimental room of CANDLES, where neutron source calibration is required. When the neutron source (^{252}Cf) passed through the detector system, the source will induce (n,γ) reaction [19] and resulted in background to the measurement of HPGe detector. Figure 3.5 shown a physics run's event rate increased after neutron source passed through the detector system for a short period (less than 15 minutes). In order to ensure the same measurement condition for all physics run, the abnormal period was split and considered as bad run.
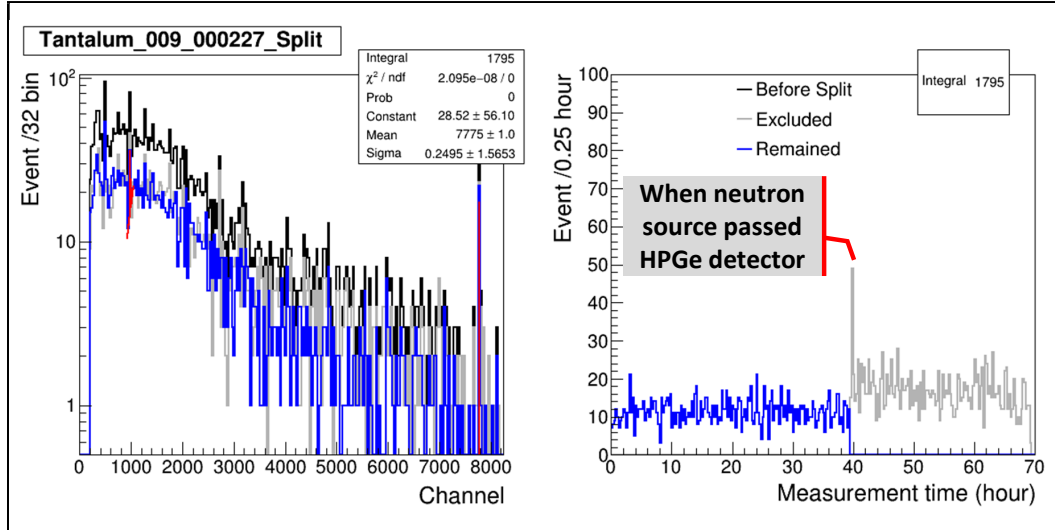
Figure 3.5: Energy spectrum (left) and event rate (right) of a physics run that affected by neutron source passing the HPGe detector. Raw data (black line), excluded bad event (grey line) and remained good event (blue line) were plotted.

3.4 Energy Calibration Run

During calibration run, the top shield of detector was opened (Figure 2.6) and calibration γ source was placed a certain distance from detector's endcap as shown in Figure 3.6. Energy calibration of HPGe detectorby γ sources was performed every one to two months. In between, the detector chamber was closed and continue taking long-term data. Calibration run is important for DSP parameter setting, energy resolution calibration, efficiency calibration and verification for simulation model.
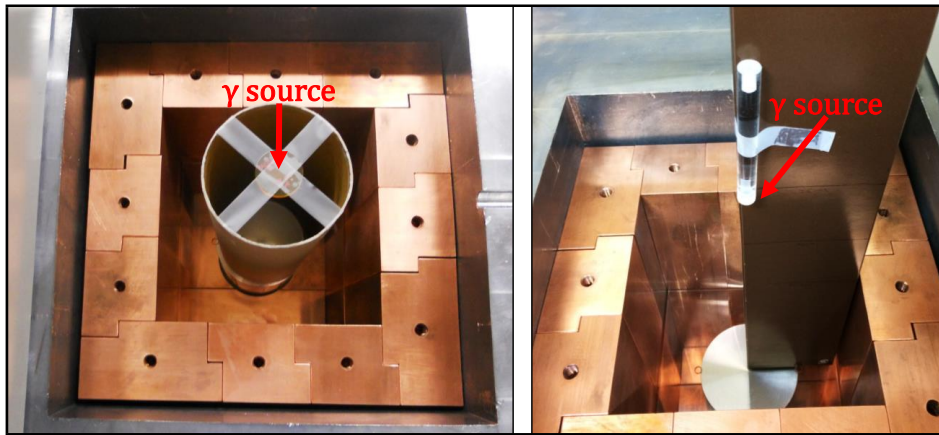
Figure 3.6: Photographic images of calibration run from top of HPGe detector. (left) Regular energy calibration run with fixed distance of 250 mm, γ source was placed at the center of paper cylinder. (right) Efficiency calibration run with variable distance from 0 mm to 250 mm, γ source was placed on a scaled paper box with scotch tape.

Without collimator   To simulate the detection efficiency of tantalum sample, calibration measurement was conducted by placing the γ source close to the detector on

acrylic cap, without any collimator (Figure 3.7). The acrylic cap can be turned freely, which is convenient to scan the detector in 360° at the same distance from top surface. In case of top surface scanning, the γ source will be placed on top of the acrylic cap.
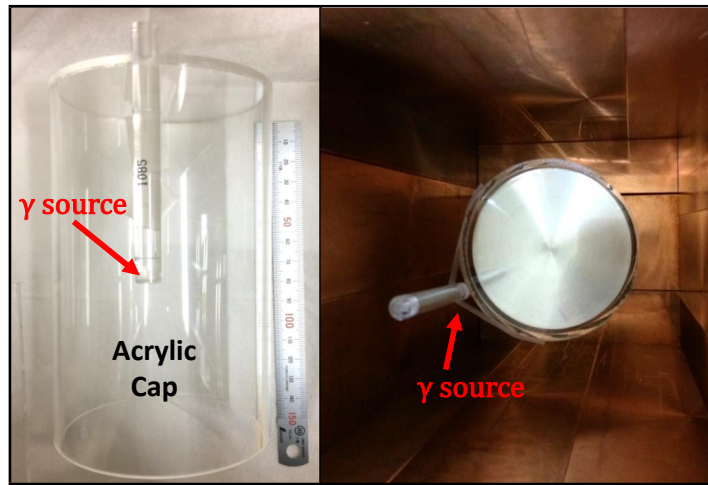
Figure 3.7: Photographic images of surface scanning without collimator. (left) γ source was placed on a acrylic cap, which distance from top surface was measured. (right) Experiment set up to scan lateral surface of HPGe detector with γ source on the acrylic cap.

With Collimator   Calibration run was also utilized to scan the top round surface and side lateral surface of the HPGe detector. The experiment set up is shown in Figure 3.8. The collimator used in this experiment was 25 mm thick lead block with 3 mm center hole for γ-rays to collimate the γ-rays emitted by radiation sources. The result of top surface scanning using lead collimator was shown in Section 3.4.2.4. This result is an important proof of the detector size during construction of detector geometry by simulation.
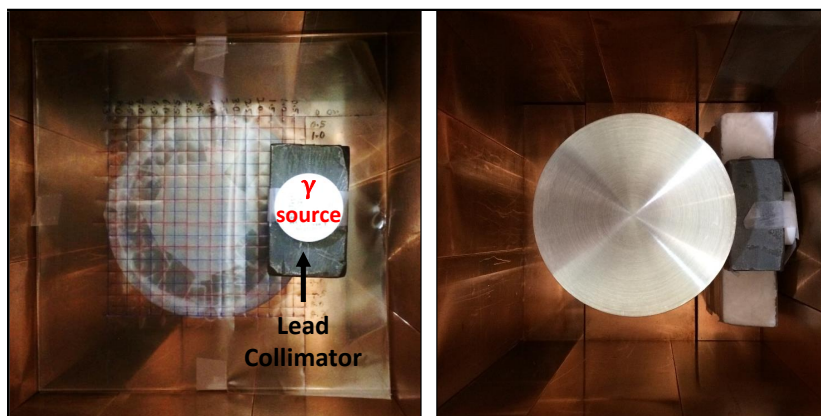
Figure 3.8: Photographic images of surface scanning with collimator. (left) γ source at the middle of 25 mm thick lead collimator and scanned through the top surface axis of HPGe detector. (right) Lateral surface scanning with lead collimator.

3.4.1 Calibration Sources

All calibration sources were borrowed from Kamioka Underground Observatory. It was kept in a safe at SuperKamiokande Experimental Hall, the geometry of γ source is point type where the source is shield with acrylic in coin or rod shape. Table 3.2 listed the γ sources that had been used for the calibration runs in this research.

Table 3.2: Gamma Sources Used for Energy Calibration

Label No.	Radionuclide	Half-life (yr)	Radioactivity (kBq)	Uncertainty (%)	Measurement Date	Shape
4	^{60}Co	5.27	30.6	4.0	30/12/2016	coin
5	^{137}Cs	30.08	253.6	4.0	30/12/2016	coin
20	^{133}Ba	10.55	12.4	1.5	30/12/2016	coin
25	^{137}Cs	30.08	13.3	2.0	30/12/2016	rod
26	^{60}Co	5.27	2.3	2.0	30/12/2016	rod
27	^{133}Ba	10.55	5.9	1.5	30/12/2016	rod
28	^{241}Am	432.60	3.7	6.0	30/12/2016	coin

3.4.2 Detector Performance

3.4.2.1 Energy Calibration by γ sources

Two types of energy calibration methods were used, calibration by using γ sources and calibration by background peaks that exist in physics run spectrum. Since tantalum measurement is long-term data, background peaks calibration method is more suitable to match the gain change of physics run. As for short-term measurement, γ sources were used for energy calibration. Figure 3.9 shown the energy calibration curve and linearity by using γ sources of ^{241}Am, ^{133}Ba, ^{60}Co and ^{137}Cs. The linearity of energy calibration was $\pm$ 0.25 keV.
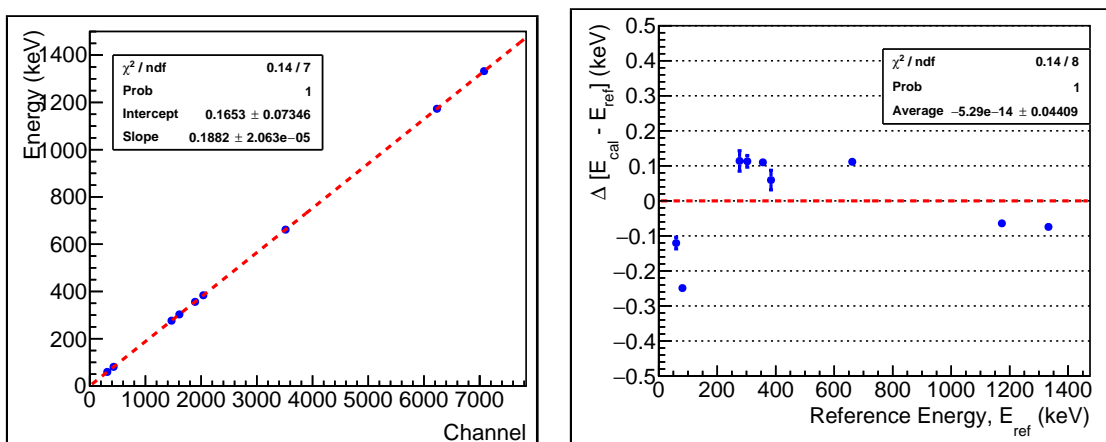
Figure 3.9: Energy calibration curve (left) and linearity (right) by γ sources

Energy Resolution The energy resolution of HPGe detector was checked by calibration sources in monthly basics during the tantalum measurement. Higher energy resolution will give a better background level since it can suppress the background event to be consider for $T_{1/2}$ limit calculation.

Energy resolution is defined as Full Width Half Maximum (FWHM) of a certain Full Energy Peak (FEP). As shown in Figure 3.10, FWHM of HPGe detectorat 1332 MeV (^{60}Co) was 2.0 keV, with fluctuation of $\pm$ 0.2 keV over few years calibration runs.
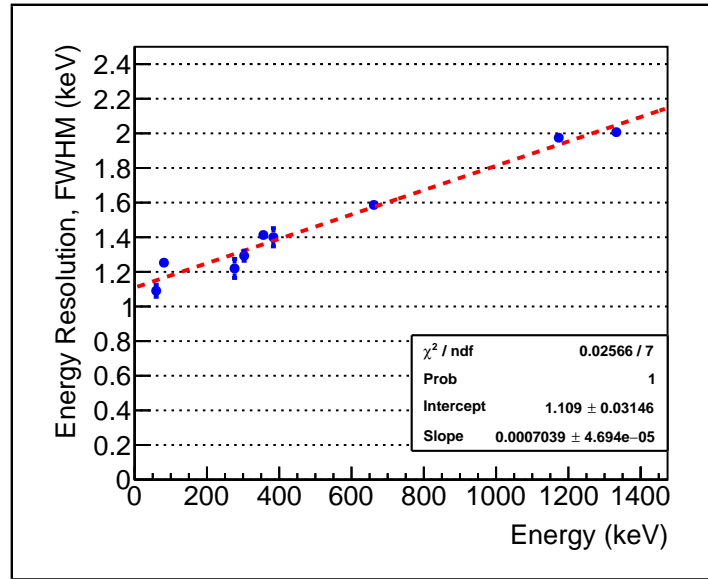
Figure 3.10: Energy resolution curve of HPGe detector

3.4.2.2 Energy Calibration by Background Peaks

Due to the long-term measurement of tantalum sample, background peaks can be observed in the spectrum. These peaks were utilized for the energy calibration, gain check and pulse shape analysis of this research. The peaks selected in tantalum spectrum is shown in Figure 3.11. The energy calibration curve and linearity is shown in Figure 3.12, where linearity was within 0.15 keV.
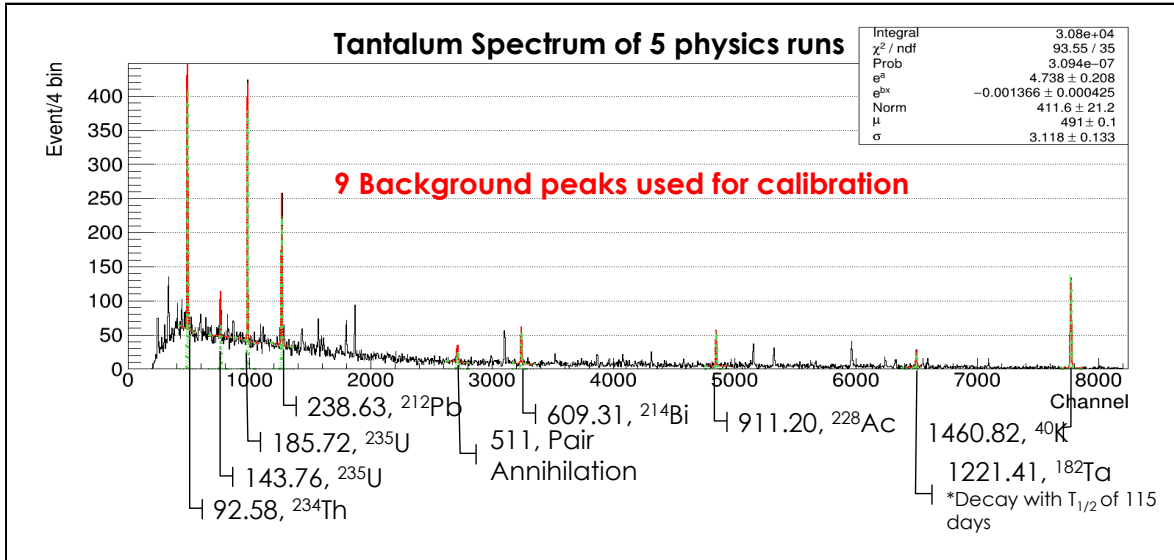
Figure 3.11: Background peaks selected for energy calibration in tantalum physics run
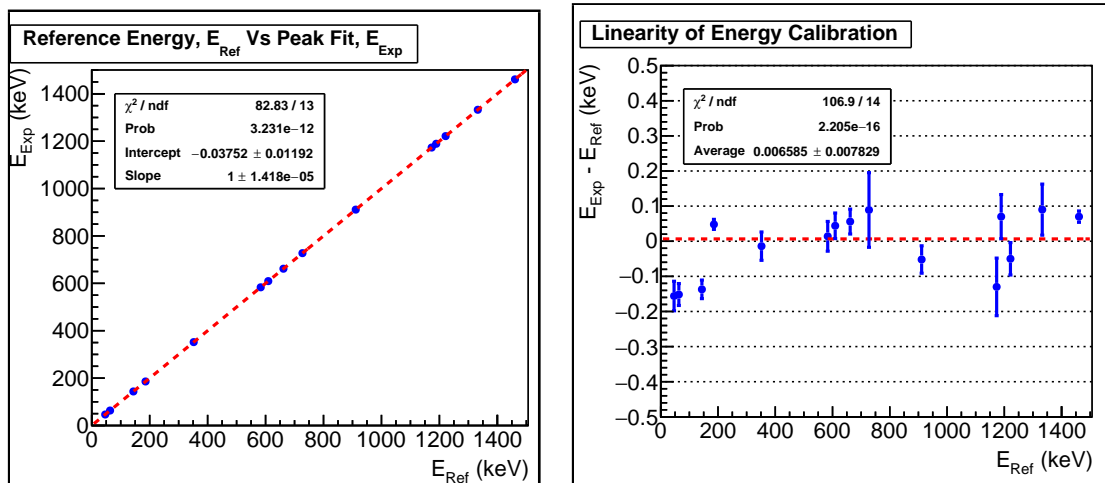
Figure 3.12: Energy calibration curve (left) and linearity (right) by background peaks

3.4.2.3 Gain Stability

Gain stability is checked by using the natural radioactivity background peaks that observed in physics run. In the coming chapter 4, detailed background peaks from different origins that commonly detected by HPGe detectorwill be discussed. In Figure 3.13, 185.7 keV peak from ^{235}U and 1460.8 keV peak from ^{40}K were selected to monitor the stability of gain over every 5 tantalum physics runs.
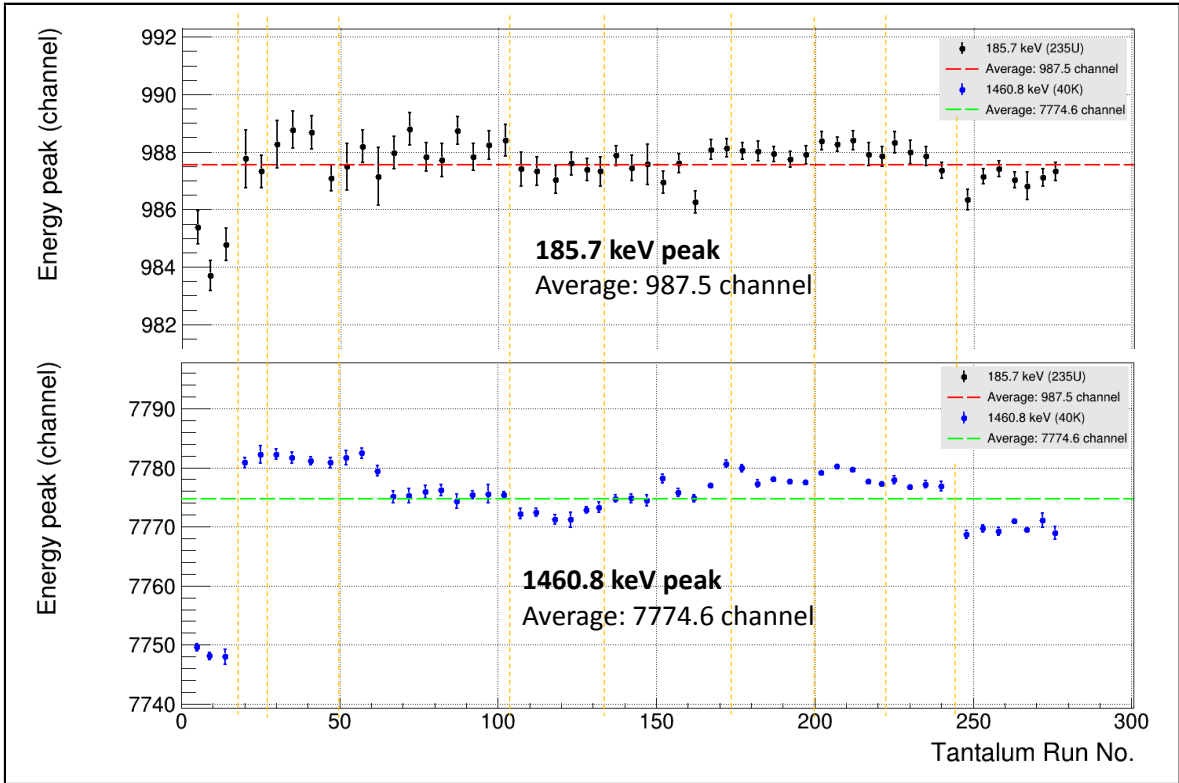
Figure 3.13: Stability of Gain - 186 keV and 1461 keV peaks. Orange color vertical lines indicate separation of physics data sets, where slight change on DAQ or detector setting were made.

3.4.2.4 Detector Surface Scanning

Top surface axis Using calibration run with collimator, the top surface and side lateral surface of HPGe detector were scanned. Figure 3.14 shown the result of top surface scanning with ^{133}Ba, 5 FEP peaks were used to plot the change of event rate as γ beam scanning from one edge to the other edge on the detector's endcap. From the result, the diameter of Ge crystal is determined to be 65 ± 2 mm, which is same as the specification given by manufacturer. In addition, a decrease of event rate is observed at he center of the detector, refer to the highest γ emission probability peak of 356 keV. This valley of low event rate is caused by the center empty core of electrode, less radiation can deposit at this position.
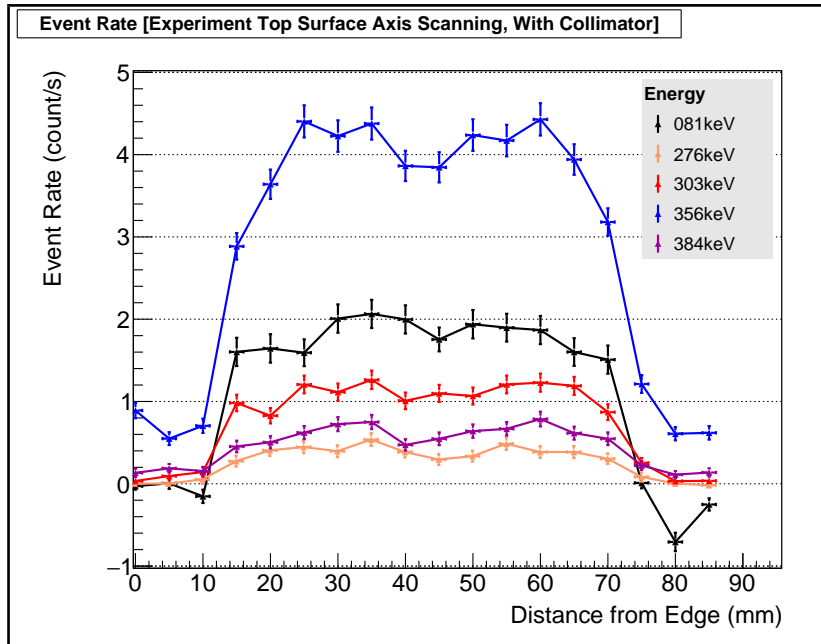
Figure 3.14: Result of top surface scanning with collimator. Total events from 5 energy peaks of ^{133}Ba were plotted.

Side lateral axis The result for side lateral scanning with collimator was shown in Figure 3.15. The length of Ge crystal is deduced to be 65 ± 5 mm (manufacturer's value is 64 mm) and distance of endcap-to-Ge crystal is 5 ± 1 mm, less than 10mm. From the energy peak of 81 keV, two valleys with lower event rate were observed at 30 mm and 50 mm from top surface. This was caused by two thicker side rings attached to the Ge crystal holder, which illustrated in Figure 2.5. Since attenuation probability of low energy γ is high, 81 keV peak is capable to shown the fine detail of inner structure of HPGe detector.

Without collimator Without collimator, the detection efficiency was obtained for lateral surface scan of the detector (Figure 3.16). 356 keV and 384 keV peaks have the same pattern, while 81 keV peak shown position dependence of detection efficiency.
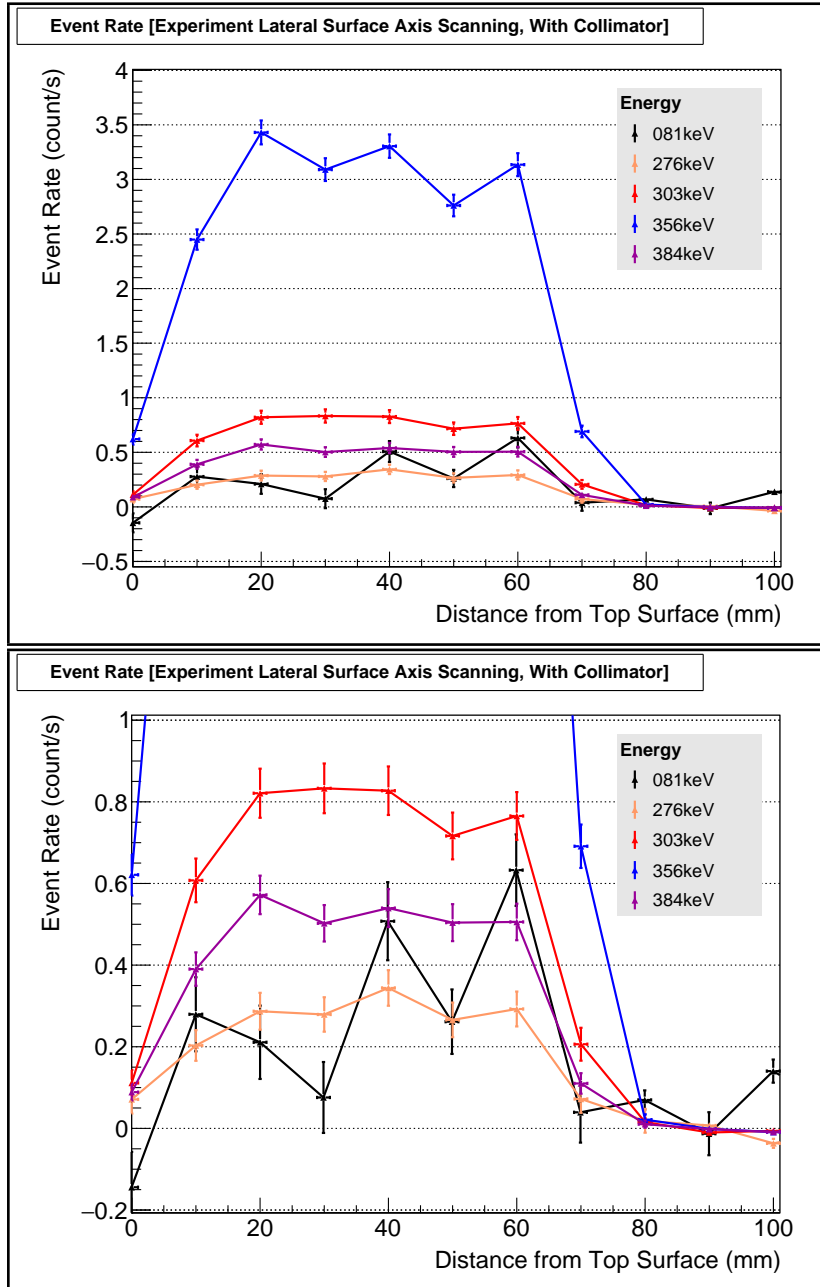
Figure 3.15: (top) Result of Lateral surface scanning with collimator. (below) Enlarge view of energy peaks with lower event rates. The distance in horizontal axis was counted from the edge of top round surface of HPGe detector.
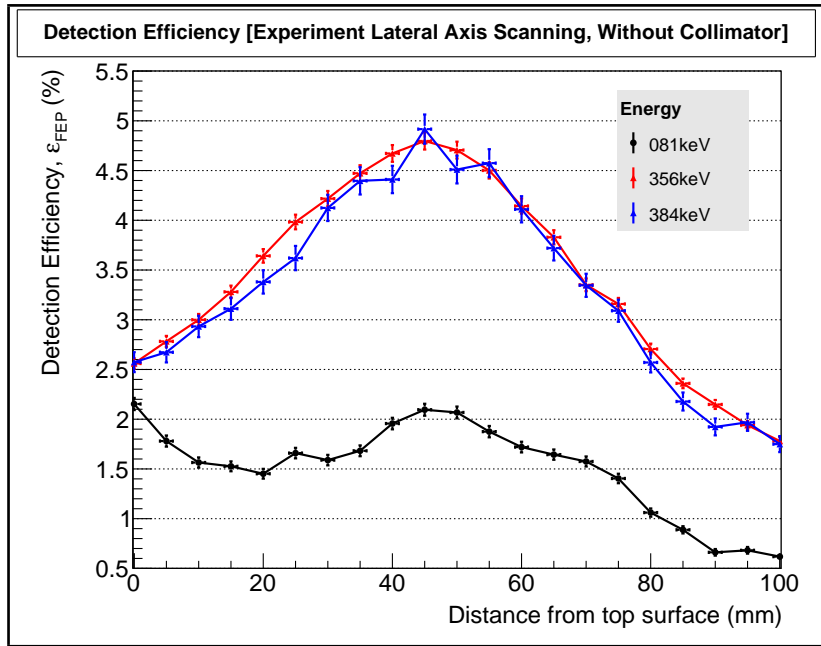
Figure 3.16: Result of lateral surface scanning without collimator.

3.5 Background Run

In order to estimate the background level of the detector system, run was taken in same condition as tantalum physics run, except that tantalum sample was not inserted in the detector chamber, refer as background run. The background runs were taken for one to two weeks, average live time of each run was 1 or 2 days. As mentioned before, the tantalum physics runs were classified into two phases. Thus, the background conditions for these two phases were not the same. In particular, for Phase II, additional inner Cu shields was inserted while Phase I was not. This changes make a great deal in background reduction and will be discussed in Chapter 4. Three sets of background runs was taken to compare the different shield configurations.
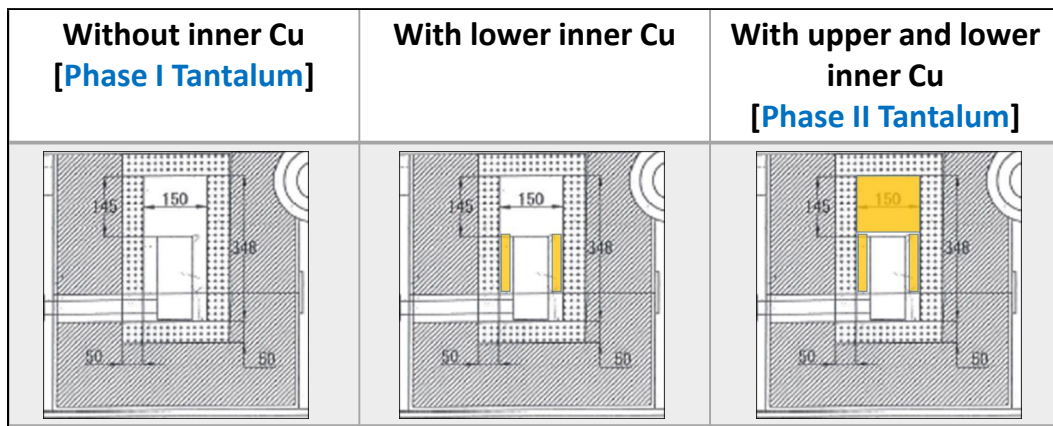
Figure 3.17: Schematic diagram of background runs with different shield configurations. Yellow blocks indicate the additional inner Cu shields

38

Tantalum Spectrum and Background Studies

4.1 Tantalum Spectrum of Phase I and Phase II

Tantalum spectrum obtained from the Phase I and Phase II measurements is presented in Figure 4.1. Background peaks that have been identified were also indicated in the plot. The ROI of ^{180m}Ta is highlighted at the bottom of the figure. From this measurement, no ^{180m}Ta event were confirmed. Hence, lower limit of $T_{1/2}$ will be deduced.

4.2 Background of HPGe Detector

Background spectrum obtained from three different shield configurations was shown in Figure 4.2, for energy region from 40 keV to 750 keV. Most of the background peaks were originated from U-chain, Ac-chain and Th-chain.

4.2.1 Peak Identification

Unlike on ground where radioactivity is high, at underground and effort to provide ultra-low background condition, many low radioactivity nuclide can be detected in the tantalum spectrum. Note that tantalum sample which is a cylinder that cover the whole detector's end-cap. Since the Z value of tantalum is 73, the sample also acts as an effective passive shield for the Ge detector. Therefore, the background level of tantalum spectrum is more than 50 % lower than the background spectrum obtained.
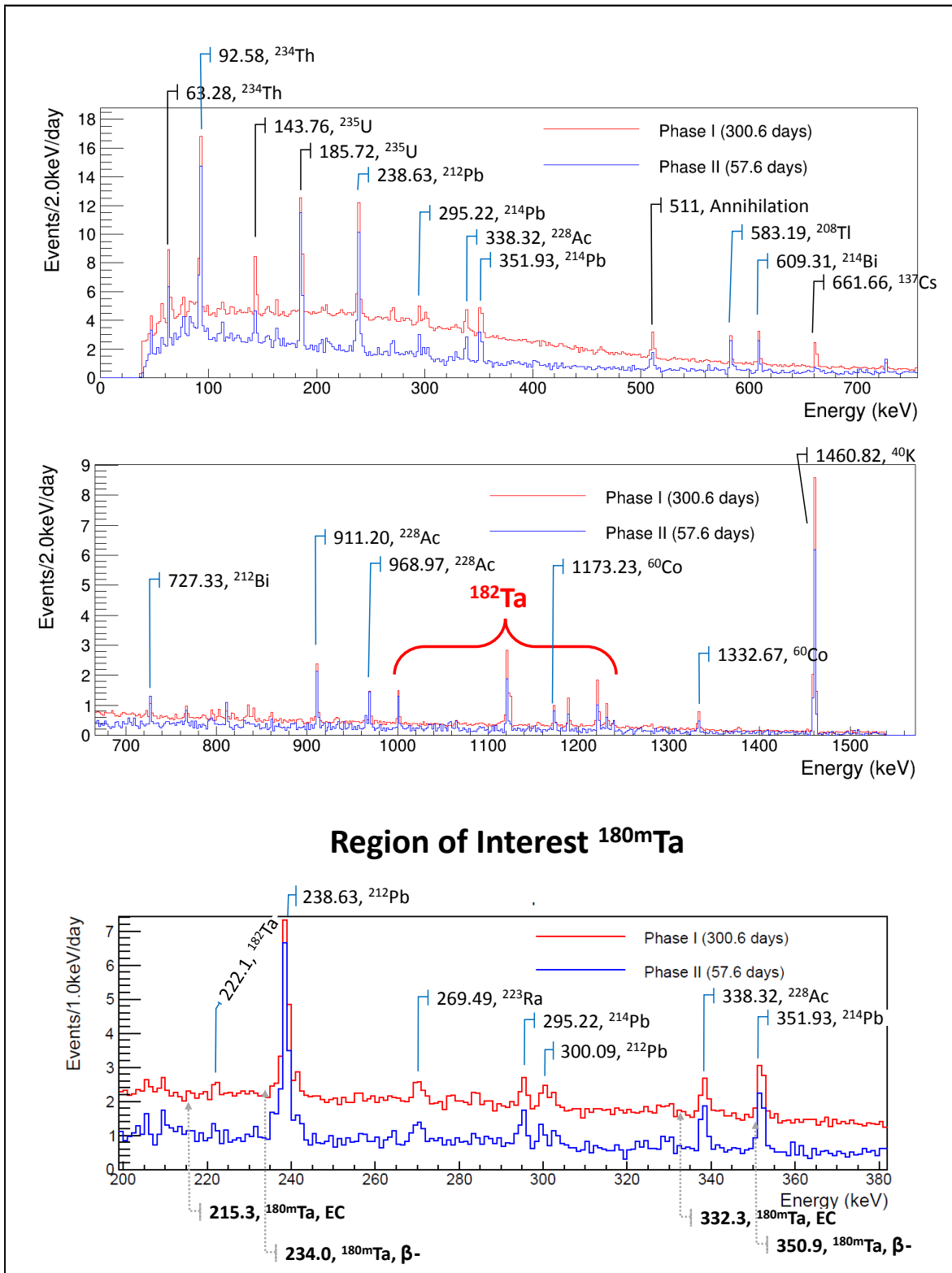
Figure 4.1: Tantalum spectrum of Phase I and Phase II
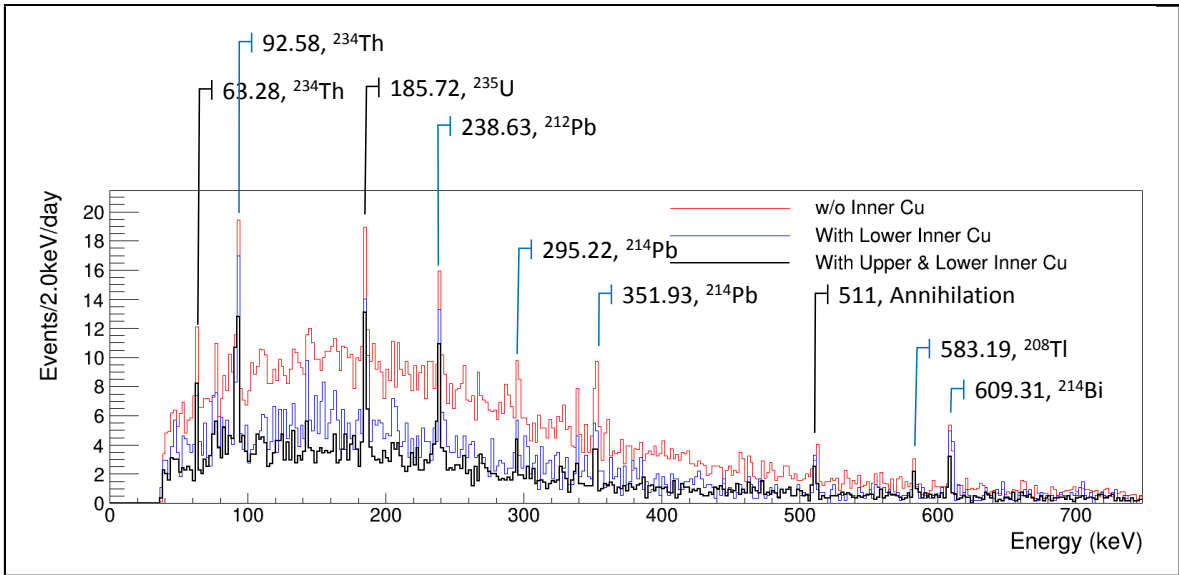
Figure 4.2: Background spectrum of different configurations of inner Cu shield

4.2.2 Origin of Background

Coming from outside the detector system,

1. Muon induced event, 511 keV peak

2. Natural radioactivity [^{40}K, Radon gas, U-chain, Ac-chain]

Within detector system,

3. Surface contamination of tantalum sample, ^{137}Cs

4. Decay of ^{182}Ta isotope

5. Broad Bremsstrahlung radiation from beta decay of ^{210}Bi (lead shield)

6. Compton backscattering event from lead shield

4.2.3 Decay of ^{182}Ta

In the tantalum physics run, energy peaks of ^{182}Ta were present. This is the intrinsic background from tantalum sample. ^{182}Ta was produced by neutron activation of ^{181}Ta on ground. Its Compton continuum has contributed to the background event. From Figure 4.3, the peaks of ^{182}Ta were reduced gradually after 27, 168 and 436 days moved to underground laboratory. Hence, tantalum sample should be stored in underground to reduce this tantalum internal background.
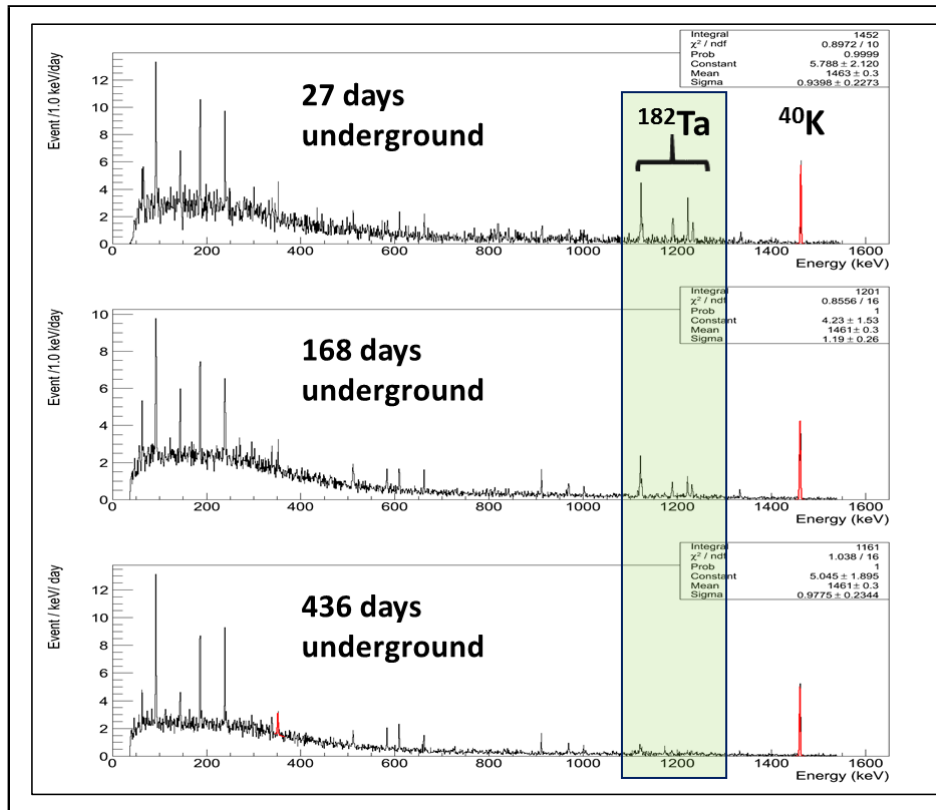
Figure 4.3: Tantalum Spectrum - Decay of ^{182}Ta

5

Pulse Shape Discrimination

5.1   Pulse Shape Discrimination Methods

The cross section of photon interaction with matter is very essential in this study, especially within the germanium detector. Mass attenuation of material is closely related to the total cross section (photoelectric effect, Rayleigh scattering (coherent), Compton scattering (incoherent)). A lot of information can be obtained from the pulse shape of each event, for example pulse height corresponds to energy, rise time and pulse shape related to position of the event happen inside the detector.

Pulse shape discrimintation (PSD) for coaxial detector is more complex compared to planer detector (BEGe type, used in GERDA experiment [38] & Majorana Demonstrater [39]). Due to the coaxial configuration (optimum for detection efficiency), pulse shape at center of the end-cap is totally different from the edge of end-cap, make it more difficult cut out event at certain depth of the detector. Extra effort is needed to develop a new PSD method aim for coaxial detector at low energy region (ROI of ^{180m}Ta is 90 - 360 keV).

The pulse shape analysis is utilized in two ways for tantalum physics runs; to reject high frequency electronic noise at the pre-analysis stage & to suppress the background level at the pulse shape analysis stage. The following sections will be focused on how pulse shape treat each methods in our analysis.

5.1.1   Rejection of Electronic Noise

High frequency electrical or microphonics noise event can be rejected by PSD Type-A. The principle of this PSD method is showned in Figure 5.1. Maximum pulse height of each event is directly proportional to its energy. For noise event, the maximum pulse height will be much greater than normal event. By making a cut for maximum pulse height,
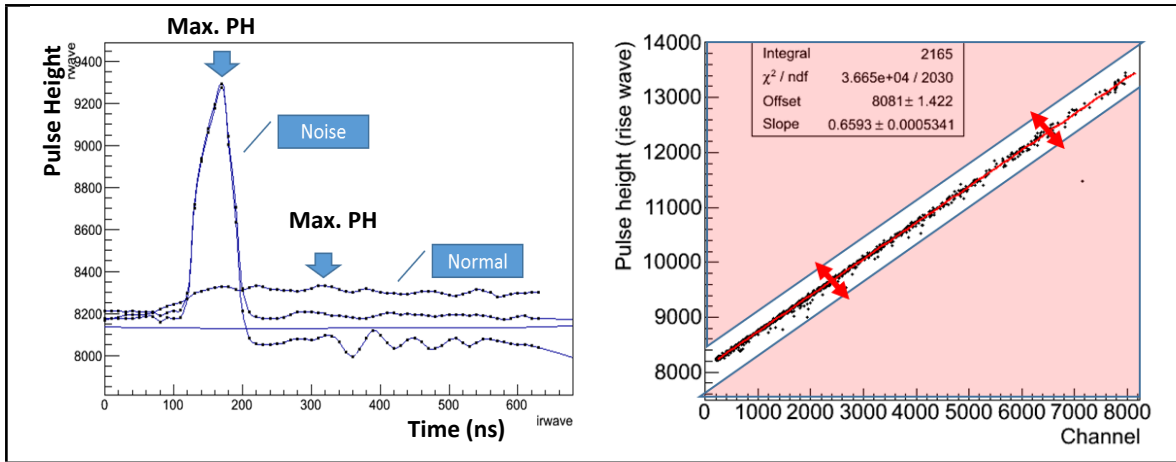
Figure 5.1: (left) Pulse shape examples of Noise event and normal event. (right) PSD Type-A to reject noise event by maximum pulse height.)

5.1.2 Position Dependence of Pulse Shape

Energy peak and Compton background event have different pulse shape distribution as compared in Figure 5.2. Using this pulse shape difference, a portion of the FEP event can be selected by apply PSD. The reason is low energy γ-ray tends to deposit all its energy at the surface of the detector and Compton background event is uniformly distributed throughout the whole active volume of HPGe detector.
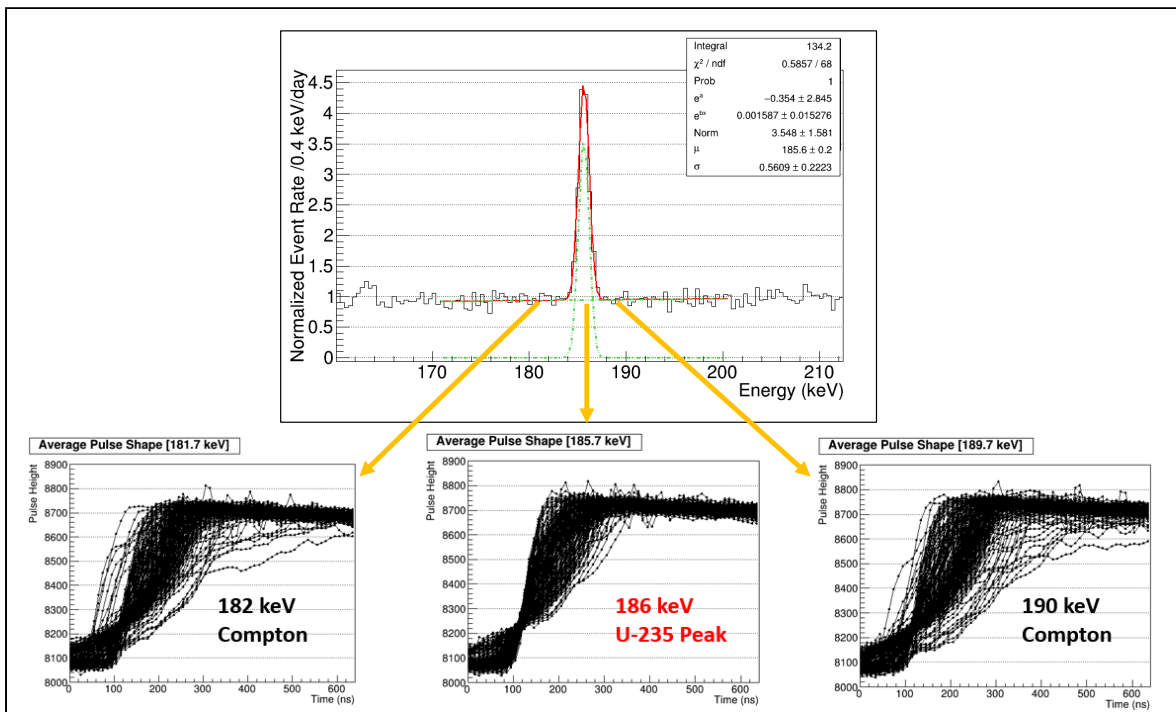
Figure 5.2: Pulse shape difference of peak vs. background (186 keV)

5.1.2.1 Maximum Current Amplitude Distribution

By differentiate each pulse shape, the current amplitude of each event can be obtained. Then, the maximum point of the current amplitude distribution was plotted with respect to the time at maximum point. This method is called current pulse amplitude method and described in Figure 5.3. This method will be refer as PSD cut in the following section.

Current Pulse Amplitude Method

Current Pulse, $I = \dfrac{dQ}{dT}$

dQ = charge integral (pulse height)
dT = time window
A = maximum amplitude

Procedure:
i. Plot pulse shape event-by-event
ii. Plot current pulse
iii. Find the maximum amplitude
iv. Plot maximum amplitude distribution
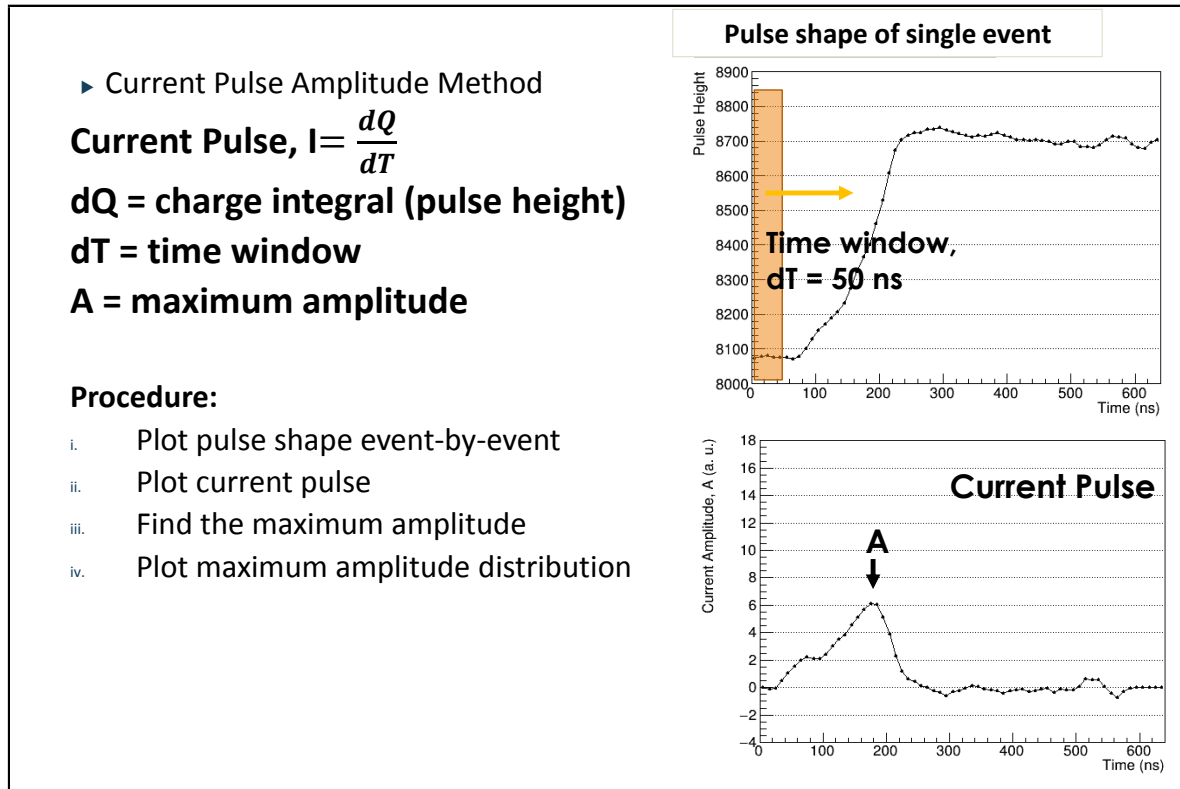
Figure 5.3: PSD - Current Pulse Amplitude Method

As shown in Figure 5.4, FEP event and Compton scattering background have different tendency of maximum current amplitude distribution. The maximum current amplitude of FEP event (186 keV) was concentrate around 100 ns, whereas Compton background around 250 ns. Hence, FEP event can be separated partially from Compton background event by PSD.

5.2 Effectiveness of PSD Cut

In order to determine which PSD cut is optimized, a parameter called effectiveness of PSD Cut, Eff was defined as shown in Figure 5.5. Seven background peaks were used to test the effectiveness of PSD Cut. If Eff is less than one, the PSD cut will be usefull to obtain a better half-life limit for ^{180m}Ta. From Figure 5.6, it was shown that this PSD method is only effective for energy region less than 200 keV.
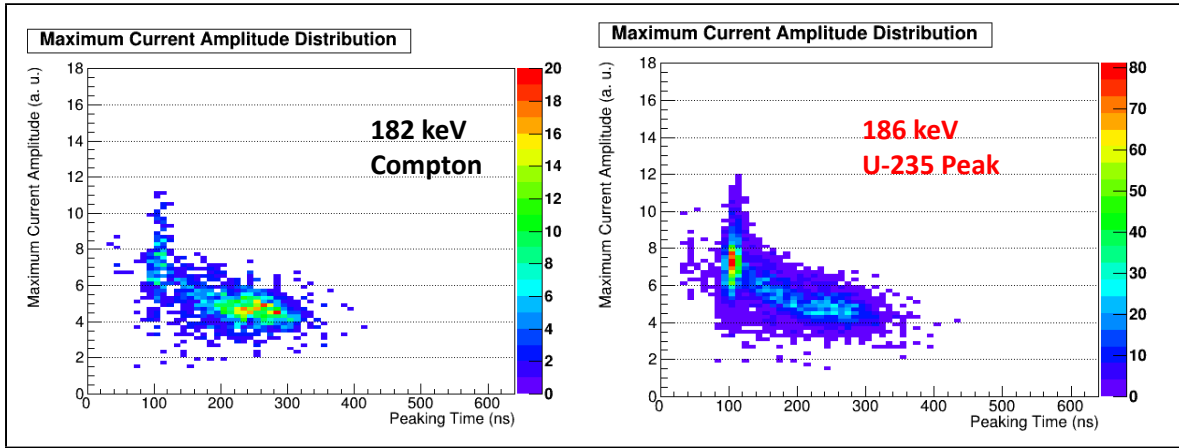
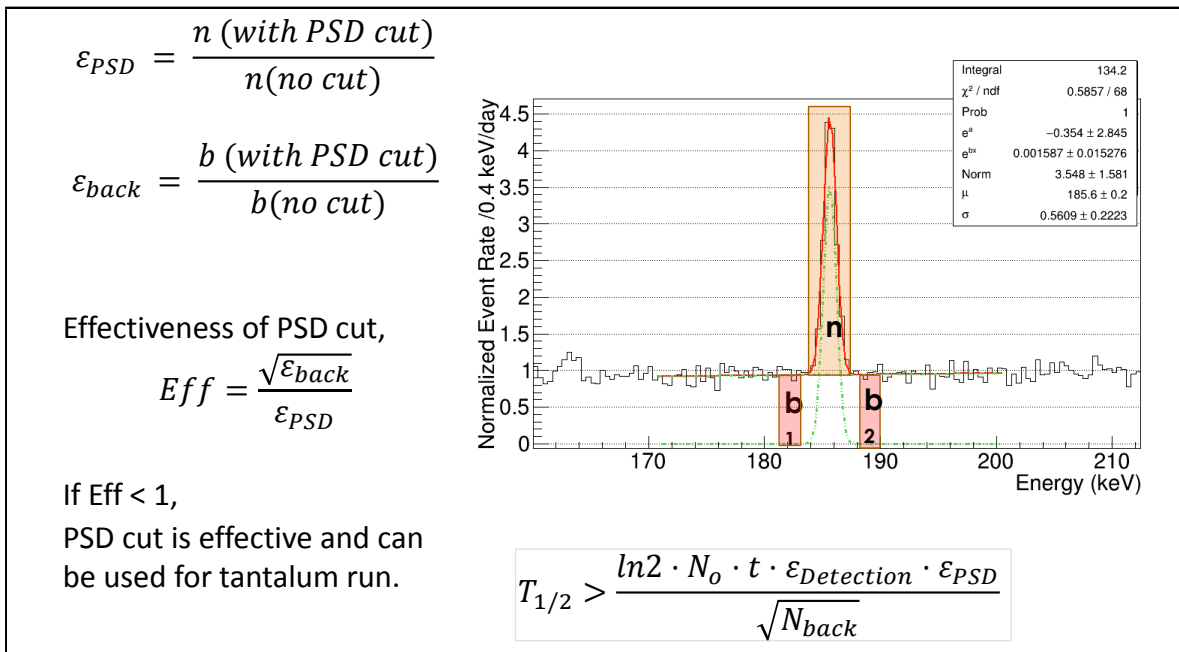Figure 5.4: Maximum point of current amplitude of peak (right) and background (left).

$$\varepsilon_{PSD} = \frac{n \, (with \, PSD \, cut)}{n(no \, cut)}$$

$$\varepsilon_{back} = \frac{b \, (with \, PSD \, cut)}{b(no \, cut)}$$

Effectiveness of PSD cut,

$$Eff = \frac{\sqrt{\varepsilon_{back}}}{\varepsilon_{PSD}}$$

If Eff < 1,
PSD cut is effective and can be used for tantalum run.

$$T_{1/2} > \frac{ln2 \cdot N_o \cdot t \cdot \varepsilon_{Detection} \cdot \varepsilon_{PSD}}{\sqrt{N_{back}}}$$

Integral	134.2
χ² / ndf	0.5857 / 68
Prob	1
e^a	−0.354 ± 2.845
e^bx	0.001587 ± 0.015276
Norm	3.548 ± 1.581
μ	185.6 ± 0.2
σ	0.5609 ± 0.2223

Figure 5.5: Definition of Effectiveness of PSD Cut

In case of ^{180m}Ta, only 103.5 keV ROI is suitable to use this PSD method. Hence, the tantalum spectrum at ROI of 103.5 keV was applied with PSD cut. The efficiency of PSD cut at 103.5 keV was 0.86338.
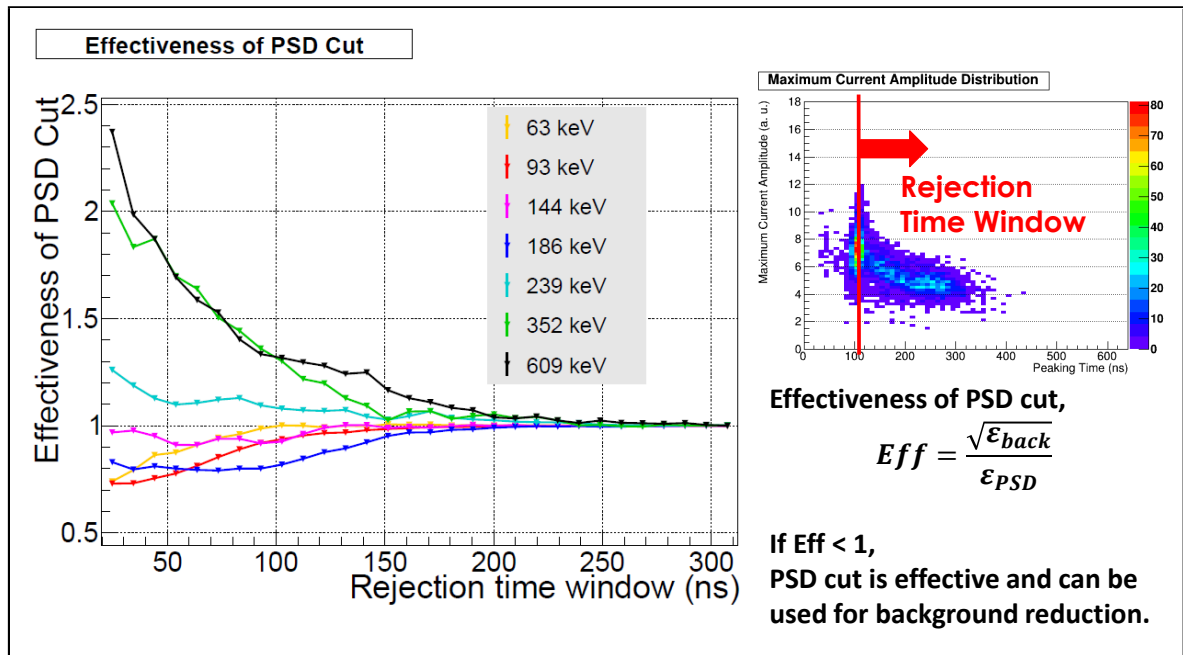
Figure 5.6: Effectiveness of PSD cut, tested with background peaks.

Chapter 6

Monte Carlo Simulation

6.1 Purpose of Simulation

In the case of point gamma source that used in calibration run, the detection efficiency of a measurement can be obtained by comparing the emitted radiation of the source given by reference data with the detected event by detector. However, in many cases, sample that need to be measured is not a point and has complex geometry. Detection efficiency is affected by many factors, for instance, distance of the source, thickness of the sample, and energy of the γ-ray. It is not practical to prepare calibration gamma source that resemble each sample's size, material and emitted radiation. In modern radiation detection, it is common to use simulation program to construct the experiment configuration and obtain the overall detection efficiency.

Moreover, simulation can used to estimate the outcome of a proposed experiment and obtain the optimum set up condition, before starting to build the detector system. Simulation in advance is critical for large scale experiment project, because sensitivity need to be estimated and the construction cost is enormous.

The tantalum sample is a cylindrical volume source, which geometry is very different from point calibration source. To obtain the detection efficiency of the tantalum Phase I and Phase II measurement, simulation is needed to reproduce the experiment condition.

6.2 Geant4 Simulation

To make a simulation of the detector configuration, GEANT4 program has been employed [40]. The Geant4 in this simulation was Ver. 4.10.02.p02. The physics list used was "shielding", which was customized for underground laboratory study.

6.2.1 Geometry Construction of Detector System

All components constructed by simulation are referred to the exact specification in the real experiment set up.

Ge Crystal   P-type Ge crystal (65 mm diameter, 64 mm length)
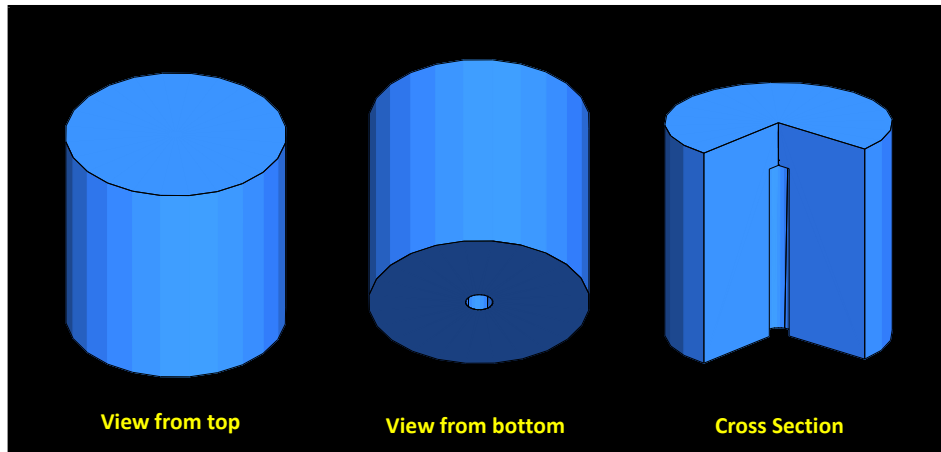
Figure 6.1: Simulation model of germanium crystal

HPGe detector   Assembly of Ge crystal, inner vacuum space, Al holder and Al endcap.
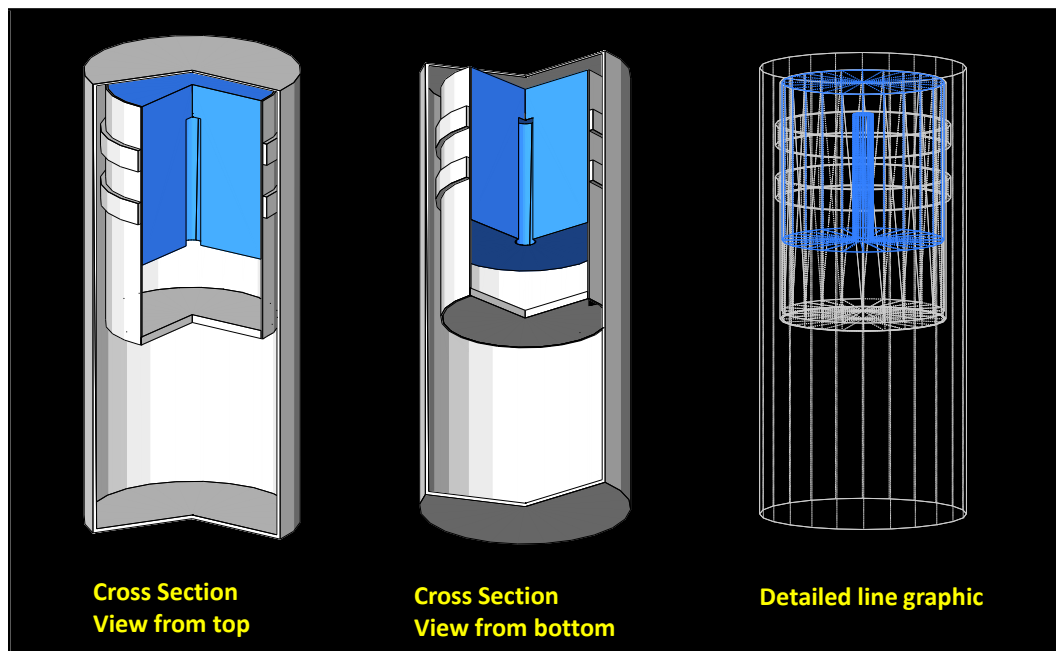
Figure 6.2: Simulation model of HPGe detector

Full Geometry of HPGe detector system The cross section view of the final geometry construction is shown in Figure 6.3. HPGe detector, tantalum sample, copper shield, lead shield and outer most iron shield were all included.
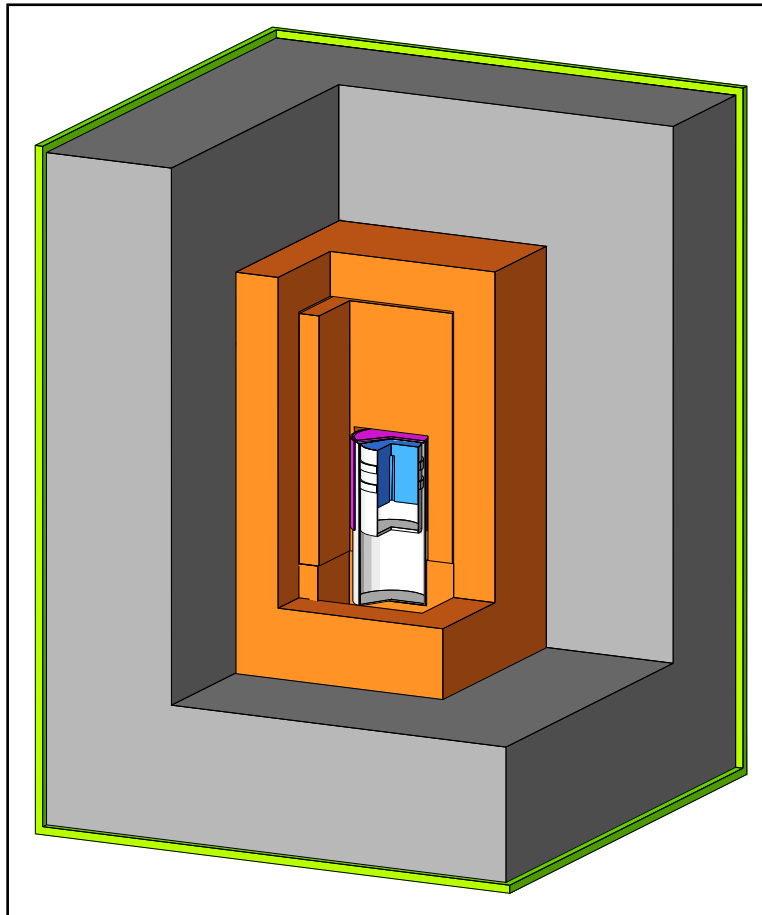
Figure 6.3: The cross section of HPGe detector in Phase II. View from top

6.3   Simulation of Calibration Run

To represent the actual calibration run, top shield of detector system was opened as shown in Figure 6.4. The calibration source can be placed at any distance and position from the detector. The source was assumed to be point source for all simulated calibration run.
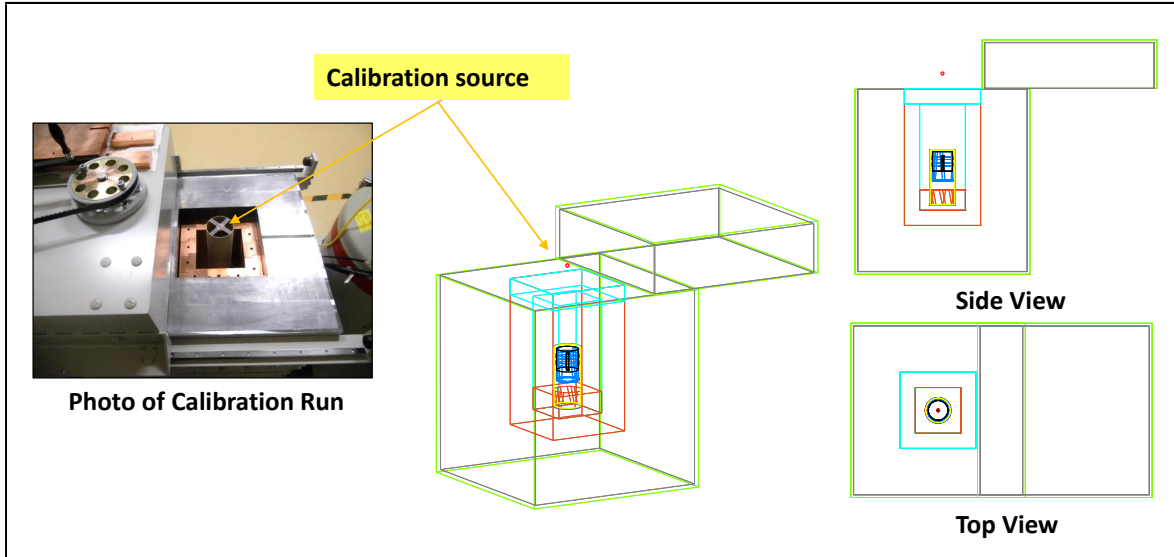
Figure 6.4: Simulation - Calibration Run

6.3.1   Primary Generator for γ Radiation

In Geant4 simulation, γ-ray is generated by setting the primary generator's particle gun. The position, energy, type, direction, momentum, etc of each beam can be defined. However, the direction of cascading γ-rays in the simulation is not correlated. Figure 6.5 shows the γ-rays path when radiation were emitted from point source. When γ source is placed at 250 mm from the detector, most of the radiation will be scattered out of the detector system. In the case of 5 mm distance, majority of the emitted γ-rays can be deposited on the detector due to large solid angle.

6.4   Comparison with Experimental Data

6.4.1   Energy Spectrum

The simulation is capable to generate energy spectrum that well resembled the experiment data. This indicated the detector system geometry is closely representing the detector system in reality. Comparison of energy spectrum between simulation and experiment was presented in Figure 6.6. There is a shortage of simulation, it can not reproduce the actual electrical response of detector. From the figure, pile-up and summing events were observed for experiment spectrum, however simulation can not reproduced any event above the energy of generated γ-ray.
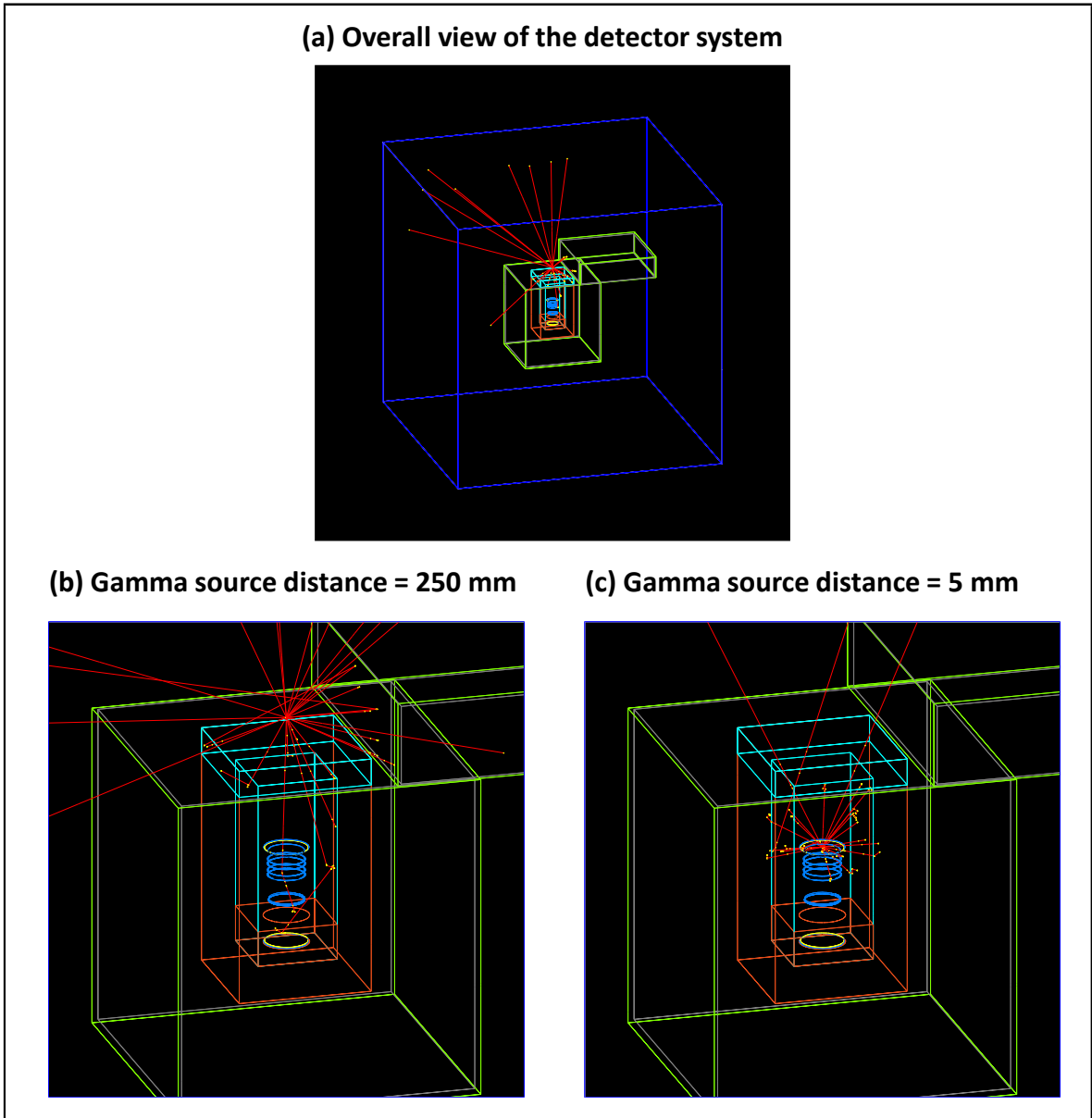
Figure 6.5: The path of γ-rays (red line) within detector system in Geant4 simulation. (a) Simulated γ-rays path with the entire detector system. The top shields was opened, which is the same configuration during calibration run with gamma sources. Blue box indicates the world, outer most boundary in simulation. Zoom in views as shown in (b) and (c). The γ source (^{133}Ba)was positioned at top of HPGe detector with distance of 250 mm (b) and 5 mm (c).
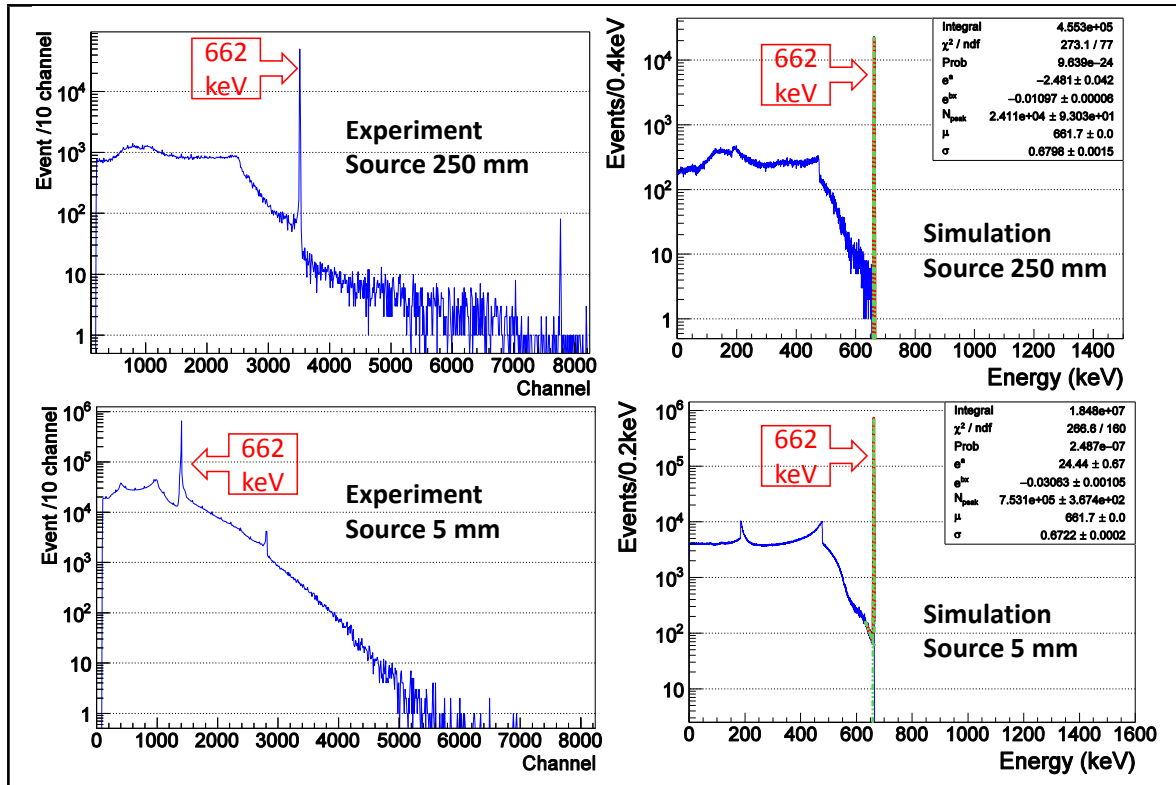
Figure 6.6: Simulation vs Experiment - Energy Spectrum of Cs-137

6.4.2 Detection Efficiency of Calibration Run

Dead Layer

The HPGe detector is a P-I-N structure semiconductor as described in section 2.3.1. Hence, the outer surface of the germanium crystal is diffused with lithium atoms and acts as ohmic contact. This area is inactive to radiation detection and referred as dead layer of HPGe detector. Manufacturer gave a typical dead layer thickness of 0.5 mm [31]. However, the actual dead layer thickness of each particular detector is vary. In this simulation, various thickness of dead layer was generated and compared with the experimental result.

For simplicity, the dead layer thickness was assumed to be uniform at all outer surfaces, including the top round surface and side lateral surface of the germanium crystal. The simulation model is shown in Figure 6.7.
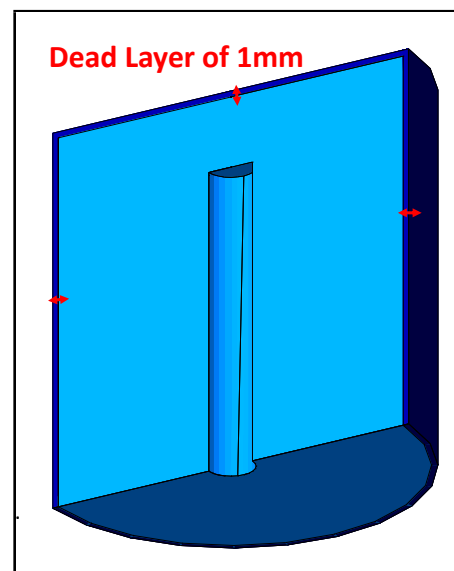
Figure 6.7: Simulation - Ge Dead Layer

Result   The change of FEP detection efficiency curve with increasing dead layer thickness is shown in Figure 6.8.
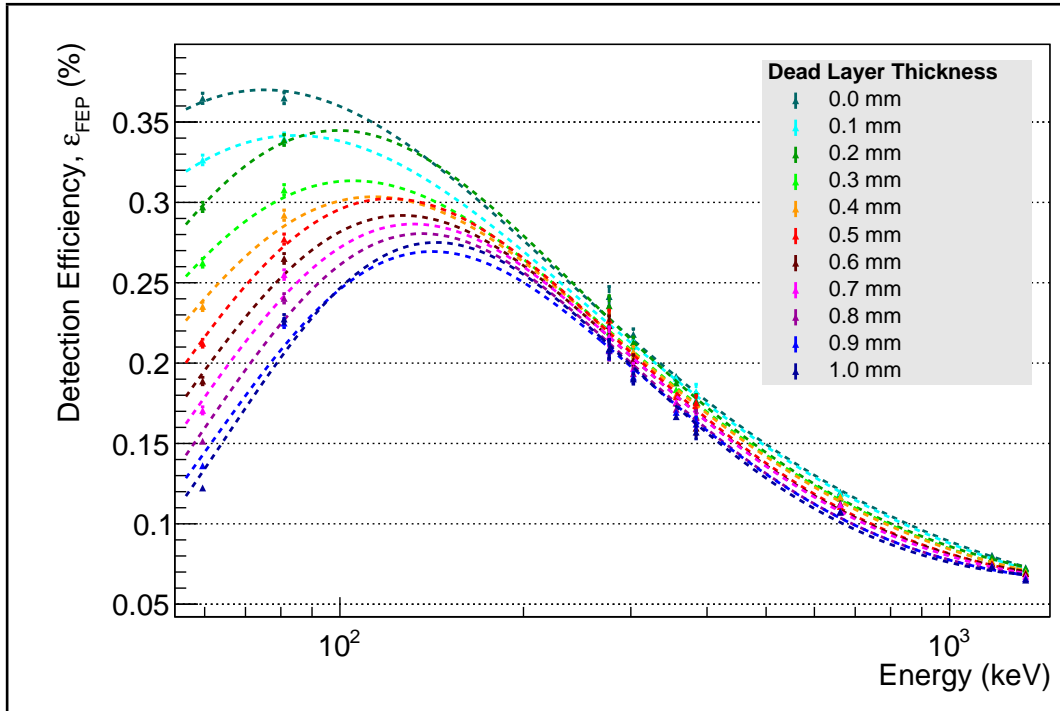
Figure 6.8: Detection Efficiency from Simulation - Adjustment of Ge Dead Layer Thickness from 0.0 mm to 1.0 mm. Distance from top of endcap of detector was set at 250 mm.

Ratio of FEP Detection Efficiency   The comparison of FEP Detection Efficiency between simulation and experiment data was shown in Figure 6.9. Comparing the shape of efficiency curve, chi-square/ndf value of ratio different and the matching of low energy peaks (less than 100 keV), dead layer of 3 mm thick is found the best simulation model to represent the experiment data. This is same as the specification given by manufacturer, that dead layer of Ge crystal is around 5 mm thick. Using the adjustment of 3 mm dead layer, tantalum spectrum was simulated.
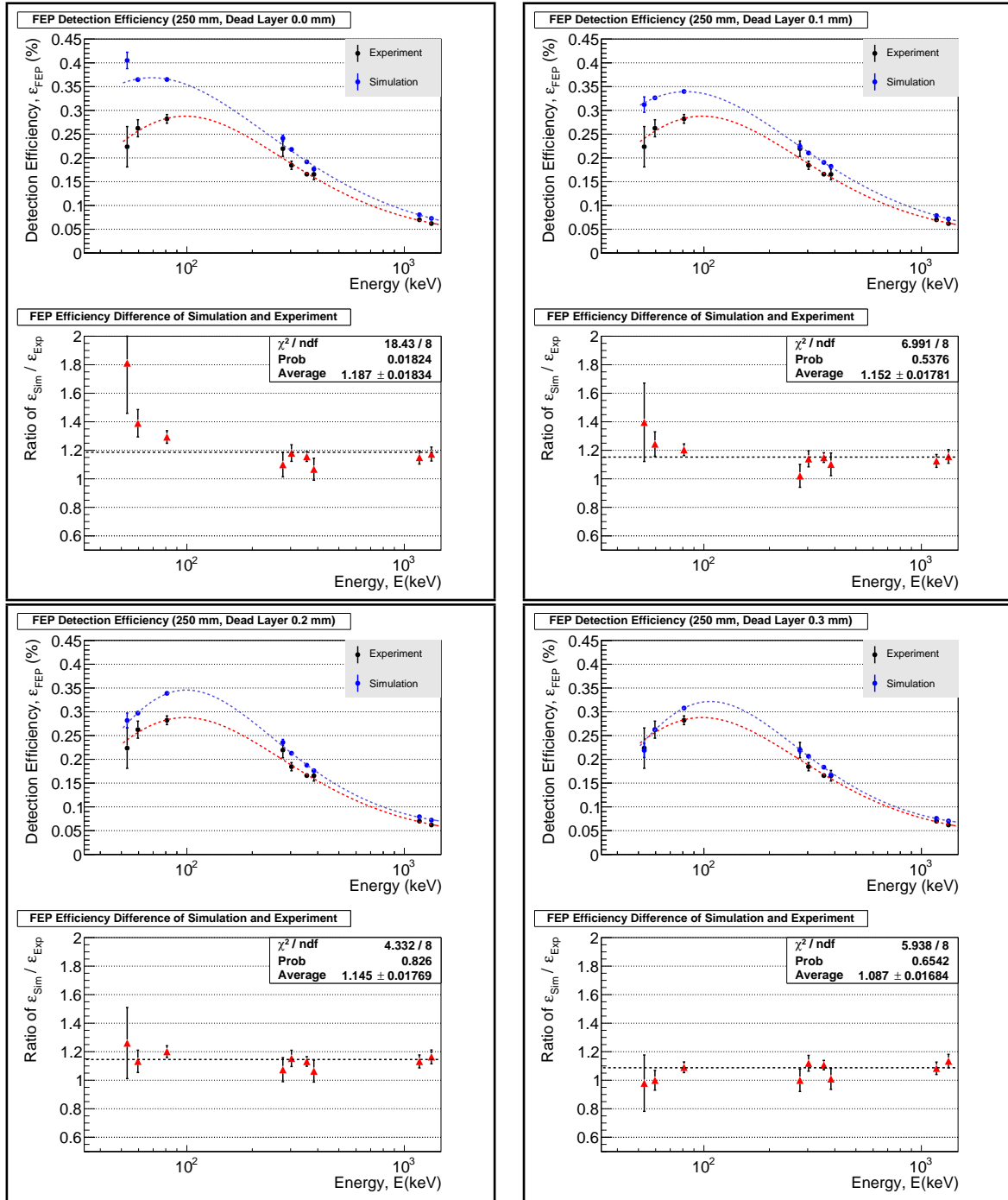
Figure 6.9: Comparison of detection efficiency curve and ratio of simulation and experiment data, by varied the Ge crystal's dead layer thickness in simulation. Dead layer thickness in simulation were 0.0 mm (top left), 0.1 mm (top right), 0.2 mm (bottom left) and 0.3 mm (bottom right). The gamma source distance was set at 250 mm from the top of endcap.
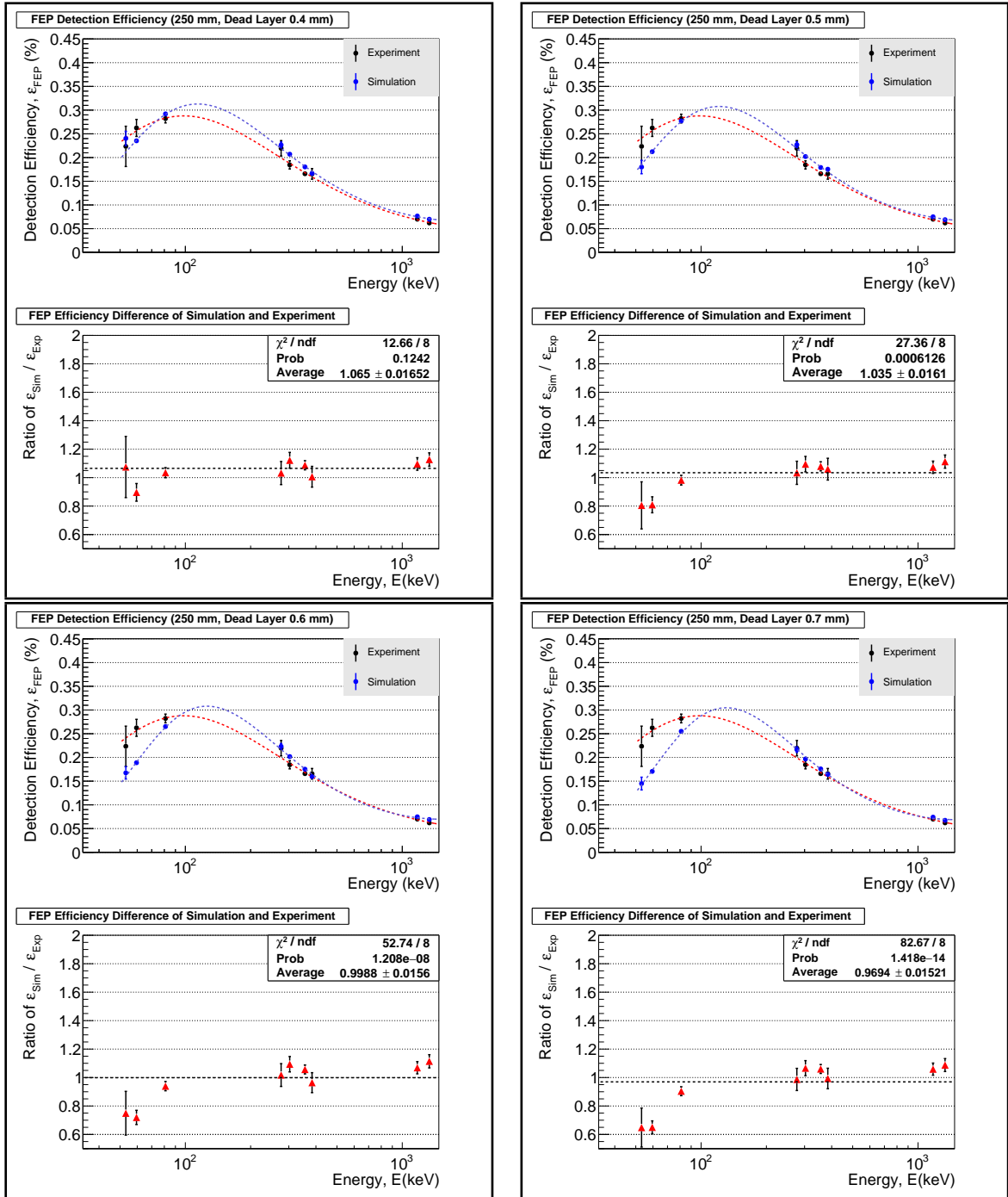
Figure 6.10: Comparison of detection efficiency curve and ratio of simulation and experiment data, by varied the Ge crystal's dead layer thickness in simulation. Dead layer thickness in simulation were 0.4 mm (top left), 0.5 mm (top right), 0.6 mm (bottom left) and 0.7 mm (bottom right).The gamma source distance was set at 250 mm from the top of endcap.

6.5   Simulation of Tantalum Measurement

The detector system and sample configurations in the Tantalum Phase I and Phase II measurement have been simulated by using the geometry as mentioned in above section. Since ^{180m}Ta emitted γ-rays in the energy range of 93 keV to 351 keV, behaviour and interaction pattern for lower energy γ and higher energy γ were different. In Figure , most of the 93.3 keV γ was self-attenuated by the tantalum sample itself, however 350.9 keVγ has higher chance to pass through the tantalum sample and entered the detector volume.

Tantalum sample   Simulation of tantalum sample, composed of two components, top round plate and side cylinder.
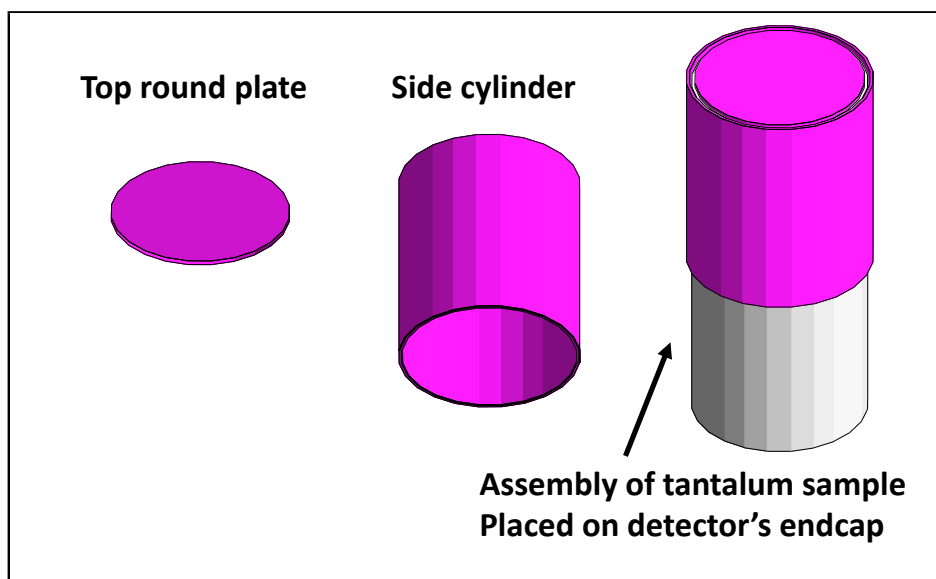
Figure 6.11: Simulation model of tantalum sample. Assembly of two components, (left) top round plate of 2 mm thick and (middle) side cylinder of 1.5 mm thick. The sample was placed on top and fit closely to the detector.

Interaction pattern   The interaction patterns of γ-rays emitted by ^{180m}Ta were energy dependence.

γ-ray from tantalum sample   The distribution of γ-rays emitted from tantalum sample and detected by HPGe detector is shown in Figure 6.13. Since only detected events were selected, position that was closest to the Ge crystal (middle of cylinder and top plate) has higher concentration of events. The x-axis and z-axis in lower plot of Figure 6.13 represent diameter (88 mm) and thickness (2 mm) of the tantalum top plate. This result indicated the self-attenuation of tantalum sample because most of the detected γ-rays were emitted from the lower part of the plate. The γ-rays that emitted from upper part of the plate has higher possibility to be self-absorbed or scattered out by the tantalum sample itself, hence can not be detected by HPGe detector.
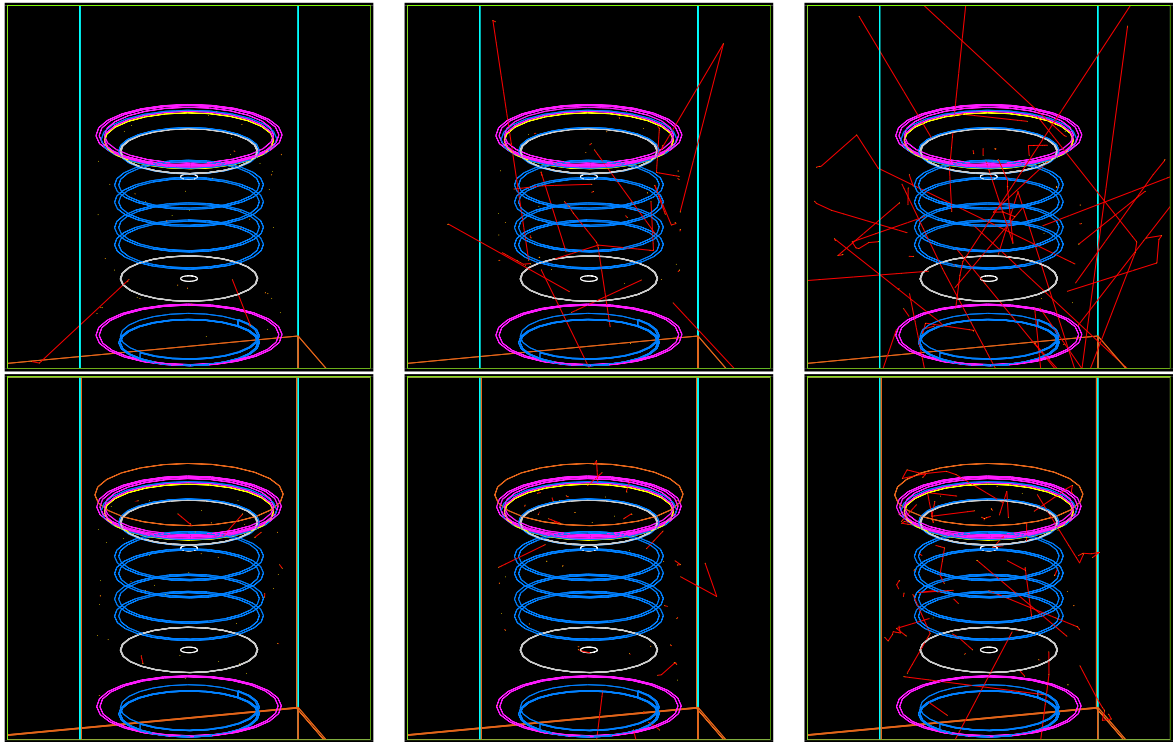
Figure 6.12: Interaction patterns of γ-rays emitted by ^{180m}Ta (purple color). Detector and sample configuration in Phase I (top row) and Phase II (lower row). The main difference for Phase II was additional inner Cu shield and smaller tantalum cylinder radius. Interaction patterns were compared between 93.3 keV (1st column), 215.3 keV (2nd column) and 350.9 keV (3rd column).
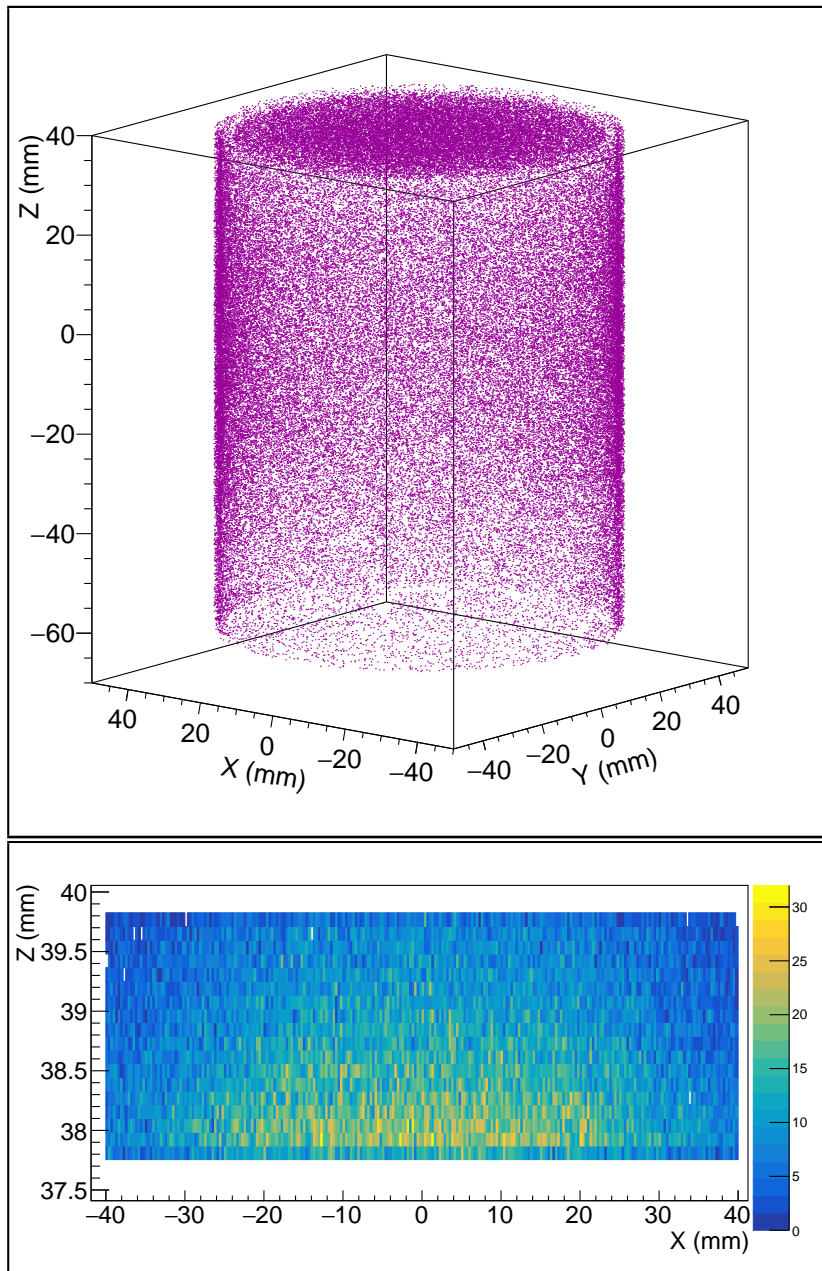
Figure 6.13: Distribution of γ-rays emitted from tantalum sample and detected by HPGe detector. (top) γ-rays were uniformly distributed within the tantalum top plate and side cylinder. (lower) Distribution of 350.9 keV γ-rays that emitted from tantalum top plate and been detected.

Distribution of energy deposition Penetration depth within Ge crystal for γ-ray coming from outside of the detector will increase with its energy. For low energy γ-ray, for example 93.3 keV γ from ^{180m}Ta, most of the radiation will deposit full energy at the surface of the detector. On the other hand, higher energy γ-ray (350.9 keV) can travel deeper into the center of the detector. Figure 6.14 shown the distribution of first interaction position of the γ-ray when entered the detector, compared between three different energy. Only events with full energy deposition were selected. By comparing these distribution, the result clearly shown that majority of the γ-ray in energy region 93.3 keV to 350.9 keV were deposited at the surface region of the detector. For 93.3 keV, almost all of the γ-ray only interact with the surface volume, whereas 215.3 keV and 350.9 keV γ-rays have increasing broader distribution.
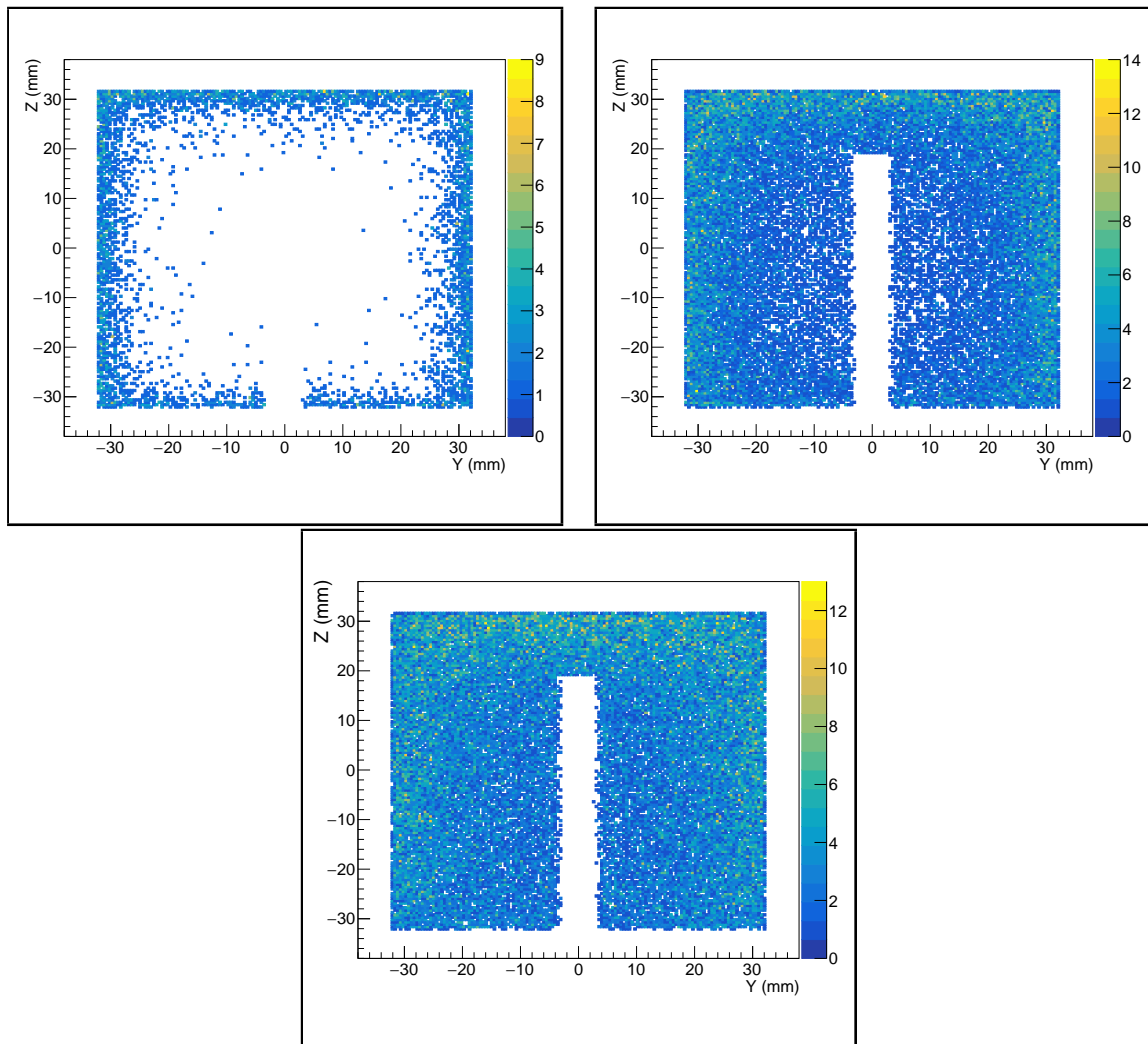
Figure 6.14: Distribution of γ-ray energy deposition within Ge crystal (center cross sectional), each point indicated the first interaction position when γ entered the detector active volume. Distribution were compared between 93.3 keV (top left), 215.3 keV (top right) and 350.9 keV (bottom middle).

Number of interaction points The number of interaction points for each γ-ray was energy dependence as shown in Figure 6.15. For low energy γ, cross section of photoelectric effect is higher than Compton scattering, hence most of the γ-rays will fully deposit its energy at 1st interaction position. For high energy γ, the radiation will undergo few scatterings within the detector volume before deposited all its energy.
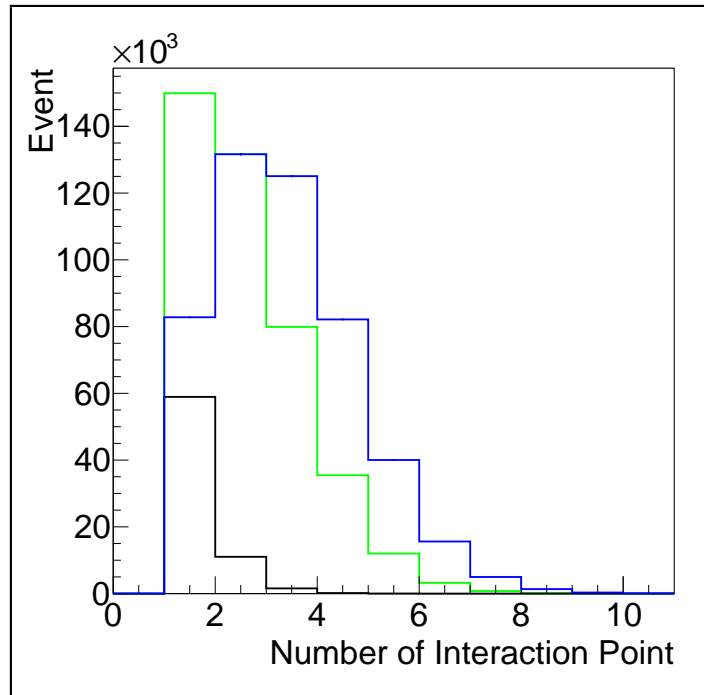

Figure 6.15: Number of interaction points for γ-rays of 93.3 keV (black), 215.3 keV (green) and 350.9 keV (blue).

6.6 Detection Efficiency of ^{180m}Ta

Using the Monte Carlo simulation by GEANT4, the FEP detection efficiency of Phase I and Phase II tantalum measurements were obtained, as listed in Table 6.1. The detection efficiency curves for Phase I and Phase II are shown in Figure 6.16. Phase II has slightly higher detection efficiency than Phase I, due to the closer distance of tantalum sample to detector. The inner radius of tantalum cylinder was 0.7 mm shorter in Phase II, hence there is no space between sample and detector.

Table 6.1: Full energy peak detection efficiency of ^{180m}Ta measurement

Decay Branch	Energy (keV)	Phase I		Phase II	
		ε (%)	$\Delta\varepsilon$ (stat.)	ε (%)	$\Delta\varepsilon$ (stat.)
EC	93.3	0.69	0.01	0.69	0.01
	215.3	4.11	0.02	4.11	0.02
	332.3	4.73	0.02	4.81	0.02
$\beta-$	103.5	0.92	0.01	0.93	0.01
	234.0	4.32	0.02	4.42	0.02
	350.9	4.74	0.02	4.78	0.02
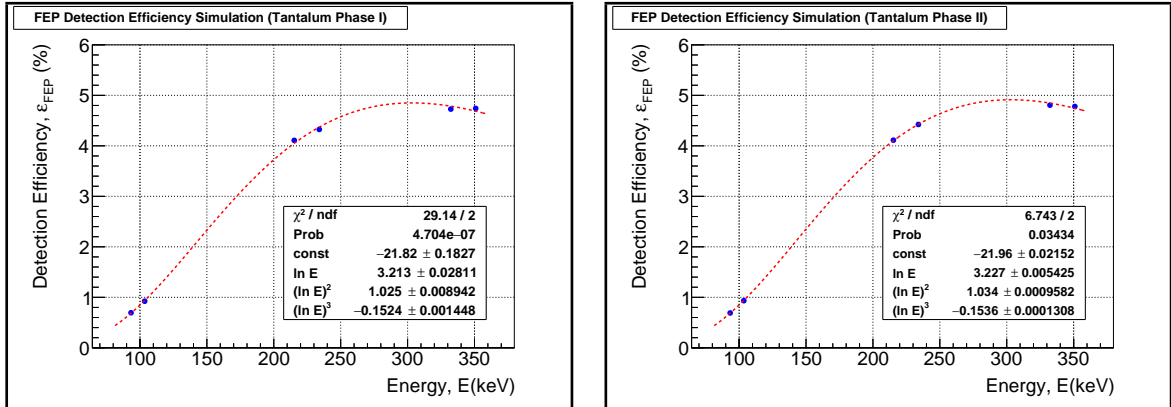
Figure 6.16: FEP detection efficiency curves of Tantalum Phase I (left) & Phase II (right) by simulation

63

Conclusion - Study of ^{180m}Ta Half-life

7.1 Event in ROI

Energy resolution of tantalum spectrum The energy calibration of every 4 to 6 tantalum physics runs with livetime around 1 week was performed by utilized background peaks. After energy calibration and summation of all physics runs, total 15 background peaks in Phase I and 13 background peaks in Phase II were selected to evaluate the linearity of energy calibration. Energy resolution corresponds to the background peak energy in tantalum physics runs were plotted as shown in Figure 7.1. Energy resolution in the peak width calibration plot is defined as the sigma, σ obtained from Gaussian fitting of each energy peak. The peak width calibration equation was then used to calculate the $\sigma_{E\gamma}$ values for ROI of ^{180m}Ta, listed in Table 7.1 .
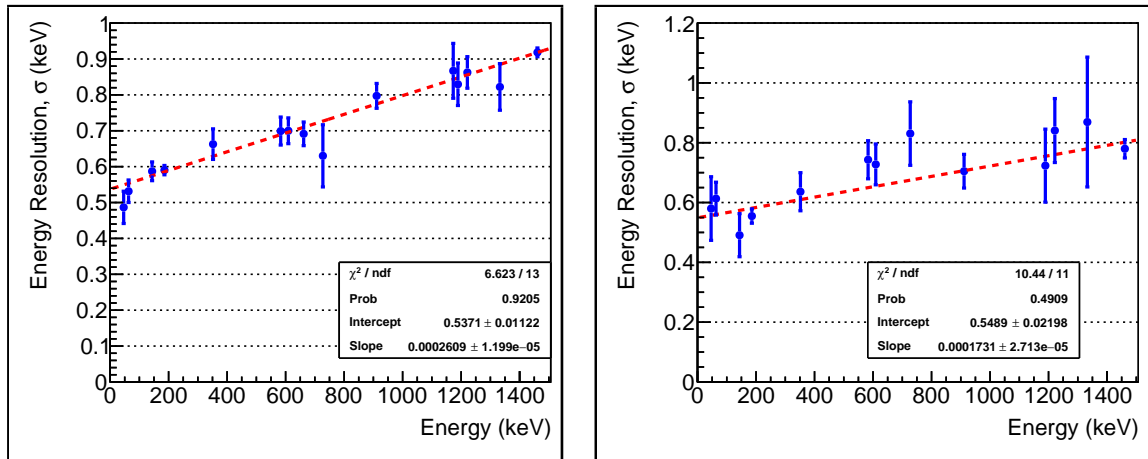
Figure 7.1: Peak width calibration in Tantalum Phase I (left) and Phase II (right)

Energy range of ROI Using the $\sigma_{E\gamma}$ values, integral events in energy range of each ROI were obtained. Energy range is defined as ROI $\pm$ 1.645$\sigma_{E\gamma}$, correspond to 90 % confidence limits. The ROI region (blue shaded region) for integral events in tantalum spectrum for EC branch and β- branch are shown in Figure 7.2 and Figure 7.3. Since PSD cut is effective for energy below 200 keV, only ROI of 103.5 was applied with PSD cut. The ROI of 93.3 keV was excluded from PSD cut because the current

energy resolution of the detector was unable to separate the ^{180m}Ta 93.3 keV peak from background peak.

The background peaks in ± 10 keV of ROI (fit with green lines) were 92.58 keV (^{234}Th), 222.1 (^{182}Ta), 238.63 (^{212}Pb), 338.32 (^{228}Ac) and 351.93 (^{214}Pb). Since no ^{180m}Ta peak is significant statistically, integral background events were obtained as listed in Table 7.1. ROI of 103.5 keV in Phase I and Phase II was applied with PSD cut.

Table 7.1: Integral background event in ROI of ^{180m}Ta

Phase (livetime)	Decay Branch	ROI (keV)	$\sigma_{E\gamma}$ (keV)	Energy Range (keV)	Integral Event, N_{back}
		93.3	0.561	92.2 - 94.4	4724
	EC	215.3	0.593	214.2 - 216.4	1462
I		332.3	0.624	331.2 - 333.4	1088
(300.6					
days)		103.5	0.564	102.4 - 104.6	527
	β-	234.0	0.598	233.0 - 235.0	1297
		350.9	0.629	349.8 - 352.0	1545
		93.3	0.565	92.2 - 94.4	781
	EC	215.3	0.586	214.2 - 216.4	129
II		332.3	0.606	331.2 - 333.4	70
(57.6					
days)		103.5	0.567	102.4 - 104.6	86
	β-	234.0	0.589	233.0 - 235.0	104
		350.9	0.610	349.8 - 352.0	197

7.2   Lower Limit of Half-life

The half-life lower limit is defined as Equation 7.1.

$$T_{1/2} > \frac{ln2 \cdot \varepsilon_{Det} \cdot N_o \cdot t}{\sqrt{N_{back}}} \tag{7.1}$$

In case of PSD cut was applied,

$$T_{1/2} > \frac{ln2 \cdot \varepsilon_{Det} \cdot \varepsilon_{PSD} \cdot N_o \cdot t}{\sqrt{N_{back}}} \tag{7.2}$$

where
ε_{Det} = Detection efficiency of detector (refer Table 6.1)
ε_{PSD} = PSD cut efficiency
N_o = Number of ^{180m}Ta nuclide
t = Livetime of the measurement
N_{back} = Integral background events in ROI (refer Table 7.1)
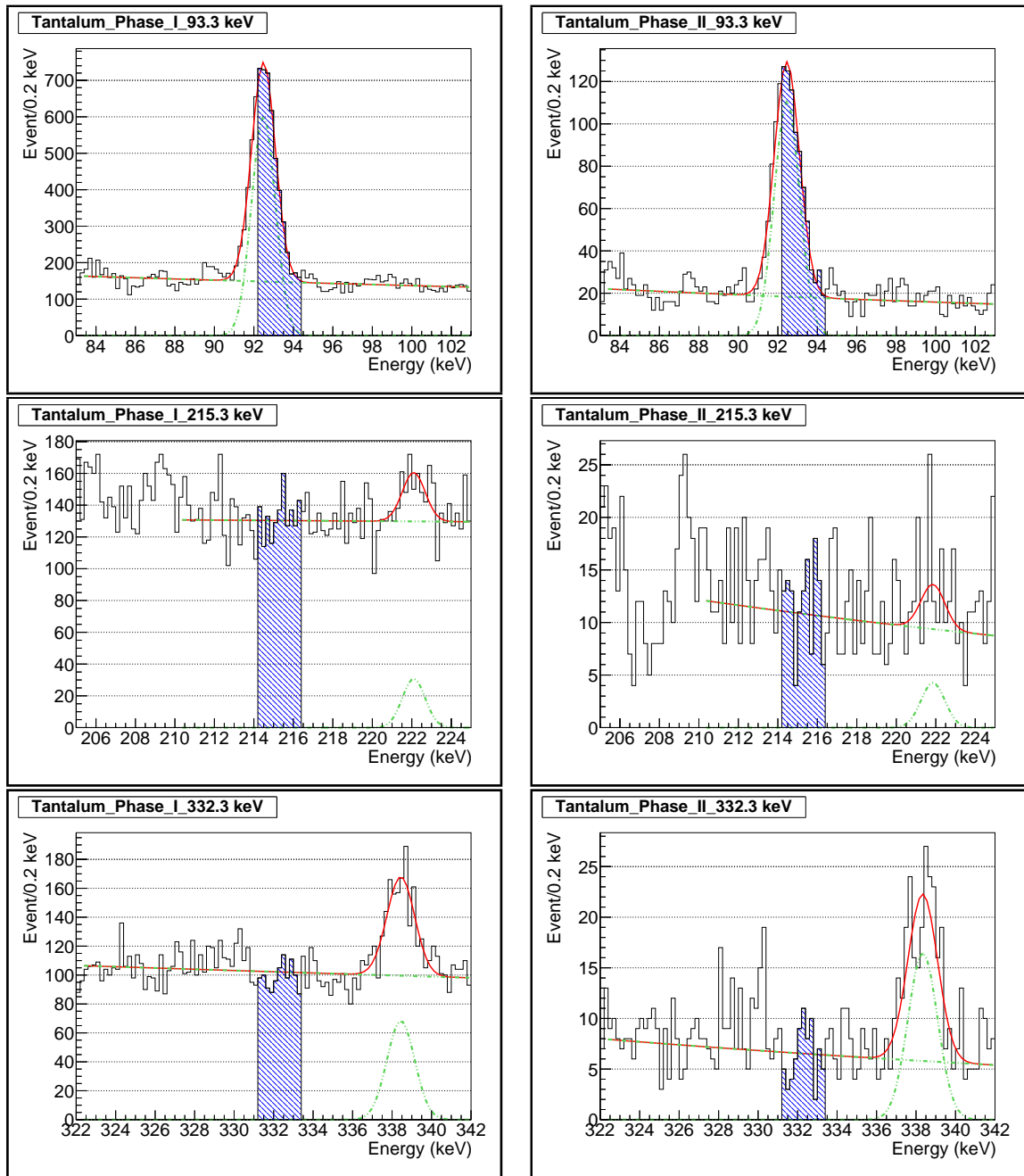
Figure 7.2: Integral events (blue shaded region) in ROI of Tantalum Phase I (1st column) and Phase II (2nd column) for EC branch. Energies of ROI are 93.3 keV (1st row), 215.3 keV (2nd row) and 332.3 keV (3rd row).
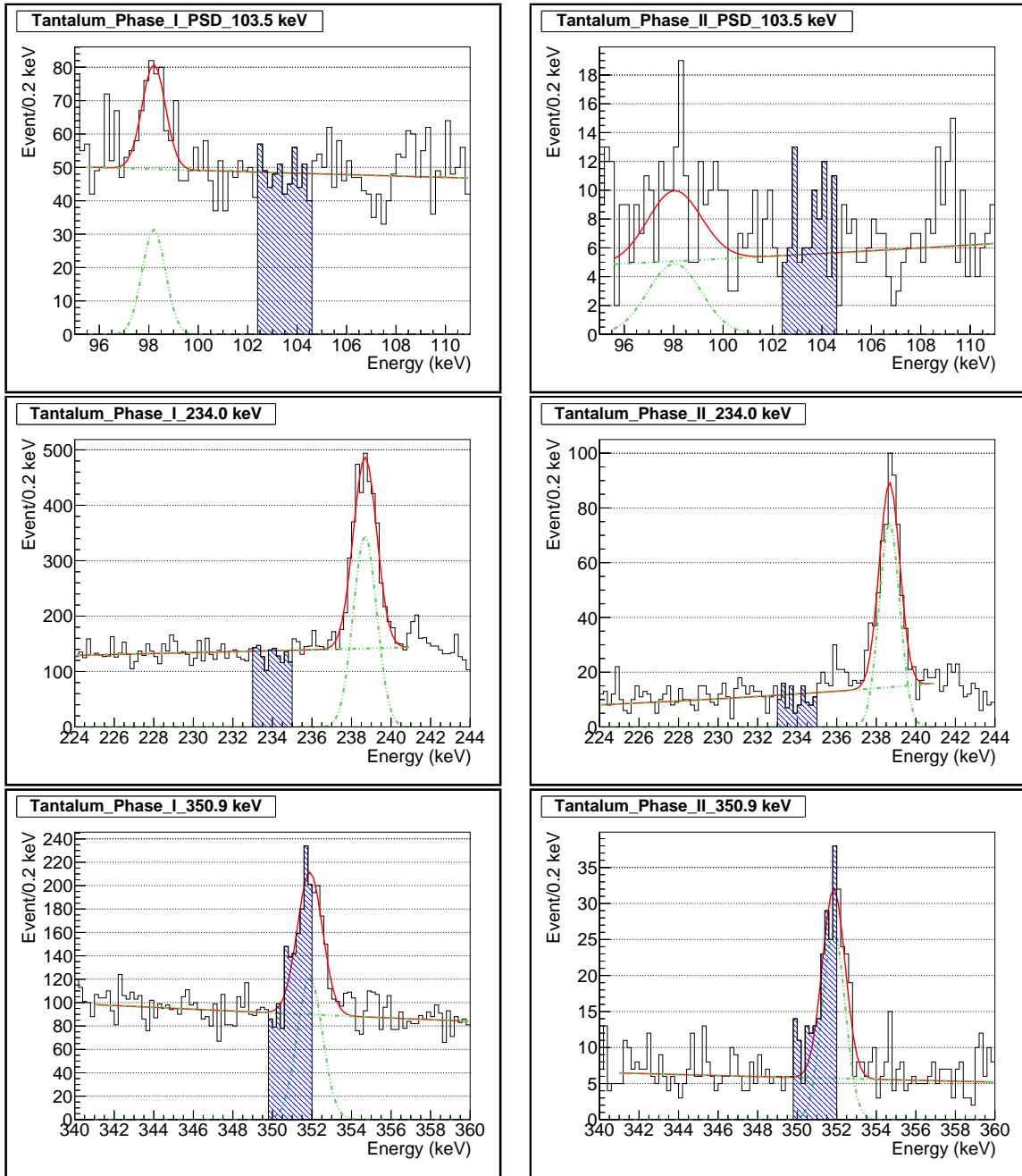
Figure 7.3: Integral events (blue shaded region) in ROI of Tantalum Phase I (1st column) and Phase II (2nd column) for β- branch. Energies of ROI are 103.5 keV with PSD cut (1st row), 234.0 keV (2nd row) and 350.9 keV (3rd row).

68

Using Equation 7.1, the half-life lower limit for ROI in Phase I and Phase II were deduced in Table 7.2.

Table 7.2: Lower limit of half-life for all ROIs in Tantalum Phase I and Phase II

Decay Branch	ROI (keV)	I_γ (%)	$\varepsilon_{Det}(\%)$		$T_{1/2}$ limit (yrs)		
			Phase I	Phase II	Phase I	Phase II	Phase I + II
EC	93.3	17.5	0.69	0.69	1.21×10^{16}	5.59×10^{15}	1.33×10^{16}
	215.3	81.5	4.11	4.11	1.29×10^{17}	8.19×10^{16}	1.47×10^{17}
	332.3	94.4	4.73	4.81	1.72×10^{17}	1.30×10^{17}	1.99×10^{17}
β-	103.5	22.5	0.92	0.93	4.15×10^{16}	1.96×10^{16}	4.58×10^{16}
	234.0	84.4	4.32	4.42	1.44×10^{17}	9.81×10^{16}	1.66×10^{17}
	350.9	94.8	4.74	4.78	1.45×10^{17}	7.71×10^{16}	1.62×10^{17}

For EC branch, the probability of γ emission, I_γ and ε for 93.3 keV are very low. Hence, this ROI is not considered for $T_{1/2}$ limit calculation. Same reasons applied to 103.5 keV for β- branch. From the calculation, the most stringent $T_{1/2}$ limit values are obtained from 332.3 keV for EC branch and 234.0 keV for β- branch.

In conclusion, the partial and total $T_{1/2}$ upper limit for ^{180m}Ta obtained from this research are

$$T_{1/2}^{EC} > 1.99 \times 10^{17} yrs$$
$$logft = 25.0$$
$$T_{1/2}^{\beta-} > 1.66 \times 10^{17} yrs$$
$$logft = 23.6$$

$$T_{1/2}^{Total} > 9.03 \times 10^{16} yrs$$

(7.3)

Both partial $T_{1/2}$ limit in EC branch and β- branch have exceed the latest published result in 2016 by research group in HADES [2]. The total $T_{1/2}$ limit has improved a factor of 2 compared to the HADES result of 4.5 $\times 10^{16}$ yrs. The most stringent lower limit of half-life for ^{180m}Ta in the world has been successfully obtained by the new ultra-low background HPGe detector system.

Appendix A

Construction of HPGe Detector System

A.1 Chronicle of Construction Work

In 2012, the construction work of the detector system was started. The assembly of the whole system was completed and data taking test using the detector was started from summer 2013. After that, this system is continuously undergo development.

Table A.1: Development time line of the HPGe detector system

Timeline (year)	Category	Progress
2012	Detector	Preparation of experiment site
		Pre-test of HPGe detector, preamplifier and liquid nitrogen dewar
	Shield	Production of lead and copper shields
2013	Detector	Full assembly of HPGe detector inside shields
		Installation of liquid nitrogen supply system (tank, pipe, dewar, level monitor, boil-off gas pipe)
	Shield	Construction of outer lead shield and middle copper shields
	DAQ	Installation of UPS, HV, preamplifier, DSP, PC, oscilloscope and cabling
	Monitor	Installation of oxygen concentration monitor, temperature monitor humidity monitor, network camera and external network connection
	Sample	Tantalum sample was moved from surface to underground
	Measurement	Phase I tantalum measurement started
2014	DAQ	DSP update with new software
	Measurement	Phase I tantalum measurement completed
		Material screening of CANDLES experiment started
	Sample	Tantalum sample was stored at underground
2015	Measurement	Material screening of CANDLES experiment
	Sample	Acid cleaning process of tantalum sample
		Reassembly of tantalum sample
2016	Detector	Installation of NaI detector for coincidence measurement
	DAQ	Installation of HV, logic circuit for NaI detector
	Shield	Production and Installation of inner copper shield
	Monitor	Installation of radon detector
	Measurement	Material screening of CANDLES experiment
		Phase II tantalum measurement

List of Figures

List of Tables

Bibliography

[1] F. A. White, T. L. Collins, and F. M. Rourke, "New naturally occurring isotope of tantalum," *Physical Review*, vol. 97, no. 2, pp. 566–567, 1955. PR.

[2] B. Lehnert, M. Hult, G. Lutter, and K. Zuber, "Search for the decay of nature's rarest isotope ^{180m}ta," *arXiv preprint arXiv:1609.03725*, 2016.

[3] Evaluated Nuclear Structure Data File (ENSDF), maintained by the National Nuclear Data Center at Brookhaven National Laboratory, in Nuclear Data Sheets (Academic Press, Elsevier Science), http://www.nndc.bnl.gov/ensdf/ENSDF.

[4] Z. Nemeth, F. Kaeppeler, and G. Reffo, "Origin of ta-180m and the temperature of the s-process," *The Astrophysical Journal*, vol. 392, pp. 277–283, 1992.

[5] M. Loewe, P. Alexa, J. de Boer, and M. Wurkner, "The ta-180 production puzzle and the classical s-process," *Nuclear Physics A*, vol. 719, pp. 275c–278c, 2003.

[6] P. Mohr, F. Kappeler, and R. Gallino, "Survival of nature's rarest isotope ta-180 under stellar conditions," *Physical Review C*, vol. 75, no. 1, 2007.

[7] T. Hayakawa, T. Kajino, S. Chiba, and G. J. Mathews, "New estimate for the time-dependent thermal nucleosynthesis of ta-180(m)," *Physical Review C*, vol. 81, no. 5, 2010.

[8] E. B. Norman, "Half-life of ^{180}ta," *Physical Review C*, vol. 24, no. 5, p. 2334, 1981.

[9] E. McCutchan, "Nuclear data sheets for a = 180," *Nuclear Data Sheets*, vol. 126, pp. 151 – 372, 2015.

[10] M. Hult, J. E. Wieslander, G. Marissens, J. Gasparro, U. Watjen, and M. Misiaszek, "Search for the radioactivity of ^{180m}ta using an underground hpge sandwich spectrometer," *Applied Radiation and Isotopes*, vol. 67, no. 5, pp. 918–921, 2009.

[11] B. Singh, J. Rodriguez, S. Wong, and J. Tuli, "Review of logftvalues in decay," *Nuclear Data Sheets*, vol. 84, no. 3, pp. 487–563, 1998.

[12] P. Eberhardt, J. Geiss, C. Lang, W. Herr, and E. Merz, "Notizen: Zur frage des zerfalls von 180 ta," *Zeitschrift fr Naturforschung A*, vol. 10, no. 9-10, pp. 796–796, 1955.

[13] J. Cumming and D. Alburger, "Search for the decay of ^{180}ta^m," *Physical Review C*, vol. 31, no. 4, p. 1494, 1985.

[14] M. Hult, J. Gasparro, G. Marissens, *et al.*, "Underground search for the decay of ta-180m," *Physical Review C*, vol. 74, no. 5, 2006.

[15] K. Wakae, T. Kanei, R. Hazama, *et al.*, "The measurement of halflife of ^{180}ta^m," *Annual Report Osaka University Laboratory of Nuclear Studies*, pp. 18 – 20, 1998.

[16] S.Shiomi, *Background from Radioactivities in Constructing Materials of ELE-GANT VI.* Master thesis, 1999.

[17] Model of Ikenoyama Mountain is belongs to Kamioka Observatory, ICRR (Institute for Cosmic Ray Research), The University of Tokyo.

[18] T. Iida, T. Kishimoto, M. Nomachi, *et al.*, "The candles experiment for the study of ca-48 double beta decay," *Nuclear and Particle Physics Proceedings*, vol. 273275, pp. 2633–2635, 2016.

[19] K. Nakajima, T. Iida, T. Kishimoto, *et al.*, "Low background techniques in candles," *AIP Conference Proceedings*, vol. 1672, p. 110004, 2015.

[20] M. Hult, "Low-level gamma-ray spectrometry using ge-detectors," *Metrologia*, vol. 44, no. 4, pp. S87–S94, 2007.

[21] Y. Suzuki and K. Inoue, "Kamioka underground observatories," *The European Physical Journal Plus*, vol. 127, no. 9, pp. 1–8, 2012.

[22] J. M. Carmona, S. Cebrin, E. Garca, *et al.*, "Neutron background at the canfranc underground laboratory and its contribution to the igex-dm dark matter experiment," *Astroparticle Physics*, vol. 21, no. 5, pp. 523–533, 2004.

[23] D.-M. Mei and A. Hime, "Muon-induced background study for underground laboratories," *Physical Review D*, vol. 73, no. 5, p. 053004, 2006.

[24] A. Bettini, "Underground laboratories," *Nuclear Instruments and Methods in Physics Research Section A: Accelerators, Spectrometers, Detectors and Associated Equipment*, vol. 626, pp. S64–S68, 2011.

[25] H. Sekiya, "Low energy investigations at kamioka observatory," in *Journal of Physics: Conference Series*, vol. 460, p. 012017, IOP Publishing, 2013.

[26] Canberra Industries Inc., *Standard Electrode Coaxial Ge Detectors (SEGe) Data Sheet*, 2013.

[27] G. Gilmore, *Practical gamma-ray spectroscopy.* John Wiley & Sons, 2011.

[28] E. Andreotti, M. Hult, G. Marissens, *et al.*, "Determination of dead-layer variation in hpge detectors," *Applied Radiation and Isotopes*, vol. 87, pp. 331–335, 2014.

[29] H. Ibach and H. Lth, *Solid-state physics : an introduction to principles of materials science.* New York: Springer, 4th ed., 2009.

[30] Canberra Industries Inc., *Flanged Cryostats Data Sheet*, 2008.

[31] Canberra Industries Inc., *Germanium detectors - Users manual*, 2003.

[32] Canberra Industries Inc., *Model 2002 Spectroscopy Preamplifier - Users manual*, 2004.

[33] T. Nakamura, M. Matsubara, S. Tasaka, *et al.*, "Development of low concentration radon detection system," in *Annual Report of Institute for Cosmic Ray Research, The University of Tokyo*, 2015.

[34] Techno AP Co. Ltd., *DSP APU8000 Series Data Sheet*, 2014.

[35] Techno AP Co. Ltd., *Digital Signal Processing - Hardware Manual*, 1.2.4 ed., 2011.

[36] Techno AP Co. Ltd., *Digital Signal Processing - Software Manual*, 2.0.8 ed., 2015.

[37] R. Brun and F. Rademakers, "Root - an object oriented data analysis framework," *Nuclear Instruments and Methods in Physics Research Section A*, vol. 389, no. 1, pp. 81–86, 1997.

[38] M. Agostini, C. Ur, D. Budjas, *et al.*, "Signal modeling of high-purity ge detectors with a small read-out electrode and application to neutrinoless double beta decay search in ge-76," *Journal of Instrumentation*, vol. 6, no. 03, p. P03005, 2011.

[39] R. J. Cooper, D. C. Radford, K. Lagergren, *et al.*, "A pulse shape analysis technique for the majorana experiment," *Nuclear Instruments and Methods in Physics Research Section A: Accelerators, Spectrometers, Detectors and Associated Equipment*, vol. 629, no. 1, pp. 303–310, 2011.

[40] S. Agostinelli, J. Allison, K. a. Amako, *et al.*, "Geant4 - a simulation toolkit," *Nuclear Instruments and Methods in Physics Research Section A: Accelerators, Spectrometers, Detectors and Associated Equipment*, vol. 506, no. 3, pp. 250–303, 2003.

Acknowledgement

The author feels enormous gratitude to a lot of people who guide, support and motivate the author during the years of doctoral study.

To all the members of CANDLES Collaboration, who involved in the construction, maintenance, data taking and analysis of CANDLES and HPGe detector system. Along the research path, the author have been blessed with a cheerful and motivated group of fellow collaborators. It is always aspiring and fruitful to learn and work with everyone. The research experiences and analysis methods that acquired in the CANDLES experiment, weekly group meeting and active discussion are golden learning opportunity for the author. Special thanks to all the staff, researchers and graduate students who have been so reliable and supportive during the preparation of this PhD dissertation.

To Prof Tadafumi Kishimoto, the author would like to offer the sincerest gratitude to his encouragement and patience supervision from the beginning until the end. The author is very grateful with the opportunity given to study in the field of experimental nuclear physics and research of tantalum-180m. He has provided a lot of chances for young students to improve and grow to become a researcher. Fully supportive in every aspects, with wisdom, experience and kindness. Thanks to the countless quality and acutely insightful discussion together. A lifelong teacher.

To Dr Saori Umehara, for the best professional guidance in running the experiment and data analysis of tantalum study. Author feels truly fortunate to do research with her very experienced supervision and commitment. The new HPGe detector system has greatly improved thanks to all her efforts. In addition, she has given many opportunities to the author to attend training workshops and present experiment result at conferences. Thank you very much.

To Kenji Matsuoka-san, who played the main role in construction work of the new HPGe detector at CANDLES Back Experimental Room. The material process, design, assembly and maintenance of the HPGe detector system and tantalum sample could not have been completed without his contribution. Author has learned a lot from his advance experience in building up various experiment facilities and research attitude with energetic passion.

To Dr Kohtaku Suzuki, who worked as a co-researcher in the preparation stage of the detector system. The tantalum measurement was first initiated at Radioisotope Research Center of Osaka University. He was actively involved in the testing of DAQ system and construction work for the new HPGe detector at Kamioka. Author is greatly in debt for his contribution and guidance on first handling of Ge detector, fine tuning of DSP, new DSP analyzer and countless discussions to perform the experiment.

To Associate Prof Sei Yoshida, for his constructive suggestions and practical support in data analysis and experimental techniques. He is always a very responsible, caring, humour and wise supervisor. Author has grew a lot by learning his research attitude in term of project planning and problem solving. A great model for becoming an excellent researcher in the future.

To Dr Kyohei Nakajima, for his professional guidance in data analysis by ROOT, GEANT4 simulation and clear presentation style. Furthermore, his passionately care to all the members has made the research life more enjoyable and appreciated. Author feels very lucky to learn and work with his interesting personality.

To Dr Takashi Iida, for his supreme multitasking research ability, encouragement and cheerful personality. His positive and forward-looking attitude has brightened many downhill during the years of doctoral study. Author is very grateful to all his contribution and utmost commitment to the CANDLES Collaboration.

To all the members of Kishimoto Laboratory, who shared all the good and bad days together in lab, like friends, like family. Assuming that 20 years from now, the author might has forgotten most of the physics equations and experimental techniques, but will always remember the nice acquaintance and good memory with everyone in Kishimoto Laboratory. Special thanks to Associate Prof Atsushi Sakaguchi and secretary Emi Matsuda-san, who are the most reliable supporters shaded at behind. They have put in a lot of efforts to make the research life very convenient and delighted for everyone. Author will like to express great gratitude to every lab members for their support on academic and personal life.

Finally, to my beloved family, who are so understandable, mind supportive and tolerance during my years of academic study. The author could not have gone this far without their dedication. Thank you.

Hissha ga koko made yatte korareta nowa, minnasama no okagesama desu.
Kokoro yori kansha moushiage masu.